1

MODULATION OF TRANSMITTER RELEASE

AT A GLOMERULAR SYNAPSE IN THE

CENTRAL NERVOUS SYSTEM

by

Simon James Mitchell

A thesis submitted for the degree of

Doctor of Philosophy

in the

University of London

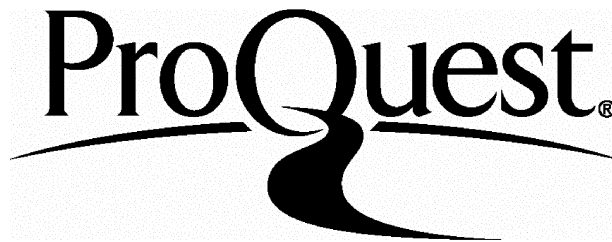Department of Physiology

University College London

2001

ProQuest Number: 10015920

ProQuest 10015920

ABSTRACT

The regulation of synaptic transmission is thought to be important for information processing and learning and memory. Synaptically-released transmitter can activate presynaptic receptors located at the same synapse to mediate homosynaptic modulation and/or spillover to neighbouring synapses to mediate heterosynaptic modulation. I investigated the properties of heterosynaptic modulation of transmitter release via metabotropic receptors at the cerebellar glomerulus using electrophysiological and modelling techniques.

Evoked inhibitory and excitatory postsynaptic currents (IPSCs and EPSCs) were recorded at 37°C from granule cells in rat cerebellar slices. Pharmacological activation of metabotropic glutamate receptors (mGluRs) on Golgi cell axons depressed evoked IPSCs by 75±5% (mean±sem; $n=6$) at 0.2 Hz, by inhibiting the release of GABA. The level of inhibition reduced with increasing stimulation frequency. Synaptically-released glutamate via mossy fibre stimulation (MFS), also induced disinhibition (50±7%; $n=6$). The magnitude of disinhibition increased with increasing MFS frequency and did not show appreciable accommodation throughout a 5 s period of MFS. Similarly, pharmacological activation of metabotropic GABA receptors (GABA$_B$-Rs) depressed evoked glutamate released from mossy fibres by 54±5% (1 Hz; $n=12$). Glutamate release inhibition was significant at 0.1-1 Hz, but not at 10-100 Hz MFS. Physiologically-released GABA from spontaneously active Golgi cells did not depress the evoked EPSC at 37°C unless a GABA uptake blocker was present, suggesting that GABA uptake maintains ambient GABA levels below that required for GABA$_B$-R

activation. However, stimulation of a single Golgi cell axon at 50 Hz depressed

the EPSC by 24±3% (n=19). Heterosynaptic $GABA_B$-R-mediated EPSC inhibition

was dependent on MFS frequency, consistent with the pharmacological data.

I investigated the effects of heterosynaptic modulation on synaptic integration

using an integrate and-fire model with granule cell properties. Activation of

mGluRs enhanced spiking driven by high frequency mossy fibres, increasing the

gain of these inputs. $GABA_B$-R activation suppressed spiking driven by mossy

fibres firing at low frequency, thereby acting as a high-pass filter. Heterosynaptic

modulation is likely to locally enhance contrast between granule cells with

different numbers of high-frequency mossy fibres. The mechanisms reported in

this thesis might shape how sensory information carried by mossy fibres is

processed at the input level, thereby determining the pattern of activation of

Purkinje cell, the output neurone of the cerebellar cortex.

TABLE OF CONTENTS

LIST OF FIGURES

LIST OF TABLES

ACKNOWLEDGMENTS

PUBLICATIONS

Mitchell, S.J. and Silver, R.A. (1999) Reciprocal presynaptic inhibition at the

cerebellar glomerulus of the rat. *J. Physiol. (Lond.)* **518.P**: 143P.

Mitchell, S.J. and Silver, R.A. (1999) Heteroreceptor mediated presynaptic

inhibition at the glomerulus of the rat cerebellum. *Society for*

Neuroscience Abstracts **25**: 189.10.

Mitchell, S.J. and Silver, R.A. (2000) Glutamate spillover suppresses inhibition by

activating mGluRs. *Nature* **404**: 498-502.

Mitchell, S.J. and Silver, R.A. (2000) GABA spillover selectively inhibits low

frequency excitatory transmission at cerebellar mossy fibres. *Society for*

Neuroscience Abstracts **26**: 332.6.

Mitchell, S.J. and Silver, R.A. (2000) GABA spillover from single inhibitory

axons suppresses low-frequency excitatory transmission. *Journal of*

Neuroscience **20**: 8651-8658.

Mitchell, S.J. and Silver, R.A. (2001) Shunting inhibition mediates a gain change

in central neurones driven by phasic synaptic inputs. *Society for*

Neuroscience Abstracts **27**: in press.

ABBREVIATIONS

7TM	seven transmembrane domains
ACPD	(±)-1-aminocyclopentane-trans-1,3-dicarboxylic acid
AMP	adenosine monophosphate
AMPA	α-amino-3-hydroxy-5-methyl-4-isoxazole-propionic acid
AP5	D(-)-2-amino-5-phosphonopentanoic acid
ATP	adenosine triphosphate
C_m	membrane capacitance
CPPG	(RS)-α-cyclopropyl-4-phosphonophenylglycine 300 μM)
CV	coefficient of variation (standard deviation/ mean)
DAG	diacylglycerol
DNA	deoxyribonucleic acid
EPSC	excitatory postsynaptic current
EPSP	excitatory postsynaptic potential
$<f>$	mean firing rate
f-F	spiking frequency versus input frequency
f-I	spiking frequency versus current amplitude
GABA	γ-amino butyric acid
$GABA_A$-R	GABA type-A receptor
$GABA_B$-R	GABA type-B receptor
$GABA_C$	GABA type-C
GC	granule cell
GIRK .	G-protein-linked inwardly rectifying potassium conductance
G_m	membrane conductance

GoS	Golgi cell stimulation
G-protein	GTP-binding protein
GTP	guanosine triphosphase
$G_{\beta\gamma}$	beta-gamma subunit complex of G-proteins
$I(0) = I_0$	initial current
$I_{inf} = I_\infty$	steady-state current
I_{inj}	current injection
I_m	*membrane current*
IP_3	inositol 1,4,5-trisphosphate
IPSC	inhibitory postsynaptic current
IPSP	inhibitory postsynaptic potential
K(ACh)	acetyl choline-sensitive potassium channels
L-AP4	L(+)-2-amino-4-phosphonobutyric acid
LTP	long-term plasticity
μ	mean PSC amplitude
MCPG	(S)-α-methyl-4-carboxyphenylglycine
MFS	mossy fibre stimulation
mGluR	metabotropic glutamate receptor
n	number of release sites
NBQX	7-chlorokynurenic acid (20 μM), 2,3-dioxo-6-nitro-1,2,3,4-tetrahydrobenzo[f]quinoxaline-7-sulphonamide disodium
NMDA	N-methyl-D-aspartic acid
PDC	L-trans-pyrrolidine-2,4-dicarboxylic acid
PIP_2	phosphatidylinositol 4,5-bisphosphate
PKA	protein kinase A
PKC	protein kinase C

PLC	phospholipase C
$P_n(0) = P_f$	probability of release failure
p_r	release probability
PSC	postsynaptic current
q	quantal size
Q_{10}	temperature coefficient
R_m	membrane resistance
R_s	series resistance
$SD = \sigma$	standard deviation
t_r	*rise time*
t_{ref}	refractory period
TTX	tetrodotoxin
VACC	voltage-activated calcium channel
V_c	command potential
V_m	membrane voltage
V_{th}	voltage threshold

CHAPTER ONE

INTRODUCTION

Modulation of transmitter release at a glomerular synapse in the central nervous system

1.1 Neurotransmission

Neurones communicate at specialised contact points called synapses. This term

was coined by Sherrington to describe areas of neuronal contiguity between spinal

motor neurones and the axons that innervate them (Foster, 1897). Later he

reasoned that synapses could perform a valve-like function, allowing the flow of

information only when the 'valve' is open. Furthermore, he reasoned that the

transduction required to propagate the signal between cells would enable

modification of the information flow possible (Schäfer, 1900). Although,

Sherrington there was no evidence when he first postulated the synapse, a

chemical mediator or neurotransmitter mediates communication at synapses. The

first evidence for chemical neurotransmission was at ganglionic and

neuromuscular synapses, where the discovery that acetylcholine was acted as

neurotransmitter made (Dale, 1935). However, it was not until the development of

intracellular recording techniques that the study of chemical transmission at the

functional level was made possible. Using these new techniques axon stimulation

evoked neurotransmission was observed at the neuromuscular junction (Fatt and

Katz, 1951), ganglionic synapses (Blackman et al, 1963) and crucially at central

synapses (Brock et al, 1952; Eccles et al, 1954). Further insights were obtained

with the arrival of high-resolution light microscopy, which enabled the

observation of granules in axon synaptic terminals (De Robertis and Bennet, 1954;

Palade, 1954; Palay, 1954). The functional significance of synaptic granules in

neurotransmission was postulated the following year (De Robertis and Bennet,

1955). These observations coincided with the development of the quantal

hypothesis for transmitter release, which suggested that discrete packets of

transmitter (quanta) are released with a finite probability from a definable number

of releasing "units" (del Castillo and Katz, 1954). A link between this functionally

derived theory and anatomical observations of discrete synaptic granules drove the

postulation of the vesicular hypothesis, which suggested that the anatomic

correlate for a quantum of transmitter may be the synaptic granule or vesicle (del

Castillo and Katz, 1956; Katz, 1962). This theory made two predictions: (1) after

the reduction in synaptic response following intense stimulation (depletion), the

number of vesicles in the presynaptic terminal should drop; (2) the vesicle

membrane should fuse during release, increasing membrane area of the

presynaptic terminal. These predictions were confirmed using anatomical

methods, supporting the vesicle hypothesis (Ceccarelli et al, 1972; Heuser and

Reese, 1973). Furthermore, the number of vesicles identified with freeze-fracture

techniques corresponds to number of functional quanta (Heuser et al, 1979;

Heuser, 1989).

Calcium has long been known to be crucial in the release of transmitter. Increasing

the extracellular calcium concentration reverses curare-induced depression (Feng,

1936) and can increase the level of neurotransmission at the neuromuscular

junction (del Castillo and Stark, 1952). In an attempt to establish whether the

calcium sensor for neurotransmission was inside or outside the terminal Miledi

and Slater exploited the ability to dialyse the presynaptic terminal at the squid

stellate ganglion giant synapse (Miledi and Slater, 1966). While electrically

stimulating the presynaptic fibre in a calcium free medium, they measure

transmitter release as they locally applied calcium by electrophoresis to the inside

or outside of the presynaptic membrane. It was found that calcium should be

applied extracellularly to evoke neurotransmission. Thus, they concluded, the

calcium sensor must be extracellular (Miledi and Slater, 1966). However,

increasing calcium concentration by intracellular electrophoresis at the same

presynaptic fibre without electrical stimulation could increase the probability of

quantal neurotransmission, to produce a slow depolarisation (Miledi, 1973). This

intracellular action locus of calcium was further supported by the observation of

highly localised depletion of vesicles following intracellular electrophoresis of

calcium (Martin and Miledi, 1978). It would appear that the calcium enters the

presynaptic terminal to act locally at a intracellular site to evoke transmitter

release.

The first direct demonstration of an increase in presynaptic calcium concentration

during an action potential were made possible with the development of calcium-

sensitive dyes. The first dye was aequorin, which is found in the luminescent

jellyfish *Aequorea victoria*. Aequorin was used to detect increases in presynaptic

calcium at the squid giant synapse following repeated stimulation (Llinas et al,

1972). The more sensitive absorbance dye, arsenazo III was used at the same

synapse to demonstrate that single action potentials could induce measurable

increases in presynaptic calcium concentration (Charlton et al, 1982; Augustine et

al, 1985). Further developments in sensitivity were made possible with the

development of fluorescent calcium-sensitive dyes by Tsien (Tsien, 1988), which

are the most widely used today.

Electrical recording of presynaptic calcium currents was first achieved at the squid

giant synapse (Llinas et al, 1981). Voltage clamp recordings of this terminal

revealed a fast inward followed by a slower outward current, similar to the results

of Hodgkin and Huxley (1952). Application of TTx and TEA showed that sodium

and potassium channels mediated these currents, respectively. Furthermore, these

drugs did not block a residual slow inward current, which was blocked by

cadmium: a calcium current (Llinas et al, 1981). Presynaptic calcium currents

have since been recorded at the calyx-type synapse at the ciliary gangion (Martin

et al, 1989; Stanley, 1989), in bipolar cells of goldfish retina (Tachibana et al,

1993) and at the calyx of Held in the MNTB (Takahashi et al, 1996). The

relationship between presynaptic calcium influx and postsynaptic response has

been quantified and appears to follow a power relationship with an exponent of 2-

4 in a wide range of central and peripheral preparations (Dodge and Rahamimoff,

1967; Jan and Jan, 1976; Andreu and Barrett, 1980; Stanley, 1986; Nachshen and

Sanchez-Armass, 1987; Seabrook and Adams, 1989; Augustine et al, 1991;

Barnes-Davies and Forsythe, 1995; Mintz et al, 1995; Takahashi et al, 1996;

Bennett, 1997; Dittman and Regehr, 1998; Reid, 1998; Kirischuk et al, 1999;

Bollmann et al, 2000; Schneggenburger and Neher, 2000; Warashina, 2001).

Therefore, changes in presynaptic calcium influx will have a profound effect on transmitter release. Indeed, repetitive stimulation of the presynaptic neurone can lead to the accumulation of residual calcium, which facilitates transmitter release (Katz and Miledi, 1968; Atluri and Regehr, 1996; Dittman et al, 2000; Tang et al, 2000). Calcium influx can also be modulated by the inactivation of calcium channels (Forsythe et al, 1998).

Released transmitter is detected by receptors that produce excitatory postsynaptic potentials (EPSPs), inhibitory postsynaptic potentials (IPSPs) or mediate modulation of transmission depending on the receptor pharmacology, signal transduction mechanism and presence on the pre- or postsynaptic membrane. These receptors can be ion selective pores (ionotropic receptors) or coupled to second messenger systems (metabotropic receptors). Synaptic transmission can be modulated via the activation of receptors by transmitter released by the same synapse (a form of homosynaptic modulation) or a neighbouring synapse (during heterosynaptic modulation). Characterising the mechanisms that modulate synaptic transmission is important since the way in which a network of neurones processes information is determined, in part, by the strength and the activity-dependent properties of its synaptic connections. Using electrophysiological and computational methods, I have investigated the presence of heterosynaptic modulation of transmitter release at the glomerulus of the cerebellar cortex and examined how this modulation affects synaptically driven spiking in model granule cells.

1.2 Receptors underlying excitation, inhibition and modulation in the CNS

To establish that a molecule acts as a neurotransmitter several criteria have to be

fulfilled. The chemical has to be synthesised and stored, released by axonal

stimulation, broken down and/ or taken up by surrounding tissue. Furthermore,

application of the molecule has to mimic the properties of endogenous transmitter

in terms of cellular action and antagonist sensitivity: that is, it must activate the

same receptors. Glutamate's role in central nervous function was first suggested

by the observation that application of glutamate could induce convulsions in dogs

(Hayashi, 1954). This suggestion was supported by the finding that glutamate

could depolarise and excite cat and toad spinal neurones (Curtis et al, 1959, 1960).

Glutamate was universally accepted as the main central neurotransmitter in the

1980s (Watkins, 2000). In this period, glutamate was found to be present at the

mossy fibre to granule cell and granule cell synapse (Somogyi et al, 1986, Ji et al,

1991), glutamate receptors had been found on granule cells (Cull-Candy and

Ogden, 1985), and the enzymes required for glutamate synthesis and breakdown

had been found in mossy fibre terminals (Kaneko et al, 1989; Wurdig and Kugler,

1991) This synapse was subsequently found to use glutamate as an excitatory

transmitter (Garthwaite and Brodbelt, 1989; D'Angelo et al, 1990; Silver et al,

1992).

GABA was first discovered to be a major inhibitory neurotransmitter in Purkinje

cells at the brain stem (Obata, 1969; Obata et al, 1970; Otsuka et al, 1971).

Bicuculine-sensitive GABA receptors were suggested to mediated inhibition in the

spinal neurones (Curtis et al, 1970a, 1970b). Morphological and physiological

evidence indicates that GABA is released as a transmitter in the retina (Sterling,

1983; Lam and Ayoub, 1983), lateral geniculate nucleus (Hendrickson et al, 1983)

and visual cortex (Gilbert, 1983). In the cerebellar granule cell layer, granule cells

have receptors have receptors for GABA and Golgi cells contain and release

GABA (Aoki et al, 1986; Gabbott et al, 1986; Kaneda et al, 1995).

Glutamate and GABA are the principle neurotransmitters in the mammalian

cerebellum. Once released into the synaptic cleft these molecules can activate

multiple receptor subtypes. Many of these receptors have been cloned and their

pharmacology is well understood (Hollmann and Heinemann, 1994; Saxena and

MacDonald, 1996; Conn and Pin, 1997; Kaupmann et al, 1997). Ionotropic

receptors make a family of receptors, which are sensitive to transmitters such as

acetylcholine, GABA or glycine, made up of 5 subunits, each with four

transmembrane domains. Excitatory transmission in the CNS is usually mediated

by glutamate, which activates ionotropic receptors that gate cation channels

sensitive to the pharmacological agonists, NMDA, AMPA or kainate to depolarise

a neurone towards, or beyond, spiking threshold on a sub-millisecond to

millisecond timescale (Bekkers and Stevens, 1989; Silver et al, 1992; Castillo et

al, 1997; Vignes and Collingridge, 1997). There is a second distinct group of

glutamate receptors that are coupled to second messenger systems via guanosine

triphosphate (GTP)-binding proteins (G-proteins), known as metabotropic

glutamate receptors (mGluRs). The majority of known mGluRs are made up of a

one of eight subunits (mGluR1-8). These are classified into three groups (I-III)

according to molecular biology and pharmacology (Conn and Pin, 1997).

Although each group share <45% DNA sequence homology, each have a similar

general structure of a N-terminal extracellular glutamate binding domain, seven

transmembrane domains (7TM) linked by alternate intra- and extracellular loops

and an internal C-terminus, which can form a fourth internal loop. This 7TM

molecular arrangement distinguishes mGluRs as part of the metabotropic receptor

family, which can also have GABA, serotonin, noradrenaline, dopamine or

acetylcholine as ligands. The second internal loop has been implicated in the

coupling and activation of G-proteins. The C-terminus of mGluR7 also been

implicated in binding of calmodulin and G-proteins in a mutually exclusive

manner (O'Conner at al, 1999). Activation of mGluRs, as well as other

metabotropic receptors, results in responses that are generally more long-lasting

than ionotropic receptors, due to their complex signal transduction mechanism.

Activation of group I mGluRs (mGluR1 and 5) activates phospholipase C (PLC)

via the α subunit of heterotrimeric G-proteins. PLC promotes the hydrolysis of the

membrane phospholipid, PIP_2, producing the two intracellular second messengers,

inositol 1,4,5-trisphosphate (IP_3) and diacylglycerol (DAG). IP_3 activates receptors

on the endoplasmic reticulum, inducing the release of calcium from intracellular

stores. Calcium acts as a third messenger to modulate ligand-gated ion channels

by acting as a cofactor for calcium/calmodulin-dependent kinase II, which can

modulate AMPA channels (McGlade-McCulloh et al, 1993) and quantal

transmitter release (Brailoiu and Miyamoto, 2000). DAG can activate protein

kinase C (PKC), which induces phosphorylation of AMPA/kainate receptors

(Wang et al, 1994) and promotes the facilitation of synaptic transmission

(Ghirardi et al, 1992). Group II (mGluR2 and 3) and group III receptors (mGluR4, 6, 7 and 8) downregulate adenylate cyclase, which catalyses the production of cyclic-adenosine monophosphate (cyclic-AMP). Cyclic-AMP regulates the actions of protein kinase A, which promotes phosphorylation of AMPA/kainate receptors (Rosenmund et al, 1994) and modulates synaptic plasticity (Ghirardi et al, 1992). The activation of mGluRs can change the excitability of the postsynaptic cells by modulating the conductance and/or the kinetics of ion channels gated by voltage or ligands.

GABA mediates inhibition by activating ionotropic $GABA_A$ (MacDonald and Olsen, 1994) and $GABA_C$ receptors (Johnston, 1996), both of which gate chloride conductances when activated. Since chloride conductances tend to have a reversal potential of around -70 mV in mature animals, due to the distribution of chloride across the cell membrane, they drive the membrane potential of a neurone below spiking threshold (typically ~ 55 mV). $GABA_B$ receptors (Bowery, 1993) have a similar 7TM structure to mGluRs (Kaupmann et al, 1997) and like mGluRs are coupled to G-protein-dependent second messenger systems. Initially, one subtype with two splice variants was cloned ($GABA_B$-R1a and 1b) (Kaupmann et al, 1997). Expression of this receptor formed functional $GABA_B$-Rs, which had a reduced affinity for GABA, compared to native receptors (Kaupmann et al, 1997). It was later found that the formation of a heterodimer between $GABA_B$-R1 and another subtype with 35% sequence homology, $GABA_B$-R2, produces $GABA_B$-Rs with a much higher affinity (reviewed in Marshall et al, 1999). $GABA_B$-Rs are negatively coupled to the production of cyclic-AMP.

The mechanisms of metabotropic receptor-mediated actions reviewed above

involve the liberation of a cytosolic second messenger: a process with slower

kinetics than ionotropic responses due to the complex signal transduction

mechanism. However, there is evidence that a second modulatory pathway might

be induced. Cell-attached recordings of acetylcholine-sensitive potassium

channels [K(ACh)] from rabbit atrial cells revealed that the application of ACh in

the patch pipette increased the open probability, while bath application did not

(Soejima and Noma, 1984). It was postulated that local activation of potassium

channels was achieved via a membrane delimited pathway, whereby the G-protein

directly regulates the channel properties, with an timescale intermediate between

those of ionotropic and second messenger pathways receptor (Hille, 1994). Direct

evidence of an interaction between G-proteins and voltage-gated ion channels has

been found in expression systems. The β-γ subunit complex of heterotrimeric G-

proteins ($G_{\beta\gamma}$) appears to bind to and be sufficient for activation of a G-protein

linked inwardly rectifying potassium conductance (GIRK1) (Reuveny et al, 1994;

Huang et al, 1995). At neuronal somata, mGluRs and $GABA_B$-Rs are known to

activate G-proteins, thereby enhancing GIRK-mediated inhibition (Andrade et al,

1986; Sodickson and Bean, 1996; Luscher et al, 1997, Dutar et al, 2000). $G_{\beta\gamma}$ also

appears to bind to the pore forming domain of voltage-activated calcium channels

(VACCs) (De Waard et al, 1997), providing a mechanism for the depression of

somal VACCs following the activation of $GABA_B$-Rs and mGluRs (Dolphin and

Scott, 1987; Scholtz and Miller, 1991; Mintz and Bean, 1993; Herlitze et al, 1996;

Ikeda, 1996; Saugstad et al, 1996; Shekter et al, 1997; Knoflach and Kemp, 1998).

G-protein-mediated regulation of ion channels such as voltage-activated calcium

and potassium channels via metabotropic receptors has also been implicated in the

regulation of transmitter release (Takahashi et al, 1996, 1998; Cochilla and

Alford, 1998); however, the specific involvement of $G_{\beta\gamma}$ in presynaptic

modulation has not been established. Although the molecular biology and

functional heterogeneity of glutamate and GABA receptors is well understood,

relatively little is known about how their physiological activation by synaptically-

released transmitter modulates synaptic transmission.

1.3 Mechanisms of homosynaptic modulation of synaptic efficacy

The efficacy with which one neurone communicates with another can change with

time due to synaptic plasticity. An increase or decrease in synaptic efficacy might

arise in response to the prior level and pattern of activity at a synapse. These

effects can persist in the short-term (milliseconds to seconds; Magleby, 1987;

Zucker, 1989), or for a longer period as typified by the phenomenon of long-term

potentiation and depression, which can last for hours in the *in vivo* preparation

(Bliss and Lømo, 1973; Ito et al, 1982). Both short- and long-term plasticity is

thought to have a role in the normalisation of synaptic efficacy according to the

rate of transmission (Markram and Tsodycks, 1996; Abbott et al, 1997). Whereas,

long-lasting plastic changes have been proposed to represent the cellular basis of

associative learning and memory (Bliss and Collingridge, 1993). Therefore,

quantification of the timescale of plasticity might give indications to its

physiological role.

The efficacy of transmission at a single synapse can be modulated by a reduction

in the release of transmitter (presynaptic mechanism) or by a reduction in the

response to released transmitter (postsynaptic mechanism). Several mechanisms

regulate the postsynaptic response to neurotransmitter. The postsynaptic response

is determined by the conductance and the kinetic properties of postsynaptic

receptors and by the excitability of the neurone. Since these parameters can be

modulated by second messenger systems, as discussed above, postsynaptic

metabotropic receptors are likely to regulate synaptic efficacy (Dutar and Nicoll,

1988; Batchelor and Garthwaite, 1997). A second mechanism that controls the

postsynaptic response is receptor desensitisation. This mechanism is activated by

the sustained exposure of receptors to transmitter, which progressively reduces the

response to further activation, reducing synaptic strength (Trussell et al, 1993;

Otis et al, 1996). Both the activation of postsynaptic metabotropic receptors and

the induction of desensitisation are likely to be important during repetitive, high-

frequency release of transmitter (Kim et al, 1997; Aria and Lynch, 1998), since

sustained release can saturate binding sites for transmitter on transporters (Tong

and Jahr, 1994; Diamond and Jahr, 1997), slowing transmitter clearance

(Overstreet et al, 1999), thus permitting more widespread diffusion (Barbour and

Häusser, 1997; Rusakov et al, 1999). The conditions that promoted the activation

of postsynaptic receptors, as discussed above, might also promote the activation of

receptors present on the presynaptic membrane.

The modulation of transmitter release was established in the form of "presynaptic

inhibition" of spinal sensory neurones (Frank and Fuortes, 1957; Eccles et al,

1961). This effect was mediated via axo-axonal synapses (Gray, 1962), which

released GABA (Barker and Nicoll, 1972; Davidoff, 1972; Nicoll, 1988),

activating $GABA_A$ receptors (Peng and Frank, 1989b); Stuart and Redman, 1992)

and $GABA_B$ receptors (Edwards et al, 1989; Peng and Frank, 1989a). The

activation of metabotropic receptors, like $GABA_B$ receptors, and the subsequent

activation of G-proteins can modulate transmitter release by inhibiting calcium

influx (Wu and Saggau, 1994, 1995; Dittman and Regehr, 1997; Takahashi et al,

1996, 1998; Cochilla and Alford, 1998). Additionally, metabotropic receptors are

also thought to modulate transmitter release by regulating processes downstream

of calcium influx (Capogna et al, 1996a, 1996b; Dittman and Regehr, 1996). The

activation of metabotropic autoreceptors has been implicated in the induction of

short-term depression of glutamate release (Barnes-Davies and Forsythe, 1995;

von Gersdorff et al, 1997; Takahashi et al, 2000) and GABA release (Davies and

Collingridge, 1993). The release probability is dependent on the size of the readily

releasable pool of vesicles (RRP), which may be related to the number of docked

synaptic vesicles (Rosenmund and Stevens, 1996). Thus, a synapse in which

vesicles are being released at a high rate will experience synaptic depression as

depletion of available vesicles occurs (Elmquist and Quastel, 1965; Kusano and

Landau, 1975), and the steady-state release probability will depend on the rate of

replenishment of the RRP. Therefore, synaptic transmission can be regulated by

many mechanisms, many of which involve the activation of pre- or post-synaptic

receptors to modulate postsynaptic responsiveness or initial release probability.

1.4 Heterosynaptic modulation

Neurotransmitter can diffuse from the synaptic cleft to activate receptors at or

around neighbouring release sites or synapses (spillover; Barbour and Häusser,

1997; Rusakov et al, 1999). Spillover of glutamate between release sites might

explain the dependence of non-NMDA receptor-mediated EPSC kinetics on

release probability at multi-site cerebellar mossy fibre to granule cell synapses

(Silver et al, 1996b). Direct evidence for the synaptic activation of NMDA

receptors by spillover of glutamate has been observed between dendrites of mitral

cells of the olfactory bulb, which do not make synapses with each other (Isaacson,

1999). GABA spillover is thought to mediate the long-lasting component of

$GABA_A$ receptor-mediated evoked IPSCs in the cerebellar glomerulus (Rossi and

Hamann, 1998). These studies show that spillover of glutamate and GABA can

activate postsynaptic ionotropic receptors to mediate excitation and inhibition,

respectively. Moreover, evidence is emerging that the heterosynaptic activation of

presynaptic receptors (heteroreceptors) sensitive to kainate and AMPA can

regulate the release of GABA (Min et al, 1999; Satake et al, 2000). However, the

activation of presynaptic metabotropic heteroreceptors via transmitter spillover

between excitatory and inhibitory fibres is better understood.

The pharmacological activation of mGluRs has been found to inhibit the release of

GABA from many preparations. Activation of group I mGluRs has been shown to

inhibition the release of GABA in CA1 area of the hippocampus (Gereau and

Conn, 1995). Group II mGluR activation suppresses inhibitory transmission in the

accessory olfactory bulb (Hayashi et al, 1993), CA3 hippocampus (Poncer et al,

1995) and inhibits spontaneous IPSCs recorded from cerebellar granule cells

(Vetter et al, 1999). Group I/II mGluRs mediate the inhibition of GABA

transmission in cerebellar molecular layer interneurones (Llano and Marty, 1995).

The activation of group III mGluRs suppresses evoked IPSCs, recorded in

mesencephalic principle neurones (Bonci et al, 1997) and developing rat

hypothalamic neurones (van den Pol et al, 1998). Group III mGluR activation also

suppresses the evoked IPSC between two CA1 hippocampal interneurones and, to

a lesser extent, between CA1 interneurones and principle neurones (Semyanov

and Kullman, 2000). Furthermore, activation of either group II or III mGluRs

suppresses inhibition in the thalamus (Salt and Eaton, 1995) and inhibits miniature

IPSCs in magnocellular neurones of the supraoptic nucleus of the hypothalamus

(Schrader and Tasker, 1997). Although activation of mGluRs by synaptically

released glutamate depresses glutamate release from excitatory terminals

(Scanziani et al, 1997; von Gersdorff et al, 1997; Vogt and Nicoll, 1999), evidence

for activation of mGluRs in interneurones by synaptically-released transmitter is

only beginning to emerge (Semyanov and Kullman, 2000).

Pharmacological activation of $GABA_B$-Rs can inhibit the release of glutamate.

This has been demonstrated in a wide range of peripheral and central preparations,

in many species (Demeneix et al, 1986; Peng and Frank, 1989b; Brooks et al,

1992; Nisenbaum et al, 1992; Wu and Dun, 1992; Morishita and Sastry, 1994;

Jiang et al, 1995; Gil et al, 1997; Shen and Johnson, 1997; Takahashi et al, 1998).

Furthermore, several studies have established that $GABA_B$-Rs on excitatory

terminals in hippocampus and cerebellar cortex can be activated by spillover of

GABA from interneurones (Isaacson et al, 1993; Dittman and Regehr, 1997; Vogt

and Nicoll, 1999). However, synchronous activation of many axons is likely

during extracellular stimulation employed in these studies so it is unclear whether

transmitter release from a single input or synchronous release from many inputs is

sufficient for heterosynaptic activation.

The distance over which transmitter can travel from the release site and activate

receptors at other synapses is dependent on diffusion and the efficacy of

transmitter uptake in the locality (Isaacson et al, 1993; Barbour and Häusser,

1997; Rusakov et al, 1999). Heteroreceptor activation is therefore likely to be

strongly dependent on temperature, because uptake mechanisms have a large Q_{10}

(~3; Wadiche and Kavanaugh, 1998). However, most of the experiments

examining transmitter spillover onto presynaptic heteroreceptors have been

performed below body temperature (26—34°C; Isaacson et al, 1993; Dittman and

Regehr, 1997; Yamada et al, 1999; Aroniadou-Anderjaska et al, 2000; Semyanov

and Kullman, 2000). This raises the question of whether the extrasynaptic

concentration of GABA or glutamate is sufficient to produce significant tonic

and/or phasic activation of heteroreceptors on synaptic terminals at body

temperature (Isaacson et al, 1993). Indeed, the physiological activation of mGluRs

on inhibitory interneurones in the hippocampus was reduced by heating the

preparation towards body temperature (Semyanov and Kullman, 2000).

Quantifying the inhibition of PSCs by synaptically released transmitter at

physiological temperature is therefore an important prerequisite for inferring how
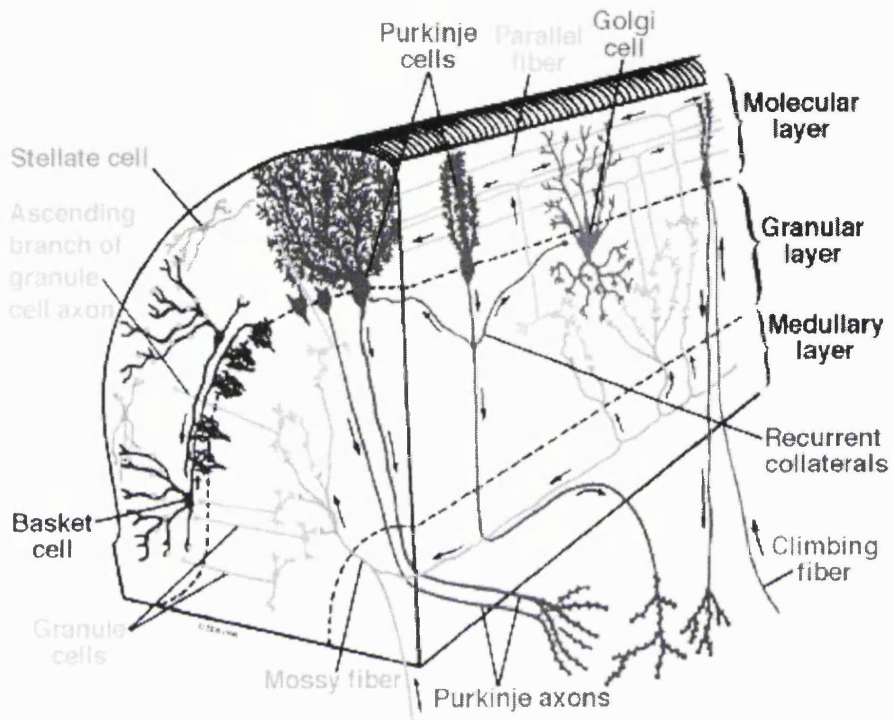
Figure 1.1 – The cerebellar cortex. See text for details. (Modified from Eccles et al, 1967)

presynaptic heteroreceptors modulate synaptic efficacy under physiological

conditions. Furthermore, the fraction of heteroreceptors occupied at physiological

temperature is a key parameter because it influences transmitter release probability

and thus determines the frequency-dependent behaviour of the synapse (Brenowitz

et al, 1998; Brody and Yue, 2000; Kreitzer and Regehr, 2000).

1.5 Heterosynaptic transmission in the cerebellar glomerulus

The cerebellum, from the Latin 'little brain', is a major part of the nervous system.

It's mass makes up 10-15 % of the brain's total weight (Inukai, 1928). The

cerebral cortex is a 1 mm thick sheet covering the folded surface of the

cerebellum. The fine folding of the cortex means that the cerebellar cortex can be

up to one third the surface area of the cerebral cortex (Ito, 1984). The cerebellar

cortex receives inputs in the form of mossy fibres from a large range of brain

regions, which can be broadly separated into three groups: cerebral cortex, spinal

cord and vestibular system (Purves et al, 2001). The cortical regions that innervate

the cerebellum are the frontal, motor, somatosensory and secondary visual cortex.

The fundamental cellular anatomy of the cerebellar cortex was discovered and

documented in great detail by the forefather of modern neuroanatomy Santiago

Ramón y Cajal (Cajal, 1911). Mossy fibres innervate the cerebellum at excitatory

synapses on granule cells within the granular layer (figure 1.1). From here,

information passes to the parallel fibres in the molecular layer, which make

excitatory synapses with Purkinje cells, whose dendritic arbour is arranged in a

perpendicular plane to parallel fibres (figure 1.1). Purkinje cells are the only

output neurone of the cerebellar cortex. These inhibitory cells send axons through

the white matter (medullary layer) and innervate neurones of deep cerebellar

nuclei (figure 1.1). There are several different types of GABAergic interneurone

including Golgi cells of the granular layer that innervate granule cells, as well as

stellate and basket cells of the molecular layer that innervate Purkinje cells (figure

1.1). In addition to mossy fibres, input from the inferior olive is conveyed via

climbing fibres to Purkinje cell dendrites and somata to form powerful excitatory

synapses. The output of the cerebellum is direct to the vestibular system and

indirect via the deep cerebellar nuclei and thalamus to red nucleus, vestibular

nuclei, superior colliculus, reticular formation and motor cortex (Purves et al,

2001). Therefore, the cerebellum is innervated by and innervates multiples

systems in the brain and can be thought of as integrating sensory and motor

information.

Most interest has been focused on the role of the cerebellum in the real-time

regulation of movement and motor learning such as proposed by Marr, Albus and

Ito (Marr, 1969; Albus, 1971; Ito, 1984). The cerebellum is therefore commonly

thought of being part of the extrapyramidal motor system, along with the basal

ganglia. The potential role of the cerebellum in motor control becomes evident

when the cerebellum is damaged, such as during trauma or disease. Often this

damage leads to cerebellar ataxia, whereby normally smooth well-coordinated

movements become jerky and imprecise. The vesibular-ocular reflex (VOR),

which ensures that the eyes remain trained to an object if the head moves, is a

model for cerebellar motor control. This reflex is plastic and can adapt to

compensate for experimental optic ligament lesions or artificial magnification of

the image (Purves et al, 2001). However, the ability to learn the VOR is

compromised by cerebellar lesions, indicating that the cerebellum has a role in

VOR. How might motor learning be achieved? Ito suggested that sensory and

other information, via mossy fibres, is processed by the granule cell layer and

projected to Purkinje cells, which compare the information with 'error signals',

carried by climbing fibres (Ito, 1984). Where parallel fibre activity is paired with

climbing fibre activity, long-lasting depression occurs at these parallel fibres,

reducing the efficacy of these pathways to induce Purkinje cell spiking. Therefore,

by modifying the pattern of parallel fibre firing, the way in which mossy fibre

information is processed at the level of the granule cell layer is crucial to the

regulation of motor learning in the cerebellum.

I have investigated the presence of heterosynaptic modulation at excitatory mossy

fibre-granule cell and inhibitory Golgi-granule cell synapses at the glomerulus of

the cerebellar cortex. This preparation has several advantages for investigating

presynaptic modulation. First, granule cells are innervated at a glomerular

structure that consists of a single large excitatory mossy fibre terminal and an

inhibitory Golgi cell axon (Eccles et al, 1967; Jakab and Hámori, 1988). The

whole structure, including the ends of the granule cell dendrites, is ensheathed in a

glial coat (Jakab and Hámori, 1988), which might localise spillover of transmitter

(Brickley et al, 1996; Wall and Usowicz, 1997; Rossi and Hamann, 1998). Each of

the three to five granule cell dendrites is innervated by a different mossy fibre, and

up to 50 different granule cells make synapses within each glomerulus (Eccles et

al, 1967; Jakab and Hámori, 1988). Second, the low density of mossy fibres and

Golgi cells in the granule cell layer allows the activation of single inputs using

local extracellular stimulation (Silver et al, 1996b). Third, the short dendrites and

small soma of granule cells form a single electrical compartment, making it

possible to obtain recordings of postsynaptic currents (PSCs) with high temporal

resolution (DC length constant 0.02-0.05, Silver et al, 1992, 1996c; D'Angelo et

al, 1993, 1995; Gabbiani et al, 1994). Fourth, immunohistochemistry has localised

the R1b splice variant of the $GABA_B$-R in the glomerulus and group II/III mGluRs

on Golgi cell axon terminals (Ohishi et al, 1994; Poorkhalkali et al, 2000),

opening the possibility that there might be functional heteroreceptors in the

cerebellar glomerulus.

In chapter 3, the role of mGluRs on inhibitory axons was investigated by making

voltage-clamp recordings of IPSCs in granule cells, evoked by minimal

stimulation of a single Golgi cell axon, under physiological conditions. The

presence of functional presynaptic mGluRs was studied by studying the effects of

mGluR agonists and antagonists on evoked IPSCs. These effects were evaluated

across a range of frequencies observed *in vivo* (Edgley and Lidierth, 1987; van

Kan et al, 1993). The physiological activation of mGluRs on Golgi cells was

investigated by stimulating single glutamatergic mossy fibres that were connected

to the same granule cell as the inhibitory fibres. The dependence of mGluR

activation on mossy fibre stimulation frequency was investigated.

In chapter 4, the role played by $GABA_B$-Rs in the regulation of glutamate release

was investigated by making voltage-clamp recordings of EPSCs in granule cells,

evoked by minimal stimulation of a single mossy fibres, under physiological

conditions. The presence of functional presynaptic $GABA_B$-Rs was studied by

examining the effects of selective $GABA_B$-R agonists and antagonists on evoked

and spontaneous miniature EPSCs. These effects were evaluated across a range of

frequencies observed *in vivo* (van Kan et al, 1993). The role of uptake on limiting

the tonic activation of $GABA_B$-Rs by spontaneously released GABA from Golgi

cells (Brickley et al, 1996) was studied using temperature and an uptake inhibitor.

The physiological activation of $GABA_B$-Rs on mossy fibres was investigated by

stimulating single Golgi cell axons that were connected to the same granule cell as

the mossy fibres. The dependence of $GABA_B$-Rs activation on mossy fibre

stimulation frequency was investigated.

1.6 Modelling synaptic integration in granule cells

Neurones integrate excitatory and inhibitory postsynaptic potentials and generate

trains of action potentials. Their firing rate depends on the balance of excitation

and inhibition, which is determined by the rate and efficacy of the individual

inputs. These factors are often interdependent, such as in the case of depression of

excitatory inputs with increasing frequency (Ch. 4; Markram and Tsodyks, 1996,

Abbott et al, 1997; Galarreta and Hestrin, 1998). Heterosynaptic interactions

between inhibitory and excitatory inputs set up further interdependencies, such as

those between release rates and initial release probabilities of neighbouring

synapses. This makes the frequency-dependence of the balance of excitation and

inhibition hard to predict.

Spillover of glutamate in the cerebellar glomerulus inhibits GABA release from

Golgi cells via mGluRs, and GABA can inhibit the release of glutamate from

mossy fibres by activating $GABA_B$-Rs (Chs 3 and 4; Mitchell and Silver, 2000a,

2000b). Suppression of inhibition occurs at glomeruli where the mossy fibre is

highly active, whereas glutamate release is selectively inhibited at low mossy fibre

firing rates. It is likely that the frequency dependences of these presynaptic

mechanisms increase the postsynaptic efficacy of high-frequency mossy fibre

transmission. However, the degree to which presynaptic metabotropic

heteroreceptors modulate neuronal spiking rate remains to be resolved as the *in*

vitro experiments required to do so are difficult to interpret and perform due to

both the unresolved mGluR pharmacology at the mossy fibre to granule cell

synapse (Vetter et al, 1999) and the difficulty in finding two inputs into the same

glomerulus (Chs 3 and 4; Mitchell and Silver, 2000a, 2000b). Although it is

ultimately necessary to demonstrate spike modulation via presynaptic

metabotropic receptors in a physiological preparation, many insights can be

obtained using computational techniques.

The modelling of complex physiological mechanisms is useful for the preliminary

testing of hypotheses and for exploring parameter space. Various models of single

neurones are available, which differ with respect to accuracy with which they

represent the morphology and electrical responses of neurones. At one end of the

scale lies the firing rate model. It integrates an injected current across a simple RC

circuit and directly derives the average firing rate from the integrated, 'generator'

potential according to a lookup table of frequency versus voltage, which is itself

derived from experimental observations (Koch, 1999). However, this model

suffers from two problems: first, the voltage response is not preserved, making it

difficult to compare data sets and second, the response kinetics do not truly

represent that of a real neuron, since the spiking mechanism can vary the

membrane time constant, which this model lacks.

Complex cellular models generally take the form of anatomically reconstructed

neuronal morphologies, divided into individual connected compartments, which

integrate and propagate signals within and between each compartment, to provide

a computational solution for the cable equation (Jack et al, 1983). The benefit of

compartmental models is that numerous voltage-dependent and independent ionic

conductances that are present in real neurones can be implemented. These models

can replicate the global spatio-temporal profile of synaptic integration. However,

compartmental models are only as accurate as the data used to construct them.

Often, they are modelled with many parameters that are unconstrained by

experimental observations, such as channel distributions. Additionally, some cells

do not benefit from the multi-compartmental approach. For example, the dendrites

and soma of the cerebellar granule cell, as mentioned above, act as an

electrotonically-compact, single compartment (Silver et al, 1992; D'Angelo et al,

1993, 1995), with an insignificant level of cable filtering occurring between the

synapse and the soma where synaptic integration occurs (Gabbiani et al, 1994;

Silver et al, 1996c).

The simplest model with a spiking mechanism is the integrate-and-fire unit. This model has been used since its conception at the beginning of the twentieth century (Lapicque, 1907; Abbott, 1999) to emulate spiking cells, before the mechanisms underlying firing were known (Koch, 1999). A variant of this single unit model, the leaky integrate-and-fire unit, can be used to integrate charge across a conductance and capacitance in parallel until a spike is generated at a specific threshold, after which the membrane potential is reset. The model is based on a single electrical compartment, and is thus useful for modelling synaptic integration in electrically compact cells like granule cells. It has also been used to model synaptic mechanisms in large cells successfully (for examples see Abbott et al, 1997 and Dittman et al, 2000). Moreover, several time-dependent conductances such as an afterhyperpolarisation and synaptic conductances can be easily introduced to mimic many properties exhibited by real cells (Koch, 1999).

In chapter 6, I have investigated how heterosynaptic inhibition of glutamate and GABA release affects the dependence of granule cell spiking rate on the frequency of mossy fibre-mediated excitation. A steady-state model of the mechanisms that control the release of transmitter from Golgi cell axons and mossy fibres was constructed from electrophysiological data (Chs 3 and 4). This model was combined with a conductance-based integrate-and-fire unit that was modified to capture some essential granule cell properties. These methods have provided a deeper understanding of the postsynaptic consequences of heterosynaptic modulation in the cerebellar glomerulus. Furthermore, by exploring the dependencies of postsynaptic spiking on heterosynaptic modulation, I was able to

test predictions regarding the network conditions under which spillover-mediated

presynaptic modulation is maximally active.

CHAPTER TWO

ELECTROPHYSIOLOGY METHODS

Heterosynaptic modulation of transmitter release in the cerebellum was investigated using a two-stage approach. First, the physiological properties of heterosynaptic modulation were quantified using electrophysiological methods in acute sagittal slices of cerebellum from juvenile rats. Second, the way in which these synaptic mechanisms affected synaptic integration was investigated using an integrate-and-fire model with the granule cell properties.

Granule cells receive synaptic input at the cerebellar glomerulus, a structure where an excitatory mossy fibre and inhibitory Golgi cell make axo-dendritic synapses (figure 2.1) onto granule cell dendrites, within a glial coat (Eccles et al, 1967; Jakab and Hamori, 1988). Synaptic modulation was studied by recording evoked EPSCs and IPSCs from granules cells in acutely isolated cerebellar slices in which the synaptic architecture remains relatively intact.

2.1 Dissection

Parasagittal cerebellar slices were prepared from 12–13 days old Sprague-Dawley rats based on a method described by Silver et al (1996b). This plane of sectioning preserves mossy fibres, which follow an approximate sagittal path as they innervate the cerebellar cortex in mice (Sultan, 2001). The animals were
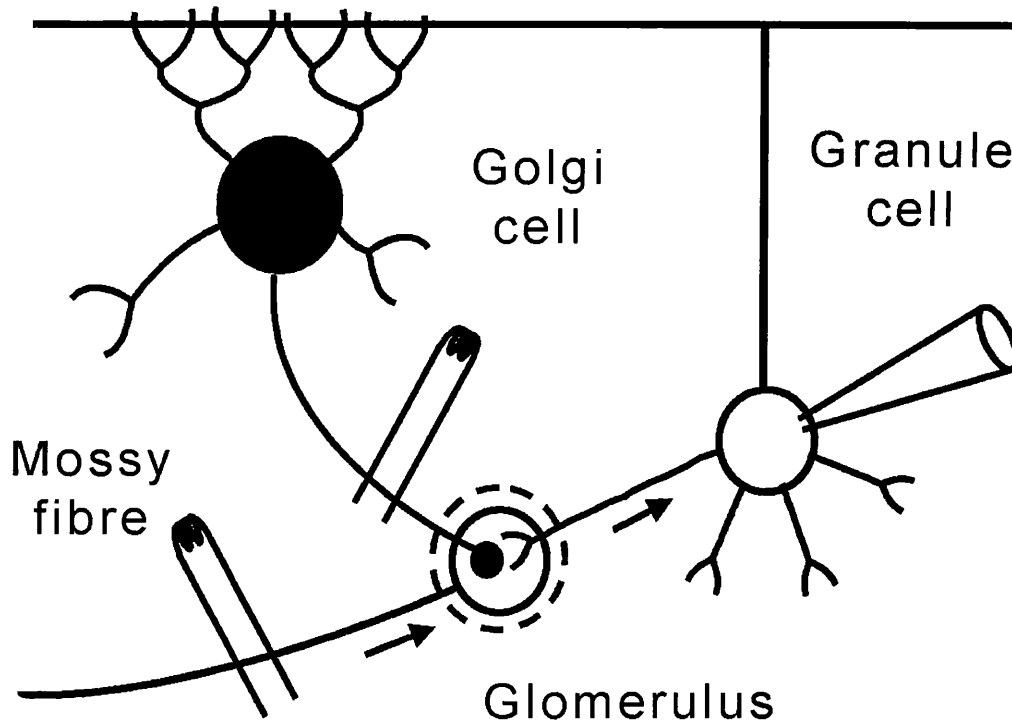
Figure 2.1 – The neurones of the cerebellar cortex. Two dimensional representation of the circuit of interest. A granule cell was whole-cell patch-clamped and single independent inhibitory (Golgi cell) and excitatory (mossy fibre) inputs were stimulated. These fibres make synapses in the cerebellar glomerulus.

decapitated in accordance with the Animals (Scientific Procedures) Act 1986. A

single cut of the skin at the midline of the dorsal surface of the skull was made in

a caudal to rostral direction; the resulting skin flaps were peeled back to expose

the skull. The skull was cut around the left side and transferred into a dish

containing ice-cold slicing solution (<5 °C; table 2.1), at which point the skull flap

was folded over to the right to expose the brain. The brain was rapidly removed

from the skull by severing the cranial nerves using a sideways motion of a small

spatula. Once removed, the brain was allowed to cool in the ice-cold slicing

solution for about 30 seconds. Mechanical damage to the tissue during the

dissection induces cell death, the production of free radicals and uncontrolled

transmitter release (Olney, 1990). Also, reduced brain respiration may cause

ischaemia, which can bring about the release of glutamate via reversed uptake

(Rossi et al, 2000). Prolonged massive excitation can promote toxic levels of

calcium influx: excitotoxicity (Olney, 1990). The brain was chilled to reduce

damage caused by these events, as these processes are temperature-dependent.

Ascorbic acid was added to the slicing solution to reduce oxidative stress in some

experiments (table 2.1).

Table 2.1 External solutions

Substance	Concentration (mM)	
	Slicing solution	Recording solution
NaCl	125	125
KCl	2.5	2.5
CaCl$_2$	2	2
MgCl$_2$	5	1
NaH$_2$PO$_4$	1.25	1.25
NaHCO$_3$	26	26
L-glucose	25	25
Ascorbic acid[1]	1	-
pH[2]	7.3	7.3
Osmolarity (mOsm)[3]	310	310

[1] Ascorbic acid not included in all experiments

[2] When bubbled with 95 % oxygen/ 5 % oxygen

[3] Osmolarity measured with vapour pressure osmometer

Table 2.2 Internal solutions

Substance	Concentration (mM)	
	Cs-methylsuphonate-based	CsCl-based
Cs-methylsuphonate	75	-
CsCl	50	140
Cs-HEPES	10	10
Cs-EGTA	10	10
NaCl	2	2
Mg-ATP	2	2
Chloride Nerst potential (mV)[1]	-24.2	1.6
Junction potential (mV)[1]	9	5
pH	7.3	7.3
Osmolarity (mOsm)[2]	290	290

[1] Calculated relative to recording solution

[2] Osmolarity measured with vapour pressure osmometer

The brain was removed to a second dish containing chilled slicing solution. This

dish had a silicone elastomer (Sylguard, Dow-Corning) base to provide a substrate

onto which the brain could be pinned. Once two pins, with one through each

cerebral hemisphere, had secured the brain, the meninges were carefully peeled

from the cerebellum with fine forceps under a dissecting microscope (6.3 times

gain; MZ 6, Leica). The hindbrain was then isolated from the forebrain by a single

dorso-ventral cut between the cerebellum and the cerebrum, through the midbrain.

The hindbrain was tilted onto the cut surface with the caudal spinal cord pointing

upwards so that the cerebellum could be sliced from the brainstem with a caudo-

rostral cut made through the cerebellar peducles. To isolate the vermis, the

cerebellum was cut in the sagittal plane through the two longitudinal furrows

between the vermis and the two cerebellar hemispheres. The vermis was mounted

onto the stage of a vibrating slicer (DTK-1000, D.S.K., Dosaka E.M. Co. Ltd.,

Japan) in the sagittal plane using cyanoacrylate glue and submerged in chilled

slicing solution, which was bubbled with 95% oxygen/ 5% carbon dioxide. Slices

of 200–250 μm thickness were cut and incubated in slicing solution at 31 °C for

45 minutes, then at room temperature (~24°C) for 0–4 hours before use.

2.2 Visual identification of cell types

Slices were placed in the recording chamber for viewing under an upright

microscope (BX 50 WI, Olympus) equipped with water immersion objective

lenses with magnifications of 20 (0.5 numeric aperture, N.A.) and 60 (0.9 N.A.),

while irrigated at a rate of 1–2 ml min^{-1} with recording solution (table 2.1), that

was heated to 34-39°C with a feedback-regulated Peltier device. The four layers of

the cerebellar cortex were clearly seen under low magnification, with bright field

illumination. The granular layer was visualised as a continuous cell-dense band

located between the outermost cell-sparse molecular layer and white matter, which

contains the cerebellum's efferent and afferent axons. Within the granular layer

individual granule cells were identified under high magnification with infrared

differential interference contrast microscopy (Stuart et al, 1993) using a CCD

camera (C3077, Hamamatsu) as numerous spherical to ovoid cell bodies of ~5-6

μm diameter (Palay and Chan-Palay, 1974). Large Golgi cells were distinguished

from granule cells by their larger somata (~10–20 μm diameter) and sparser

distribution within the granular layer (Palay and Chan-Palay, 1974).

2.3 Drugs

The recording solution (table 2.1) was supplemented, where appropriate, with

D(-)-2-amino-5-phosphonopentanoic acid (AP5, 10 μM), 7-chlorokynurenic acid

(20 μM), 2,3-dioxo-6-nitro-1,2,3,4-tetrahydrobenzo[f]quinoxaline-7-

sulphonamide disodium (NBQX, 2 μM), bicuculline methobromide (15 μM) and

strychnine hydrochloride (0.3 μM), to block conductances mediated by N-methyl-

D-aspartic acid (NMDA), non-NMDA, γ-aminobutyric acid type-A (GABA$_A$) and

glycine receptors. The drugs (±)-1-aminocyclopentane-trans-1,3-dicarboxylic acid

(ACPD, 20–100 μM), L(+)-2-amino-4-phosphonobutyric acid (L-AP4, 50 μM),

(S)-α-methyl-4-carboxyphenylglycine ((S)-MCPG, 1 mM) and (RS)-α-

cyclopropyl-4-phosphonophenylglycine (CPPG, 300 μM) were added to activate

and block mGluR receptors. Baclofen (50-100 μM) and CGP 35348 (500 μM)

were added to activate and block GABA$_B$ receptors, respectively. Spontaneous

miniature postsynaptic currents were recorded in 0.5 µM tetrodotoxin (TTX) to

block voltage-activated sodium channels. GABA uptake was blocked by NO711

(50 µM), which is not a substrate for uptake (Zeevalk & Nicklas, 1997).

Glutamate uptake was inhibited by L-trans-pyrrolidine-2,4-dicarboxylic acid

(PDC, 1 µM), which is a substrate for the transporter and therefore induces

glutamate release via heteroexchange (Volterra et al, 1996). TTX and strychnine

were bought from Sigma, Poole, UK. NO711 was bought from Sigma-RBI, Poole,

UK. CGP 35348 was the kind gift of Novartis Pharmaceuticals UK Ltd,

Camberley, UK. All other drugs were sourced from Tocris Cookson Ltd,

Avonmouth, UK.

2.4 Patch-clamp techniques for slice preparations

Patch-clamp recordings were made from visually identified granule and Golgi

cells, using an Axopatch 200B (Axon Instruments, Inc, Foster City, CA).

Recordings were made using whole-cell voltage clamp as well as cell-attached

current and voltage clamp configurations (Hamill et al 1981). Patch

microelectrodes were manufactured from standard wall borosilicate capillaries

(1.5 mm outside diameter × 0.86 mm inside diameter; GC150F-7.5, Harvard

Apparatus Ltd, Edenbridge, UK) using either a two-stage vertical puller (PC-10,

Narashigi) or a multistage horizontal puller (P-97, Sutter). The recording pipettes

were filled with a caesium-based recording solution (table 2.2), to impose an open

channel block of potassium channels at negative potentials (Hille, 1992). No

correction was made for the liquid junction potentials between the internal and
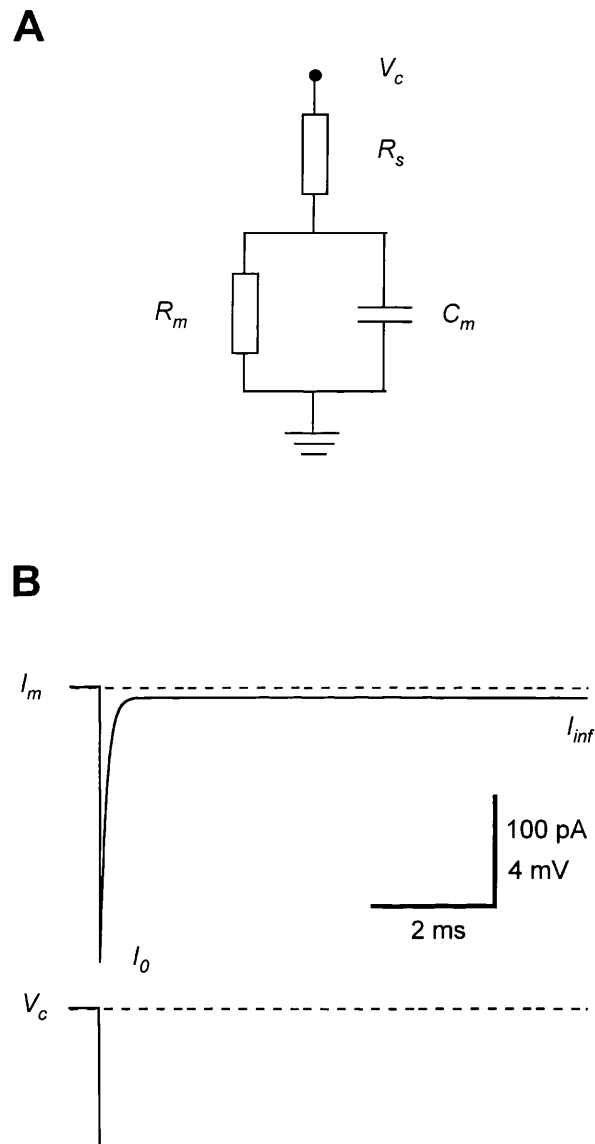
Figure 2.2 – Whole-cell parameter analysis. **A**, Circuit diagram for single compartment neurone with whole-cell patch pipette. Command potential (V_c) is applied through a series resistance (R_s) to the cell, which is represented as a membrane resistance (R_m) and a membrane capacitance (C_m) in parallel. **B**, *Bottom trace*, Step pulse of -5 mV. *Top trace*, Current response of a neurone with the properties: R_m = 500 MΩ; R_s = 10 MΩ; C_m = 3.1 pF.

external solutions (table 2.2). A square voltage-clamp pulse of -10 mV was

applying to assess the resistance of the microelectrodes in recording solution. The

resistance of the electrode was calculated by dividing the applied voltage by the

induced steady-state current response according to Ohm's Law ($V_c = I_p \cdot R_p$; where

V_c is the command potential in Volts, I_p is the pipette current in amps and R_p is the

pipette resistance in Ω). In the presented work this was found to be 4—10 MΩ.

Cells in the brain slice are surrounded by debris and other cells, which impairs

seal formation between the patch pipette and the cell. Therefore to aid patching,

the cell of interest was mechanically cleared of debris by applying positive

pressure (60—150 kPa) to the microelectrode. The pressure was then dropped to

~50 kPa and the microelectrode lowered onto the cell. Once the pipette was on the

cell, as indicated by a the appearance of a 'halo' of refracted light on the

membrane surrounding the pipette, the pressure was reversed to -10— -50 kPa,

and held until a seal was formed between the microelectrode and cell. When the

gigaohm seal (Hamill, et al, 1981) was achieved, 30 s was allowed for the contents

of the pipette reach equilibrium. A sharp pulse of negative pressure was applied to

rupture the patch, providing low resistance access to the cell.

2.5 Whole cell parameters

The circuit between a patch electrode and a cell can be modelled using an

electrical circuit (figure 2.2A). The cell is represented by a resistance (R_m) and

capacitance (C_m) in parallel. V_c is injected into the cell through a series resistance

(R_s), which is primarily set by the electrode-cell interface. The R_s can have a

profound effect on the quality of recordings achieved with patch-clamp as the

membrane voltage is measured at the same time as injecting current to maintain

the holding potential with the patch electrode. This creates a voltage drop at the

pipette tip, which is equal to the current injected times the series resistance

(Ohm's law). This voltage drop will induce a voltage error in the clamped

membrane potential, which will be equal to the command potential minus the

voltage drop. A second problem relates to the fact that the cell has a capacitance

(C_m). When you pass current into (or measure current from) the membrane

through a series resistance (the pipette) the signal will be low-pass filtered by this

RC circuit. The R_s was therefore monitored throughout the experiment to ensure

that it remained constant (< 25 % change throughout).

The parameters R_s, C_m as well as the input resistance of the cell (R_m) were derived

from the current response (referred to as capacitance transient in text) to a square

voltage-clamp hyperpolarising pulse (V_c = -5 mV), as shown in figure 2.2**B**. The

current response, $I_m(t)$, is made up of an initial rapidly rising and decaying

component followed by a steady-state component, which represent the

capacitative and resistive elements of the cell membrane (figure 2.2**B**). The time

course can be estimated by the following equation (Tessier-Lavigne et al, 1988),

$$I_m(t) = \frac{V_c}{R_m + R_s} \cdot \left(1 + \frac{R_m \cdot e^{-t/\tau}}{R_s} \right),$$ (2.1)

where,

$$\tau = C_m \cdot \left(\frac{R_m \cdot R_s}{R_m + R_s} \right).$$ (2.2)

At $t = 0$, equation 2.1 reduces to,

$$I_m(0) = \frac{V_c}{R_s},$$
(2.3)

thereby allowing the R_s to calculated. Obtaining an accurate measurement of $I_m(0)$

for this calculation is hampered by filtering of the instantaneous current by the

cell-pipette-amplifier circuit. A practical solution to this was to fit the current

waveform decay with an exponential function and extrapolated the resulting fit to

$t = 0$. The granule cell capacitance transient exhibited a decay that had two kinetic

components. The fast component (~80 µs; ~95 % of fit) was due to the fast

response of the small cell body, whereas the slower kinetic component (~800 µs)

was probably due to stray capacitance from the electrode and/or the cell's axon

(Silver et al, 1996a). Another source of measurement error is that the records were

filtered at 5 kHz, which will force a slower estimation of the kinetics of the

granule cell capacitance transient. The fitted R_s was 16 ± 4 MΩ (n = 15). At $t = \infty$,

equation 2.1 reduces to,

$$I_m(\infty) = \frac{V_c}{R_m + R_s}.$$
(2.4)

The current value obtained 8 ms after application of the hyperpolarising step was

taken to be the steady-state current as this was at ~100-times the fast and ~10-

times the slow time constant, of the typical granule cell. This enables the input

resistance to be calculated using equation 2.4 and the previously calculated R_s. In

the present thesis the mean input resistance was calculated as 2.4 ± 0.6 GΩ (n =

15), which is high due to the inclusion of Cs^+ in the patch pipette (table 2.2).

Finally, the C_m was calculated using the time constant derived from the fit and

equation 2.2. The mean C_m was 6.4 ± 0.5 pF (n = 15). This value is double that

expected (~3 pF, Silver et al, 1992) due to pipette capacitance, the contribution of

axon capacitance and filtering as discussed above for the apparent time constant

Golgi cell and mossy fibre axons were stimulated at 0.1–100 Hz (5—80 V; 40—

100 µs) using patch pipettes filled with recording solution and driven by isolated

constant-voltage devices (DS2, Digitimer). Single fibres were identified on the

basis of an all-or-none presence of a granule cell postsynaptic current (PSC),

elicited by stimuli of graded intensity and the presence of an event with one

temporally distinct component. The stimulation voltage was set 5–10 V above

threshold to ensure reliable fibre stimulation (Silver et al, 1996a).

2.6 Data analysis

For all recordings, data were acquired for analysis using Axograph 4 software

(courtesy of John Clements). Data were digitised online by an Instrutech ITC-18

interface at 10–25 kHz after low-pass filtering at 2–5 kHz (2-pole Bessel filter,

Axon Instruments). Data were analysed both online and offline by Axograph 4,

and offline with Igor Pro 3.1 (Wavemetrics, Lake Oswego, Oregon), at times

utilising custom written procedures in both packages.

PSCs were aligned on their stimulus artefact and the baseline holding current was

measured from a 0.2 – 0.6 ms region before the stimulus artefact and subtracted

from the records before analysis of the PSCs. For each cell the events were

averaged across trials to allow the mean peak position in time to be established. A

measurement window of 0.2 – 0.6 ms was centred at this peak. For each event, the

mean current within the measurement window was recorded as the peak PSC.

Background current fluctuations were estimated in the same manner with the two

measurement regions shifted into the pre-event baseline. For coefficient of

variation (CV) and variance analysis the background variance was subtracted from

the measurements at the event position (Silver et al, 1998). The stability of

synaptic current amplitude over time was assessed using Spearman rank order

correlation analysis implemented in Igor. Epochs that were stable to the 5 % level

were regarded as steady state. Spontaneous PSCs were detected with the scaling

template detection method implemented in Axograph (Clements and Beckers,

1997).

The kinetics of the PSCs were obtained by first aligning and averaging the

individual currents as described in the previous section. The rise time was

quantified as the time to pass from 10 to 90 % of peak current, relative to baseline.

This rise time (t_r) was estimated by a single exponential function with a time

constant τ_r according to,

$$\tau_r = \frac{t_r}{0.3321 \cdot 2\pi}.$$
(2.5)

To ascertain the decay kinetics the PSC was fit from the 10-20 % decay time point

with a two component exponential function. To ensure the reliable estimation of

the relative amplitude of the two components, $t = 0$ was set at the time of peak

PSC. Means were expressed ± standard errors. Groups of data were tested for

differences using a paired Student's $t$test, unless stated otherwise.

Figure 2.3 – Simple binomial model of transmitter release. **A**, Central synapse represented as presynaptic neurone with $n = 4$ active zones, each made up of a single independent release site and a postsynaptic density. **B**, Variance-mean amplitude plots for a synapse with different release sites (n) and quantal sizes (q; in pA). **C**, CV-mean amplitude plots for same synapse.

A

Presynaptic terminal

Postsynaptic cell
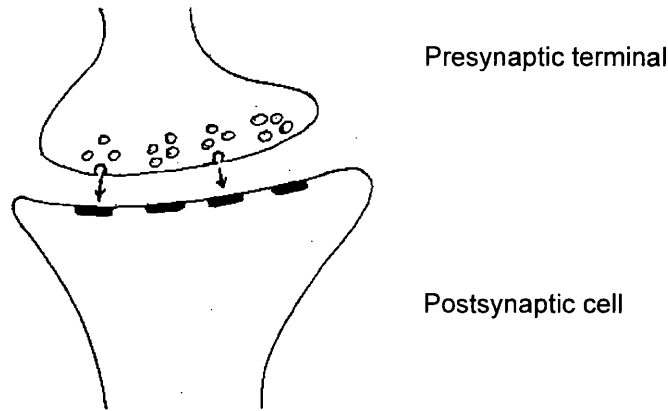
B
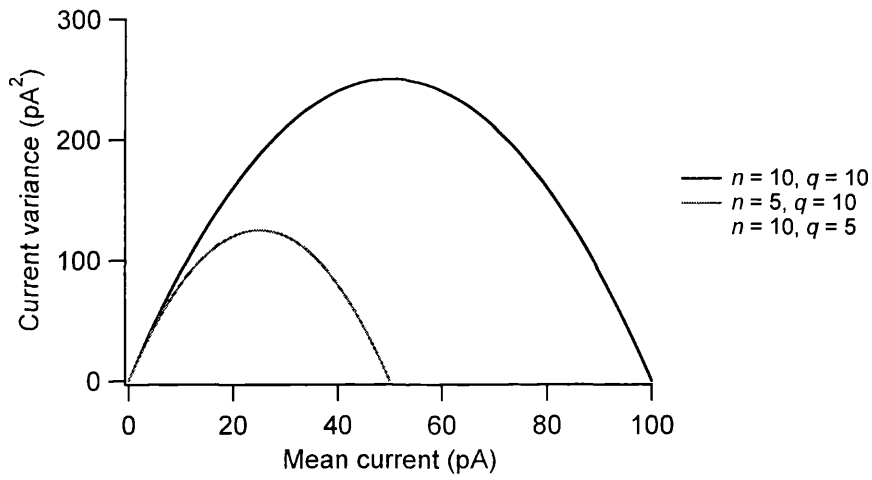
C
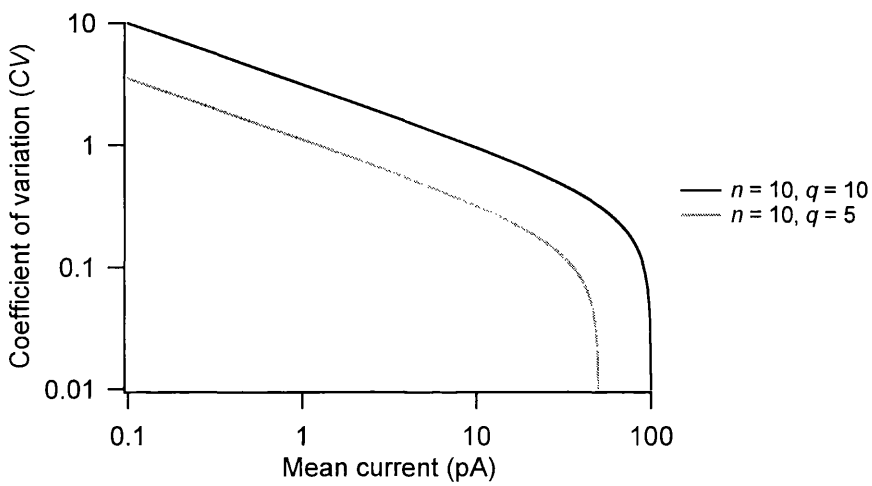
2.7 Binomial model of transmitter release

The simplest expression of quantal neurotransmission describes the release of packets (quanta) of transmitter from a number of independent release sites (n, figure 2.3**A**). Each release site releases a quantum of transmitter in an all-or-none manner with a finite mean probability (p_r) that is controlled by calcium influx during a presynaptic action potential. The weighted mean response of the postsynaptic cell to each quantum is defined as the parameter q (figure 2.3**A**). The size of the synaptic response is equal to $n \cdot p_r \cdot q$.

A key question in synaptic physiology is whether a modulation of synaptic efficacy is expressed as a change in n, p_r or q. We can use the binomial model for release to address these questions (Silver et al, 1998; Reid and Clements, 1999; Clements and Silver, 2000). To do this we need to express the model in terms of parameters we can measure: that is, mean postsynaptic current (μ). The mean PSC is given by,

$$\mu = n \cdot p_r \cdot q. \tag{2.6}$$

The standard deviation of the PSC, σ^2, is given by,

$$\sigma^2 = n \cdot p_r \cdot (1 - p_r) \cdot q^2. \tag{2.7}$$

Substituting for p_r and rearranging we finally get,

$$\sigma^2 = q \cdot \mu - \frac{\mu^2}{n}. \tag{2.8}$$

Using measured data, mean current-variance plots can be constructed under different release probability conditions and fit with equation 2.8 to derive n and q. When p_r is small (<0.3), equation 2.8 is well described by the linear relationship,

$$\sigma^2 = q \cdot \mu,$$ (2.9)

which allows q to be determined simply by measuring the slope of the mean

current-variance plot (Silver et al, 1998; Reid and Clements, 1999).

If a change in synaptic efficacy is caused by a postsynaptic modification (q) the

initial slope of the current-variance plot will change (figure 2.3**B**). However, if a

presynaptic change has occurred, q will not change and the modulated mean

current-variance plot will overlay the control, if only p_r has been affected. If n has

been modulated, the initial slope will remain unchanged and $n \cdot q$ will be modified

(figure 2.3**B**). This multiple probability fluctuation analysis (MPFA) (Silver et al,

1998) or variance-mean analysis (Reid and Clements, 1999) is related to a method

by Sigworth (1980) for the analysis of single channel parameters from

macroscopic current data.

Changes in the statistics of release can also be inferred from a movement in the

CV. The CV of release can be calculated by,

$$CV = \frac{\sigma}{\mu}.$$ (2.10)

Raising this to the power of 2, substituting for σ^2 according to equation 2.8 then

rearranging we get,

$$CV = \frac{q}{\mu} - \frac{1}{n}.$$ (2.11)

This relationship is shown in figure 2.3**C** that shows the CV as a function of μ.

If we substitute for μ according to equation 2.6 we get the following expression,

$$CV = \sqrt{\frac{1-p_r}{n \cdot p_r}} .$$

(2.12)

Equation 2.12 shows that the CV is insensitive to changes in q and can therefore

be used to monitor presynaptic modifications independently of postsynaptic.

Therefore, if q is constant, a change in CV indicates a change in release properties.

Furthermore, inspection of equation 2.12 and figure 2.3C reveals that under these

conditions, an increase in CV indicates that p_r has decreased, and vice versa.

Another property of the binomial model is that we can infer information about the

mechanism underlying modulation from release failure analysis. If a nerve is

stimulated N times, the number of times zero quanta will be released

simultaneously (N_0) is,

$$N_o = P_n(0) \cdot N,$$

(2.13)

where

$$P_n(0) = (1 - p_r)^n$$

(2.14)

according to the binomial distribution for zero quanta.

Rearranging and substituting for $P_n(0)$ we get,

$$\frac{N_0}{N} = (1 - p_r)^n .$$

(2.15)

In this thesis N_0 was computed as the number of failures of transmission as

defined as an event that was less that 2 times the standard deviation of the

background noise. The ratio of N_0 to N was referred to as P_f in the text.

CHAPTER THREE

GLUTAMATE SPILLOVER SUPPRESSES INHIBITION BY ACTIVATING PRESYNAPTIC MGLURS

3.0 Abstract

Metabotropic glutamate receptors (mGluRs) found on synaptic terminals

throughout the brain are thought to be important in modulating transmitter release,

neuronal excitability and may have a role in short- and long-lasting synaptic

plasticity. Activation of mGluRs by synaptically released glutamate depresses

glutamate release from excitatory terminals but the physiological activation of

mGluRs on inhibitory terminals has not been demonstrated. I have investigated

activation of mGluRs on inhibitory terminals within the cerebellar glomerulus, a

structure in which GABA-releasing inhibitory terminals and glutamatergic

excitatory terminals are in close apposition and make axo-dendritic synapses onto

granule cells. Here I show that 'spillover' of glutamate, which is released from

excitatory mossy fibres, inhibits GABA release from Golgi cell terminals by

activating presynaptic mGluRs under physiological conditions. The magnitude of

the depression of the inhibitory postsynaptic current is dependent on the frequency

of mossy fibre stimulation, reaching ~50% at 100 Hz. Furthermore, the duration of

inhibitory postsynaptic current depression mirrors the time course of mossy fibre

activity. These results establish that mGluRs on inhibitory interneurone axons

sense the activity of neighbouring excitatory synapses. This heterosynaptic

mechanism is likely to boost the efficacy of active excitatory fibres by locally

reducing the level of inhibition.

Figure 3.1 - Activation of presynaptic mGluRs depresses IPSCs in

granule cells. **A, B**, Average IPSCs evoked by Golgi axon stimulation

at 0.2 Hz in control solution and 100 μM ACPD (**A**) or 50 μM AP4

(**B**). **C**, Pooled results (n = 4) showing effect of 20 μM trans-ACPD and

its block by the antagonists (Ant) MCPG (1 mM) and CPPG (300 μM).

D, Steady-state frequency response normalised to 1 Hz value of control

evoked IPSCs (*filled circles*) and in 100 μM ACPD (*open circles*; n =

7; 20 Hz and 50 Hz, n = 6). **E**, Variance-mean relationship of IPSCs

recorded at 5 Hz with different external Ca^{2+}/ Mg^{2+} (*filled symbols*). A

parabolic fit gave a weighted mean quantal size of 357 pS for this cell.

This remained unchanged during 100 μM ACPD application (*open*

symbol).

A

ACPD

Control

40 pA

5 ms

B

AP4

Control

40 pA

5 ms

C

D

E
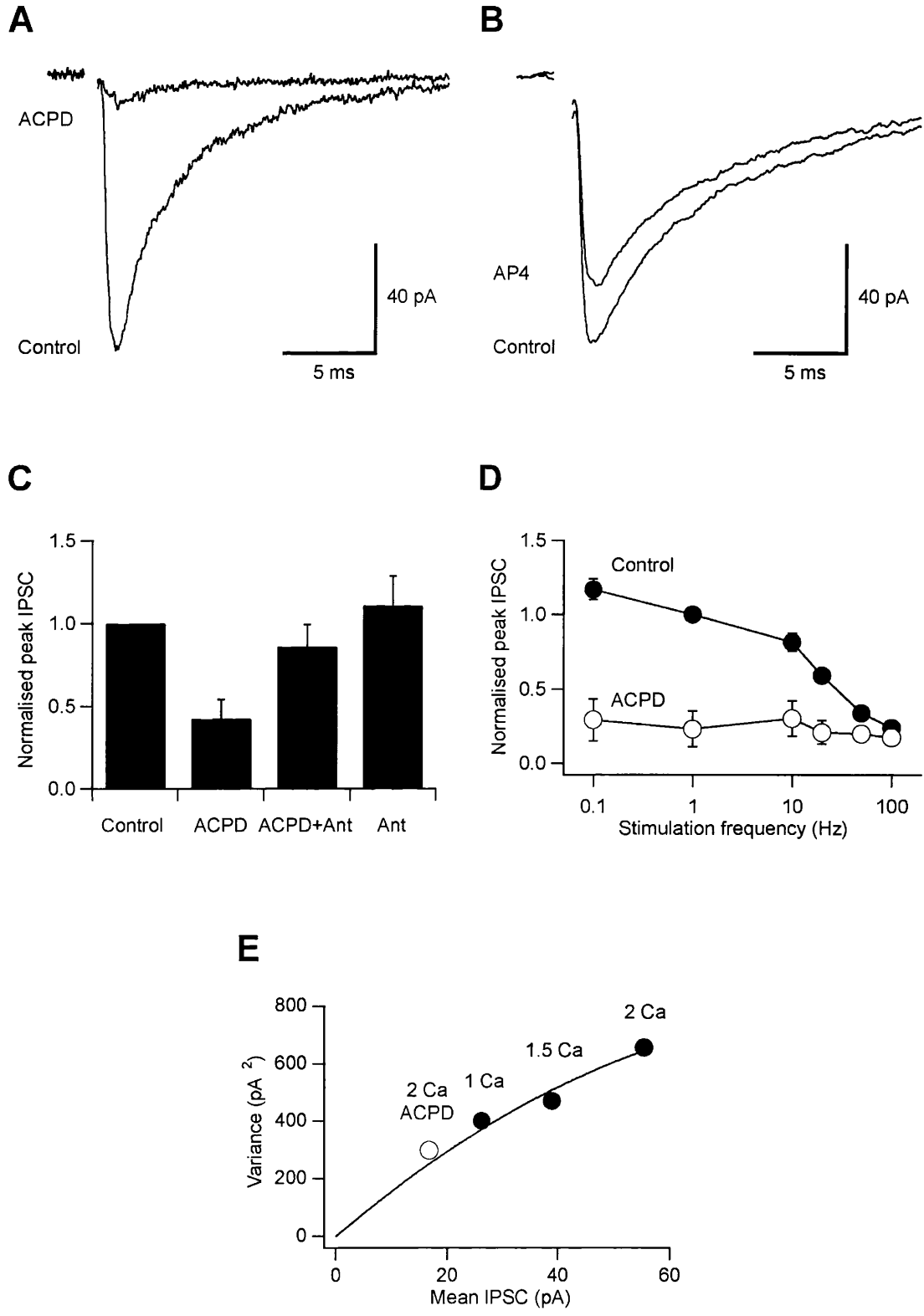
3.1 Evoked IPSCs in granule cells

Whole-cell patch clamp recordings of inhibitory postsynaptic currents (IPSCs)

were made from visually identified granule cells at 37 °C. The currents were

evoked by minimal stimulation of single Golgi cell axons in the presence of

ionotropic glutamate and glycine receptor antagonists (figure 3.1**A**, control). In 7

cells detailed analysis of the kinetics and mean amplitude of the conductance

underlying the IPSC was performed. Individual IPSCs were aligned on their

stimulus artefact and the mean was calculated. The 10-90 % rise time was

measured as 0.60 ± 0.13 ms (figure 3.1). The rising phase of the IPSC was

modelled in chapter 5 as an exponential expression. The measured 10-90 % rise

time was approximated by a single exponential rise with a time constant of 0.29 ±

0.06 ms. The mean conductance IPSC was measured as 3100 ± 680 pS at a

holding potential and driving force of –70 mV. The decay phase was fit with a

dual component exponential function with time constants of 4.1 ± 0.4 ms and 22.5

± 3.4 ms. The fast component of the decay made up 40.5 ± 13.0 % of the

exponential fit amplitude at the peak of the waveform.

3.2 Pharmacological activation of mGluRs depresses evoked GABA release

3.2.1 Activation of mGluRs with ACPD and AP4 depress IPSC
Immunohistochemical (Baude et al, 1993; Ohishi et al, 1994; Neki et al, 1996;

Jaarsma et al, 1998) and electrophysiological studies (Knoflach and Kemp,1998;

Vetter et al, 1999) have shown that mGluRs 1/5 and 2/3 (groups I and II) are

present on cerebellar Golgi cell somal-dendritic compartment, and that group II

mGluRs are on the axon terminal (Ohishi et al, 1994). Therefore, the possibility

that these mGluRs are functional and that activation of these receptors might

regulate the Golgi to granule cell synapse was investigated. Bath application of the

group I/ II receptor agonist trans-ACPD (Conn and Pin, 1997) at 100 μM

reversibly depressed the mean IPSC by 75 ± 5 % ($n = 6$; $P < 0.001$; figure 3.1**A**),

at a stimulation frequency of 0.2 Hz. In a separate set of experiments the selective

group III receptor agonist, AP4 (Conn and Pin, 1997; 50 μM) was found to also

depress the mean IPSC albeit by a lesser degree (0.2 Hz; 27 ± 6 %; $n = 3$; $p =$

0.05; figure 3.1**B**). To block the activation of these mGluRs, the broad-spectrum

combination of antagonists, 1 mM (S)-MCPG (group I/ II selective) and 300 μM

CPPG (group II/ III selective), was used. Bath application of these mGluR

blockers reduced IPSC depression, induced by 20 μM ACPD application, from 57

± 18 % ($n = 4$; $p = 0.05$) to 14 ± 27 % ($P > 0.3$; figure 3.1**C**). confirming that the

depression was mediated via mGluR receptors. These results establish that a

heterogeneous population of mGluRs are present and functional at the Golgi to

granule cell synapse and activation of these receptors can depress the IPSC.

3.2.2 ACPD removes frequency dependence of release

Golgi cells can fire at >100 Hz *in vivo* (van Kan et al, 1993). Therefore, any

investigation of the modulation of the Golgi to granule cell synapse should assess

the regulation of synaptic efficacy over a wide range of transmission frequencies.

First, presynaptic depression was characterised over a physiological range of Golgi

cell axon stimulation frequencies (0.1-100 Hz). Under control conditions, the

synapse exhibited frequency-dependent depression, with the steady-state mean

IPSC amplitude decreasing with increasing stimulus frequency (figure 3.1**D**). The

ratio of peak IPSC amplitudes at 100 to 1 Hz was 0.24 ± 0.04 ($n = 7$). The effects

of mGluR activation were examined on IPSCs evoked at 0.1 to 100 Hz. ACPD

(100 µM) depressed the mean steady-state current at 0.1 to 50 Hz ($n = 7$; $p < 0.01$)

but not at 100 Hz (figure 3.1**D**; $n = 7$; $P > 0.3$). Furthermore, ACPD removed the

frequency-dependence of the IPSC amplitude as this relationship in the agonist

had a shallower slope than control, with the 100 to 1 Hz ratio equal to 1.08 ± 0.19

($n = 7$; $P < 0.01$). These results show that ACPD-induced depression of the Golgi

to granule cell synapse is frequency dependent, and the frequency dependence of

the mean IPSC was removed by ACPD.

3.2.3 IPSC depression is mediated by presynaptic mGluRs

Synaptic currents can be modulated by activation of receptors present on the pre-

or postsynaptic membrane. I therefore sought to establish the locus of effect of

ACPD. To determine whether ACPD had postsynaptic effects under my

experimental conditions (caesium based internal solution) the whole cell

conductance was monitored during the application of the mGluR agonist. The

control input resistance was unaffected by the application of 100 µM ACPD ($1.9 \pm$

0.2 vs. 1.9 ± 0.4 MΩ; $n = 5$; $p = 0.85$), indicating ACPD depresses the IPSC by a

mechanism independent of postsynaptic input resistance modulation.

To quantify the presynaptic action of mGluR activation, the trial-to-trial

fluctuations in IPSC amplitude were analysed using a binomial model of release.

Coefficient of variation (CV; standard deviation (SD) / mean) analysis revealed

that ACPD-mediated depression in IPSC amplitude was associated with an

increase in the CV (221 ± 59 % of control; $n = 4$; $P < 0.02$). This point was

quantified further with the use of multiple-probability fluctuation analysis (MPFA;

Silver et al, 1998; Clements and Silver, 2000) as outlined in the methods. Briefly,

IPSCs were evoked at 5 Hz under different release conditions, induced by

changing the ratio of calcium and magnesium concentration in the external

solution (changes release probability) or by applying 20 μM ACPD to the bath.

Measurements of the mean and variance (SD^2) of the peak IPSC amplitude were

derived from stable epochs. The variance was then plotted against its mean for

each calcium/ magnesium ratio (figure 3.1**E**). This near-linear relationship was

then fit with a simple binomial model to derive the quantal size for the synapse.

This quantal size was not different from that derived from the slope between the

ACPD-induced variance-mean relationship and the origin (99 ± 9%; $n = 3$; $p =$

0.9; figure 3.1**E**). These results suggest that ACPD-induced depression of the

Golgi to granule cell IPSC is mediated by a reduction in the release probability of

GABA.

The effect of AP4 on release parameters was also evaluated with a binomial

release model. CV analysis revealed that AP4-mediated depression of IPSC

amplitude was associated with an increase in the CV (127 ± 5 % of control; $n = 3$;

$P < 0.03$). As with the ACPD data, these results suggest that a component of AP4-

induced depression of the Golgi to granule cell IPSC was mediated by a reduction

in the release probability of GABA.
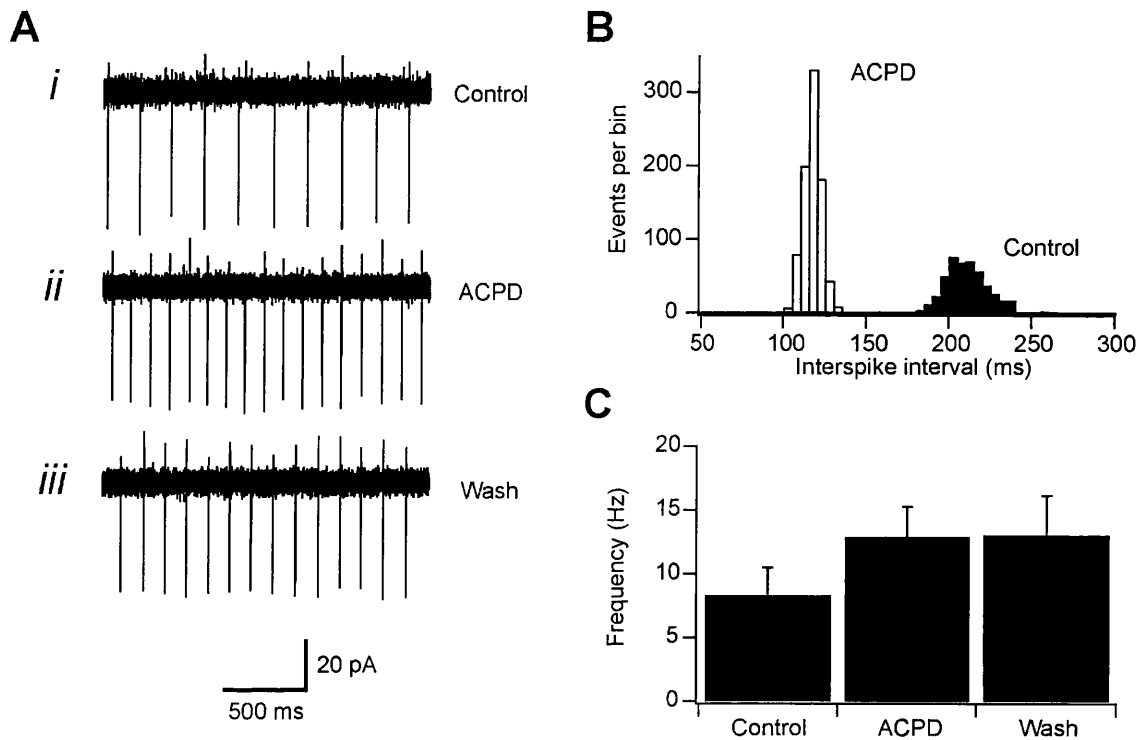
Figure 3.2 – Activation of mGluRs increases Golgi cell spontaneous firing rate. **A**, Cell-attached current recordings from Golgi cells: *i*, under control conditions; *ii*, during application of 100 μM ACPD and *iii*, after 10 minutes ACPD washout. **B**, Amplitude histogram showing distributions of interspike intervals under control and ACPD conditions. **C**, Histogram of mean firing rate in control, during ACPD application and in wash (*n* = 8).

3.2.4 ACPD increases the firing rate of Golgi cells

During the above experiments it was noticed that the rate of spontaneous IPSCs in granule cells increased upon application of ACPD. The possibility that this effect of ACPD was induced by an increase in Golgi cell firing rate was investigated by making cell-attached recordings from Golgi cells. The firing rate in control solution of 8 ± 2 Hz ($n = 8$) increased to 13 ± 2 Hz ($n = 8$; $p = 0.003$) upon bath application of 100 μM ACPD (figures 3.2). This suggests that activation of mGluRs on Golgi cells may reduce the IPSC amplitude indirectly by increasing firing rate; an indirect mechanism of depression.

The impact of indirect inhibition was quantified using information derived from the above sets of experiments. The basic pharmacological data revealed that the IPSC was depressed by 75% by 100 μM ACPD (at 0.2 Hz stimulation frequency, which was assumed to be superimposed onto the spontaneous firing rate of 8 Hz). As described above, application of ACPD increased the firing rate of Golgi cells by 5 Hz. The amount of depression one would expect to arise from the shift from 0.2 Hz to 5.2 Hz can be derived from log-linear interpolation of the frequency-IPSC relationship (figure 3.1**D**), which is 22 %. Therefore, if the evoked firing rate is linearly superimposed onto the spontaneous firing rate, direct inhibition of the IPSC accounts for around 70 % ($100 \times [1-(22 / 75)]$ %) of the total inhibition induced by 100 μM ACPD.
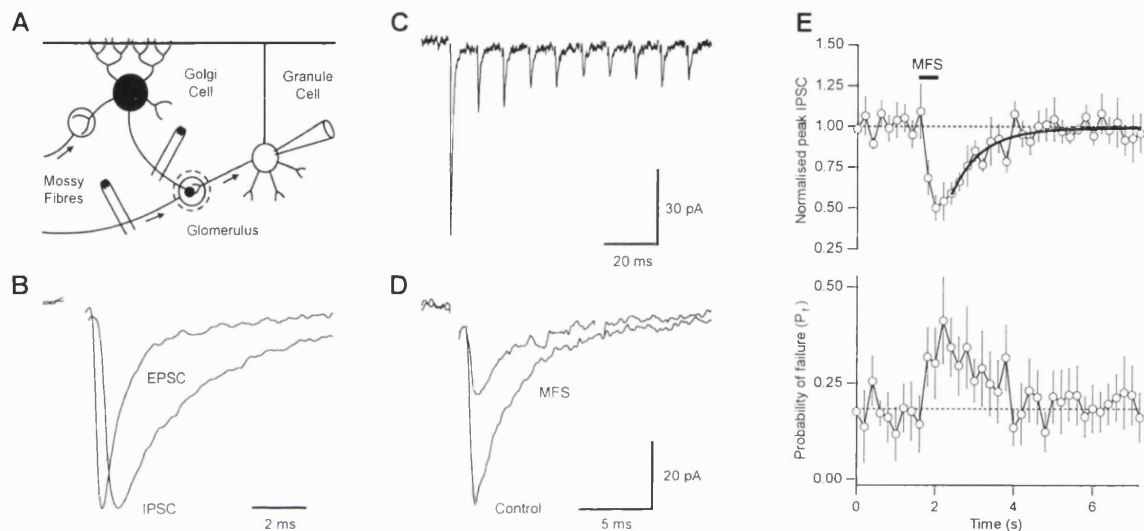
Figure 3.3 - Mossy fibre stimulation depresses GABA release from Golgi cells in the absence of fast excitatory transmission. **A**, Recording configuration. Whole-cell patch-clamped granule cell and independent stimulation of inhibitory and excitatory inputs. **B**, Normalised EPSC and IPSC exhibit different kinetics. **C**, Averaged non-NMDA EPSCs depress rapidly at 100 Hz. **D**, Average IPSC waveforms from control period and during mossy fibre stimulation (MFS). **E**, *Top panel*, normalised IPSC amplitude during 5-Hz Golgi cell stimulation in ionotropic glutamate receptor antagonists. *Bar* indicates timing of 0.5 s burst of 100-Hz MFS. *Bold line* shows single exponential function fit to IPSC recovery ($\tau = 770$ ms). *Bottom panel*, probability of failure increases during IPSC depression.

3.3 Physiological activation of mGluRs on Golgi cells depresses IPSC

So far I have presented pharmacological data that suggests that mGluRs are

present and functional on Golgi cells, and that these receptors mediated inhibition

of GABA release. The source of the mGluRs' endogenous ligand, glutamate, is

likely to be the mossy fibre terminal, the only excitatory terminal in the

glomerulus (figure 3.3**A**). This possibility was investigated by determining if

glutamate released from a mossy fibre could depress the Golgi to granule cell

IPSC amplitude.

3.3.1 Physiological activation of mGluRs by brief mossy fibre stimulation

A single Golgi cell input to a granule cell was established using minimal

stimulation. This was based on the all-or-none presence of a $GABA_A$-mediated

IPSC in the granule cell. A mossy fibre input that could be stimulated

independently of the Golgi cell was then established onto the same granule cell. It

was possible to discriminate between excitatory and inhibitory inputs on the basis

of different PSC kinetics (Figure 3.3**B**). Furthermore, I used an intracellular

solution that allowed EPSCs and IPSCs to be distinguished by their reversal

potentials of 0 and −24 mV, respectively. Once an excitatory and inhibitory input

had been established, their identity was confirmed by the application of the

antagonists NBQX, AP5 and 7-chlorokynurenic acid, which blocked the fast

EPSC evoked by mossy fibre stimulation but not the Golgi cell IPSC.

To give adequate characterisation of the time course of depression, the Golgi cell

was stimulated at 5 Hz. After 10 s, when the IPSC had reached a stable amplitude

level, the mossy fibre was stimulated with a 100 Hz train for 0.5 seconds. In the

absence of ionotropic glutamate receptor antagonists, the evoked non-NMDA

EPSC during this train depresses on a tens of milliseconds timescale (figure 3.3**C**).

This protocol was repeated 10-20 times, with the peak IPSCs recorded and

averaged across trials. When the mossy fibre was stimulated, the IPSC depressed

16 of 33 cells (48 %). In responding cells, IPSC depression was present in all

repetitions, although occasionally IPSC rundown was observed throughout the

experiment. Figure 3.3**E** shows the average time course of depression of the IPSC

peak amplitude. The maximal mean depression of 50 ± 7 % ($n = 6$; $p = 0.001$) was

achieved at 400 ms after the onset of mossy fibre stimulation (figures 3.3**D**, **E**),

which is an order of magnitude slower that the depression of the evoked EPSC

during the train (figure 3**C**). The peak IPSC recovered from depression with a time

course that was well approximated by a single exponential with a time constant of

770 ms (figure 3.3**E**). These results suggest the IPSC amplitude is dependent on

the activity of the mossy fibre.

The conditional probabilities for establishing the Golgi cell input following the

mossy fibre input and the recording lasting long enough to test for synaptic

activation of presynaptic receptors was quantified for the experiments carried out

to generate figure 3.3. In the 62 granule cells in which I could establish a stable

mossy fibre input for this experiment, the probability of finding a stable,

independent Golgi cell input was 0.484. Of these 30 cells the probability of the

recording lasting long enough to perform the test protocol was 0.333. Of these 10

cells, only 6 exhibited IPSC depression following mossy fibre stimulation,

Figure 3.4 - Metabotrophic glutamate receptors mediate MFS-induced IPSC depression. **A**, 100-Hz MFS (timing indicated by *ticks*) at 0 mV and -80 mV without glutamate receptor blockers. The lack of evoked IPSCs, which had a reversal potential of -24 mV, shows that MFS evoked no inhibitory input. **B**, Simultaneous 5-Hz Golgi cell stimulation (GoS) and 100-Hz MFS in ionotropic glutamate receptor blockers. The IPSC depresses during the 0.5-s MFS, whereas no currents were associated with the MFS (small currents throughout are averaged spontaneous IPSCs). **C**, Stimulus-averaged currents. GoS indicates IPSC at 5 Hz and MFS shows that IPSCs were not evoked during 100-Hz MFS. *Dashed line* shows, for comparison, 100-Hz GoS for 0.5 s. **D**, Averaged IPSCs before, during and after 100-Hz MFS for control and in the presence of mGluR antagonists MCPG (1 mM) and CPPG (300 µM).

A

MFS

0 mV

-80 mV

20 pA

100 ms

B

MFS

GoS

-80 mV

20 pA

100 ms

C

MFS

GoS

20 pA

2 ms

D

MFS

Control

Antagonist

20 pA

5 ms
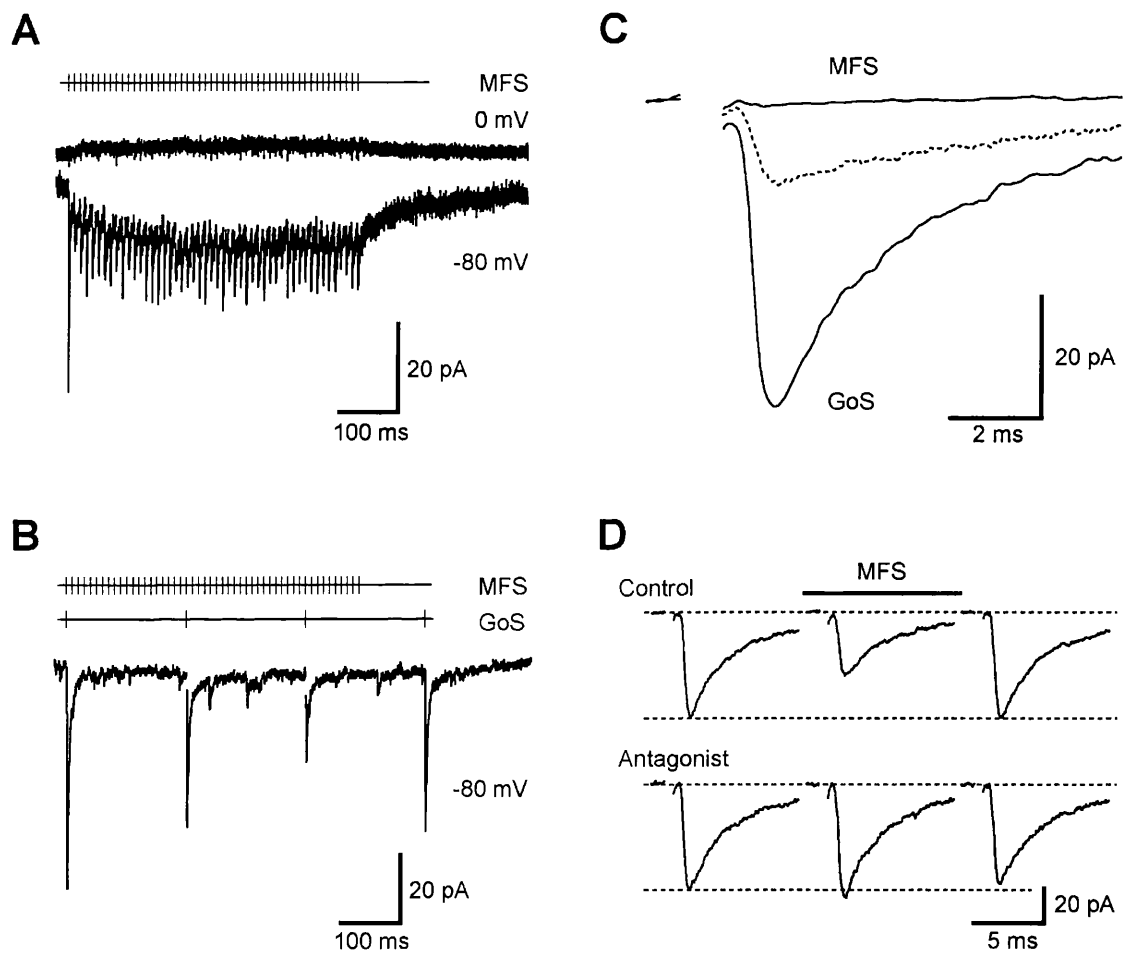
possibly due to the inputs innervating different dendrites of the granule cell (see

discussion of this chapter). Therefore, conditional probability of demonstrating

mossy fibre stimulation-dependent IPSC depression, following the stable

recruitment of a mossy fibre input was 0.097.

3.3.2 Mossy fibre activity activates mGluRs on Golgi cell

To investigate the locus of mossy fibre-mediated depression of inhibition, the

probability of failure for GABA release upon stimulation (P_f) and the CV of the

IPSC were calculated at each time series point. P_f was observed to increase

substantially, concomitant with the depression of the mean IPSC amplitude (figure

3.3**E**; 0.18 ± 0.06 to 0.34 ± 0.07; n = 6; p = 0.03). Also, the CV increased with

IPSC inhibition (not shown), similar to observations during pharmacological

activation of mGluRs. These data suggest that stimulation of the mossy fibre

reduced in the release probability of GABA from Golgi cell axon terminals.

One possible mechanism for IPSC depression is direct stimulation of the Golgi

cell by high-frequency mossy fibre activity, inducing frequency-dependent

depression as shown in figure 1. It was therefore crucial to demonstrate that the

mossy fibre electrode did not recruit IPSCs during the high frequency train.

Analysis of the whole-cell recordings during mossy fibre stimulation period

revealed that IPSCs were only evoked when the Golgi cell axon was stimulated

and not while the mossy fibre was stimulated in isolation (figures 3.4**A**, **B**). If an

IPSC was recruited at 100 Hz its amplitude would be small due to frequency-

dependent depression (figure 3.1**D**). To ensure that it was possible to detect such

an IPSC, a Golgi cell that innervated a different granule cell was stimulated at 100

Hz for 0.5 s. The normalised average IPSC was larger than the mossy fibre

induced response, but smaller than the lower frequency Golgi cell response, as

expected (figure 3.4**C**; middle trace), suggesting that no IPSCs were evoked by

mossy fibre stimulation.

The involvement of presynaptic mGluR receptors in mossy fibre-induced

depression of GABA release was tested directly using the mGluR antagonists (S)-

MCPG (1 mM) and CPPG (300 μM). This was done by confirming that the IPSC

amplitude could be depressed by mossy fibre stimulation, then repeating the

protocol on the same cell in the presence of mGluR antagonists. For each half of

the experiment the protocol was repeated only 5-10 times, to minimise the

possibility of rundown of the mGluR response. Mossy fibre-induced depression

was completely blocked by the mGluR antagonists (106 ± 8 % of control; $n = 4$; p

$= 0.77$; figure 3.4**D**). These results show that glutamate released from mossy

fibres can inhibit GABA release via activation of mGluRs on Golgi cell axons.
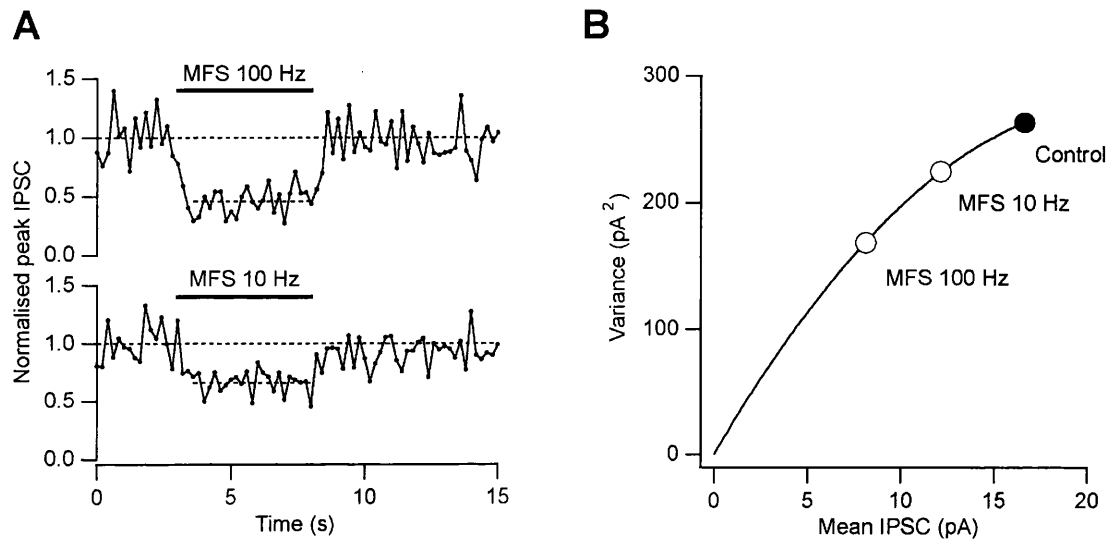
Figure 3.5 - IPSC depression depends on duration and frequency of

MFS. **A**, Normalised IPSC amplitude during Golgi cell stimulation at 5

Hz in ionotropic glutamate receptor antagonists. *Bars* indicate timing of

prolonged MFS at 100 Hz and 10 Hz. *Dashed lines* indicate mean

values for the baseline and during MFS. **B**, Variance-mean relationship

for IPSCs evoked at 5 Hz for control (*filled circle*) and during

prolonged MFS at 10 Hz and 100 Hz (*open circles*). The parabolic fit

gave a weighted mean quantal size of 456 pS for this cell.

3.3.3 Physiological activation of mGluRs by sustained mossy fibre stimulation

To further characterise mGluR regulation of GABA release, the dependence of the

IPSC amplitude on mossy fibre stimulation duration and frequency was

investigated. As before, an independent mossy fibre and Golgi cell axon was

stimulated. The Golgi cell was stimulated at 5 Hz until the IPSC amplitude

reached steady state. At this point, the mossy fibre was stimulated (figure 3.5**A**)

for 5 seconds at either 10 or 100 Hz. These protocols were interleaved as an

internal control for any possible rundown in mGluR action. This protocol was

repeated 10-20 times, with the peak IPSCs recorded and averaged across trials.

Figure 3.5**A** shows the average time course of the peak amplitude of the IPSC for

4 cells. It is clear that the depression associated with mossy fibre stimulation is

sustained throughout the train at both 100 and 10 Hz. At 100 Hz the mean

depression was 54 ± 11 % ($n = 4$; figure 3.5**A**). However, at 10 Hz the degree of

depression was significantly lower (34 ± 10 %; $n = 4$; $p = 0.03$; figure 3.5**A**).

These results suggest that the efficacy of the Golgi to granule cell synapse is

dependent on the duration and frequency of mossy fibre activity.

3.3.4 Quantal size estimated using physiological activation of mGluRs

The quantal size of the evoked IPSC was established above using standard MPFA,

by analysing changes in the mean and variance of the peak IPSC under different

release probabilities induced by changes in the calcium/ magnesium concentration

ratio. If physiological activation of mGluRs induces a change in release

probability, variance-mean analysis of these data should yield a similar value for

the quantal size as standard MPFA. To test this, a variance-mean plot was

constructed using IPSC data under control conditions and during sustained mossy

fibre activation at 10 and 100 Hz (figure 3.5B). The quantal size derived from the

fit of a simple binomial function to the data (350 ± 60 pS; $n = 4$) was similar to

that previously obtained with MPFA (410 ± 60 pS; n = 10; $p = 0.30$; unpaired

t-test). This result confirms that sustained IPSC depression was also mediated by a

change in the GABA release probability.

3.3.5 Physiological activation of mGluRs may be localised to glomerulus

Activation of mGluRs on Golgi cells by sustained high-level release of glutamate

from mossy fibres might increase the firing rate of the cell, as with ACPD-

mediated mGluR activation (figure 3.2). This could induce frequency-dependent

depression of the IPSC amplitude. To test this possibility, spontaneous IPSCs

were detected during mossy fibre stimulation using a scaling template protocol

(Clements and Bekkers, 1997). The frequency of spontaneous IPSCs remained

unchanged during mossy fibre stimulation ($n = 4$; $p = 0.92$), suggesting that single

mossy fibres do not affect the firing rate of Golgi cells via mGluRs. Furthermore,

in contrast to evoked IPSCs, the weighted mean amplitude of spontaneous IPSCs

was unchanged by mossy fibre stimulation ($n = 4$; $p = 0.31$), indicating that IPSC

depression occurred only at glomeruli activated by mossy fibre stimulation.

The activation of extrasynaptic receptors is dependent on diffusion and transmitter

uptake (reviewed by Barbour and Häusser, 1997). Therefore, the role of glutamate

transporters in limiting mGluR activation was investigated. Application of the

uptake blocker PDC (1 µM), which raises extracellular glutamate through

heteroexchange, produced a substantial tonic IPSC depression ($51 \pm 12\%$; $n = 3$; p

$= 0.05$). Sustained mossy fibre stimulation while applying PDC reliably depressed

the IPSC further (to $64 \pm 11\%$ at 10 Hz, $n = 3$; $p = 0.05$), consistent with mGluR

activation by glutamate.

3.4 Discussion of results

In this chapter I have investigated the role of mGluRs in regulating synaptic

efficacy at the Golgi to granule cell synapse. The results show that group I/ II

mGluRs are functional in cerebellar Golgi cells, as pharmacological activation of

mGluRs with ACPD was found to depress the release of GABA. This is consistent

with immunohistochemical (Ohishi et al, 1994; Neki et al, 1996; Jaarsma et al,

1998) and a recent electrophysiological study (Vetter et al, 1999). Physiological

activation of mGluRs on Golgi cells is mediated by synaptically released

glutamate from mossy fibres at physiological temperatures.

3.4.1 Locus of depression

ACPD- and glutamate spillover-mediated depression of the IPSC were not caused

by a change in quantal size. The presynaptic effect of ACPD was achieved by two

mechanisms. First, around 30 % of the inhibition was induced by a small increase

in the Golgi cell spontaneous firing rate, which caused frequency-dependent

depression. Second, most of the depression was likely to be mediated by a direct

reduction in release probability via mGluRs on the Golgi cell axon terminals

(Ohishi et al, 1994). Inhibition of GABA release may be mediated by a reduction

in calcium influx at the terminal, since avtivation of mGluRs inhibits somal

calcium influx in cultured Golgi cells (Knoflach et al, 2001). This dual effect of

APCD has been observed in the cerebellar molecular layer to be mediated by

group I/ II receptors (Llano and Marty, 1995).

In situ hybridisation studies show that mRNA for group I and III mGluRs are

present in granule cells (Abe et al, 1992; Shigemoto et al, 1992; Ohishi et al,

1993; Tanabe et al, 1993). Extracellular recordings from cerebellar slices suggest

these receptors may play a role in mossy fibre synaptic integration (Vetter et al,

1999). Therefore, to isolate and establish presynaptic mGluR actions, a caesium-

based internal solution was employed to block postsynaptic potassium currents,

which can be coupled to mGluRs (reviewed by Conn and Pin, 1997). The fact that

no change in input resistance was induced by ACPD application indicates that this

strategy was successful. It is also possible that mGluR activation could modulate

the properties of the postsynaptic $GABA_A$ receptor ion channel. However,

variance-mean analysis established that the quantal size was unchanged during

mGluR-mediated depression of inhibition, indicating that the depression is not

mediated via direct modulation of $GABA_A$ receptor conductance or a change in

channel open probability.

3.4.2 Physiological activation of mGluRs at a glomerular synapse

Agonist application will tend to activate all receptors on the cell according to the

drug's dose-response characteristics. However, the occupancy of the receptors

induced by synaptically-released transmitter will depend, not only on how much

transmitter is released, but also the spread of transmitter from the release site. This

is related to how many terminals are active and the diffusion barriers present. It

was therefore important to establish that synaptically-released glutamate could

activate mGluRs on Golgi cells and to compare the resulting effects with those

observed with exogenous agonists.

The primary finding in this chapter was that, during excitatory mossy-fibre activity, glutamate depresses GABA release by activating mGluRs. This occurred on a sub-second timescale. This mechanism is likely to involve spillover of transmitter from a single terminal onto an inhibitory Golgi cell terminal, as there are no identifiable synaptic active zones between mossy fibre and Golgi cell axons (Jakab and Hamori, 1988). This contrasts with a related mechanism in the olfactory bulb where there are reciprocal synapses (Hayashi et al, 1993). Suppression of inhibition via spillover of glutamate from multiple fibres has recently been established in synapses onto inhibitory neurones in the CA1 region of the hippocampus (Semyanov and Kullman, 2000). The hippocampal mechanism was mediated entirely by group III mGluRs, whereas, it is likely that a heterogeneous population of mGluRs regulate inhibition in the cerebellar cortex, since both ACPD and AP4 inhibited evoked IPSCs.

An important feature of physiological activation of mGluRs on Golgi cells is that it is likely to be locally restricted to the axon terminals within active glomeruli because the concentration of glutamate falls rapidly with distance from the release site due to diffusion and uptake (Barbour and Häusser, 1997) and glomeruli are partially encapsulated by glia at this age (Hamori and Somogyi, 1983), which may impede diffusion. In support of this, the spontaneous IPSC rate was unaffected by prolonged mossy fibre stimulation, making it unlikely that spillover-mediated depression involves receptors in neighbouring Golgi cell axons or on their somato-dedritic compartment. Such local activation of presynaptic mGluRs by glutamate spillover allows modulation of inhibition at the level of the individual synaptic

input. mGluR activation may occur in this way at other glomerular synapses in the

central nervous system, such as in the olfactory bulb, spinal cord or thalamus

(Shepherd, 1972; Duncan and Morales, 1978; Mason et al, 1996).

3.4.3 Functional implications

Communication between excitatory and inhibitory synapses provides a local

feedforward disinhibitory mechanism that contrasts with depolarisation-induced

suppression of inhibition, an mGluR-mediated feedback mechanism observed at

other synapses that depends on postsynaptic activity through a retrograde

messenger (Glitsch et al, 1996; Morishita et al, 1998). The spillover-mediated

disinhibition of granule cells will selectively boost the excitation in granule cells

with active mossy fibres, thereby enhancing contrast between inputs firing at

different rates. As the mechanism underlying suppression of inhibition showed

little accommodation, presynaptic mGluRs on Golgi cells are likely to be

important for processing information encoded as tonic firing rate, such as joint

angle (van Kan et al, 1993). While, the rapid kinetics of the mechanism enables

mGluRs to follow sub-second changes in mossy fibre firing rate with high

temporal fidelity. The firing rate of Golgi cells *in vivo* (van Kan et al, 1993)

reflects the level of excitation in the regional population of mossy fibres and

granule cells (Eccles et al, 1967; Marr, 1969; Ito, 1984). As inhibition of GABA

release by mGluRs is reduced at higher Golgi cell firing rates, contrast

enhancement by glutamate spillover is likely to be most effective when synaptic

excitation of Golgi cells is low.

CHAPTER FOUR

GABA SPILLOVER ATTENUATES EXCITATION BY ACTIVATING PRESYNAPTIC GABA$_B$-RS

4.0 Abstract

GABA type-B receptors (GABA$_B$-Rs) are present on excitatory terminals throughout the CNS, but surprisingly little is known about their role in modulating neurotransmission under physiological conditions. I have investigated activation of GABA$_B$-Rs on excitatory terminals within the cerebellar glomerulus, a structure where glutamatergic excitatory and GABAergic inhibitory terminals are in close apposition and make axo-dendritic synapses onto granule cells. Application of the GABA$_B$-R agonist baclofen depressed evoked mossy fibre EPSCs by 54% at 1 Hz. The amplitude of miniature EPSCs recorded in tetrodotoxin was unchanged in the presence of baclofen, but the frequency was significantly reduced, indicating a purely presynaptic action of baclofen under the recording conditions. At physiological temperature (37°C) presynaptic GABA$_B$-Rs were not tonically activated by spontaneous GABA release from Golgi cells, which fire at ~8 Hz in slices at this temperature. However, tonic activation could be induced by blocking GABA uptake or by lowering temperature. GABA$_B$-Rs were activated at physiological temperature when Golgi cell firing was increased above the basal level by stimulating a single inhibitory Golgi cell input at 50 Hz, suppressing the mossy fibre-evoked EPSC by 24% at 1 Hz. Furthermore, glutamate release was selectively inhibited at low-frequency mossy fibre inputs (<10 Hz) during Golgi cell stimulation. These findings suggest that GABA spillover in the glomerulus modulates sensory input to the cerebellar cortex.

Figure 4.1 - Pharmacological activation of presynaptic GABA$_B$-Rs depresses glutamate release from mossy fibres. **A**, Average non-NMDA receptor-mediated EPSCs evoked by mossy fibre stimulation at 1 Hz in control solution and in 100 μM baclofen. **B**, Bath application of 100 μM baclofen reduced the EPSC amplitude in a reversible manner (each point is the average of 10 EPSCs, *top trace*). The coefficient of variation (CV) of the EPSC amplitude (*bottom panel*) increased during depression, indicating reduced glutamate release. **C**, Superimposed average spontaneous miniature EPSCs recorded in tetrodotoxin (0.5 μM) in control solution and in the presence of 100 μM baclofen. **D**, Histogram showing mean frequency of miniature EPSCs in control and in 100 μM baclofen ($n = 6$).
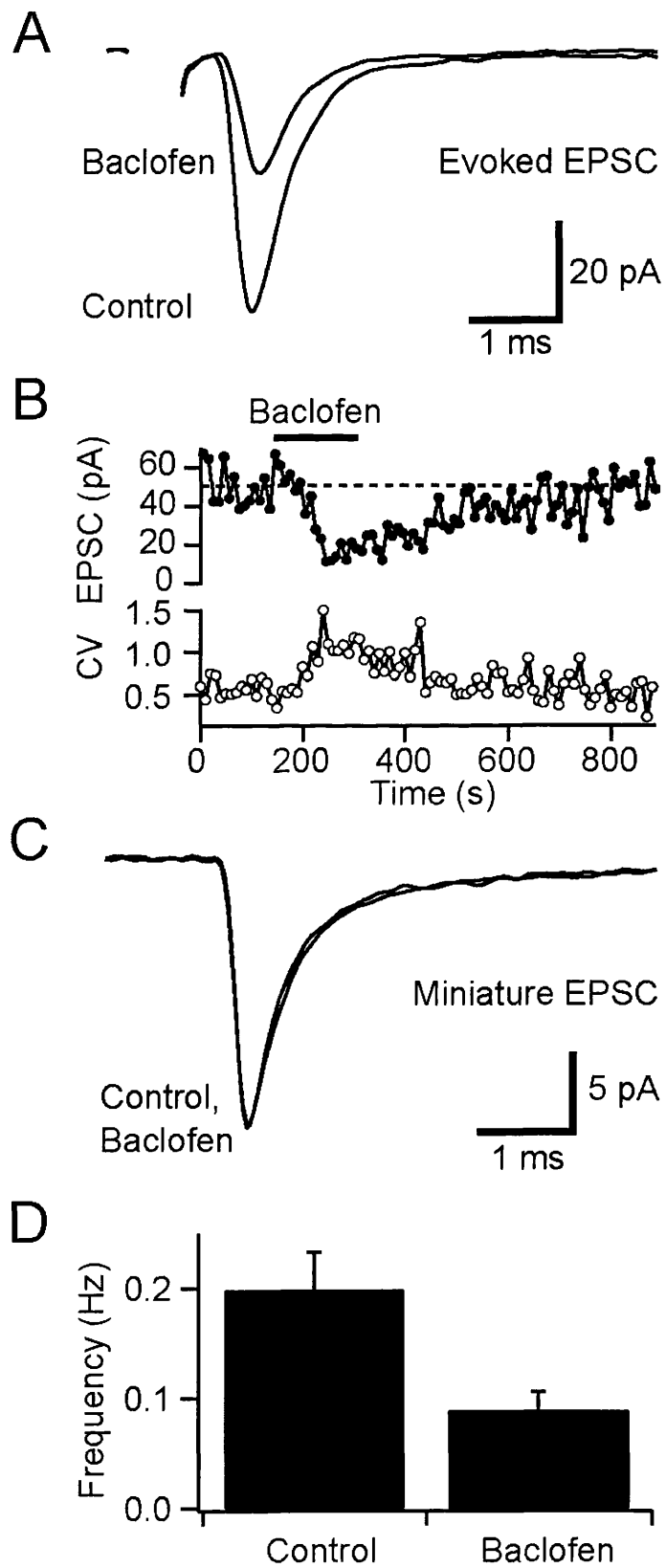
4.1 Evoked EPSCs in granule cells

Whole-cell patch clamp recordings of excitatory postsynaptic currents (EPSCs) were made from visually identified granule cells at 37°C unless stated otherwise. The currents were evoked by minimal stimulation of single mossy fibres in the presence of NMDA, $GABA_A$ and glycine receptor antagonists (figure 4.1**A**, control). In 4 cells detailed analysis of the kinetics and mean amplitude of the conductance underlying the EPSC evoked at 1 Hz was performed. Individual EPSCs were aligned on their stimulus artefact and the mean was calculated. The 10-90 % rise time was measured as 0.60 ± 0.13 ms (figure 4.1). The measured 10-90 % rise time was approximated by a single exponential rise with a time constant of 0.17 ± 0.04 ms. The mean conductance EPSC was measured as 661 ± 173 pS at a holding potential of –70 mV. The decay phase was fit with a dual component exponential function with time constants of 0.92 ± 0.19 ms and 8.8 ± 3.2 ms. The amplitude of the fast component made up 86.6 ± 2.6 % of the peak waveform.

4.2 Pharmacological activation of $GABA_B$-Rs on mossy fibre terminals

I first established whether functional presynaptic $GABA_B$-Rs were present on mossy fibre terminals by using a conventional pharmacological approach. Application of the $GABA_B$-R agonist baclofen (100 μM) reduced the mean amplitude of the evoked non-NMDA receptor-mediated EPSC by 54 ± 5%, in a reversible manner at 37°C (1 Hz, $p < 0.001$, $n = 12$; figure 4.1**A**, **B**), without affecting the input resistance of the granule cell (data not shown). A similar level of inhibition of the EPSC was observed at room temperature (45 ± 1%, $p = 0.41$, $n = 3$, unpaired t test). The coefficient of variation (CV; standard deviation / mean)
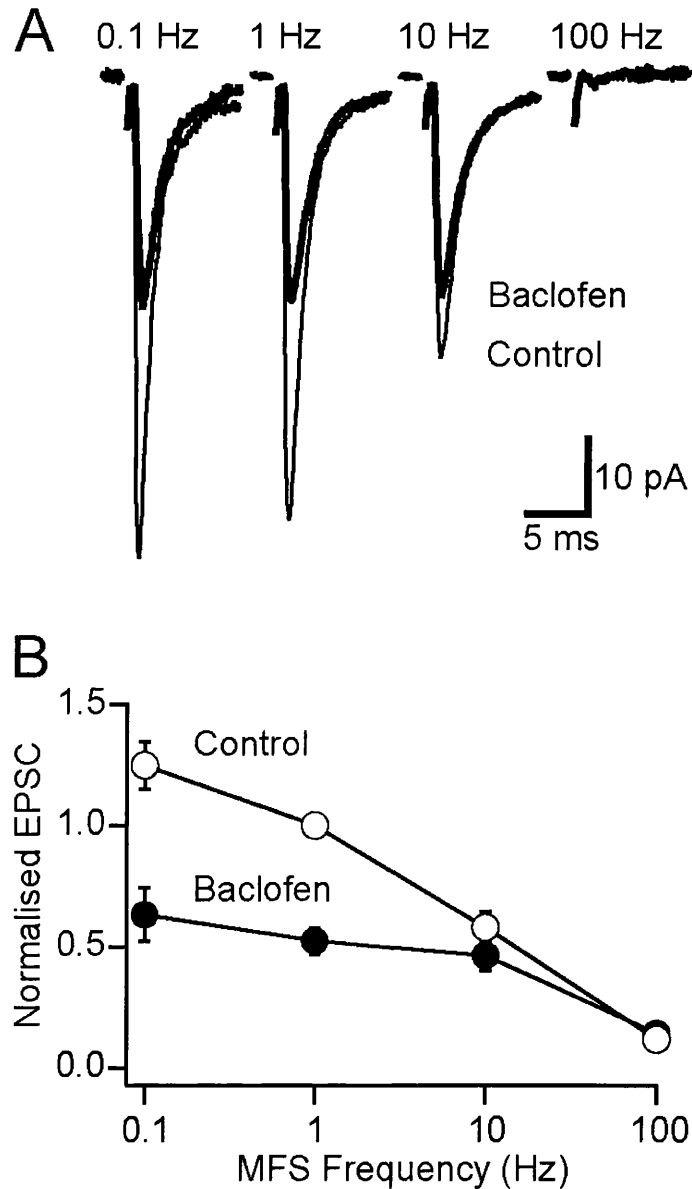
Figure 4.2 - Frequency dependence of GABA_B-R-mediated EPSC depression. **A**, Averaged steady-state EPSCs from the same cell recorded at different stimulation frequencies in control solution (*thin trace*) and in the presence of 100 μM baclofen (*thick trace*). **B**, Steady-state frequency dependence of EPSC amplitude in control (*open symbols*) and in the presence of 100 μM baclofen (*filled symbols*). The relationship shows the average of eight cells normalised to the 1 Hz EPSC amplitude in control solution.

of the EPSC increased in the presence of baclofen ($200 \pm 20\%$ of control, p =

0.002, n = 12; figure 4.1**B**), consistent with the EPSC depression being mediated,

at least in part, by a reduction in glutamate release onto the granule cell. The locus

of the GABA$_B$-R action was investigated further by examining the effect of

baclofen on miniature currents recorded in the presence of tetrodotoxin (0.5 μM).

The mean amplitude of miniature EPSCs in the presence of baclofen was similar

to control (quantal size = 12.9 ± 1.9 pA; $p > 0.05$, n = 6; figure 4.1**C**), but the

miniature frequency was significantly reduced ($50 \pm 12\%$ $p = 0.01$, n = 6; figure

4.1**D**), as expected for a purely presynaptic mechanism. These results are

consistent with the present experimental conditions, which employed a caesium-

based internal solution to block postsynaptic potassium currents.

The effects of presynaptic GABA$_B$-R activation on the EPSC were examined over

a range of mossy fibre stimulation frequencies that were similar to the firing rates

observed *in vivo* (van Kan et al, 1993). Under control conditions the steady-state

amplitude of the evoked mossy fibre EPSC declined as the stimulation frequency

increased (figure 4.2**A, B**). In the presence of a saturating concentration of

baclofen (100 μM; Takahashi et al, 1998) the frequency dependence of the EPSC

was flattened because of selective depression at frequencies less than 10 Hz ($p <$

0.001, n = 8; figure 4.2**B***). However, at stimulation frequencies of greater than or

equal to 10 Hz GABA$_B$-R activation had no statistically significant effect on the

amplitude of steady-state EPSC ($p \geq 0.28$, n = 8; figure 4.2**B***).

Figure 4.3 - Tonic activation of $GABA_B$-Rs is temperature-dependent. **A**, Averaged EPSCs evoked at 1 Hz in control and in 500 μM CGP35348 at 37°C. **B**, Steady-state frequency dependence of EPSCs for control solution (*open symbols*) and in the presence of 500 μM C0P35348 (*filled symbol*) at 37°C. The relationship shows the average of three cells normalised to the 1 Hz EPSC amplitude in control solution. **C**, Averaged EPSCs evoked at 1 Hz in control solution and in the presence of the $GABA_B$-R antagonist CGP35348 (500 μM) at room temperature. **D**, Histogram of normalised EPSC amplitudes during control, 50 μM baclofen, 500 μM CGP35348, and 500 μM CGP35348 plus 50 μM baclofen at room temperature ($n = 4$).

A Physiological temperature

Control
CGP35348

40 pA

1 ms

B

Normalised EPSC

Control
CGP35348

1.0

0.5

0.0

1   10   100

MFS Frequency (Hz)

C Room temperature

Wash
Control

CGP35348

20 pA

2 ms

D

Normalised EPSC

1.5

1.0

0.5

Control   Baclofen   CGP   Baclofen + CGP
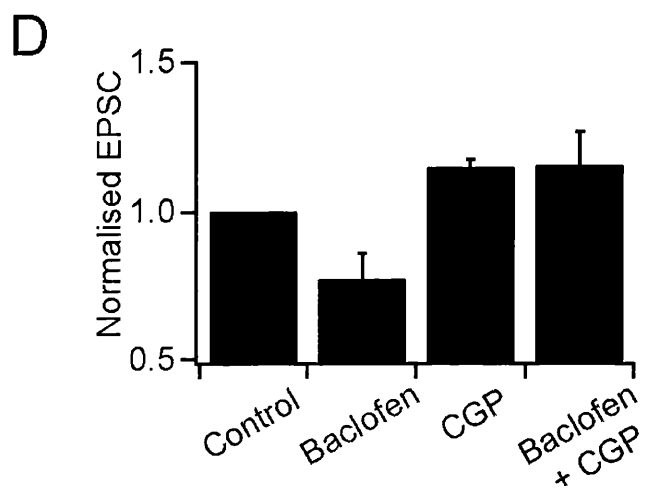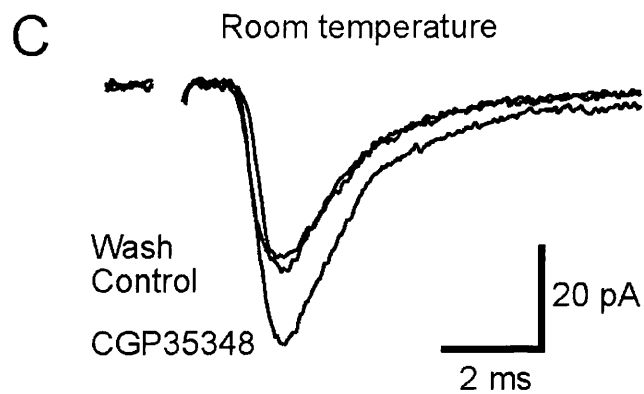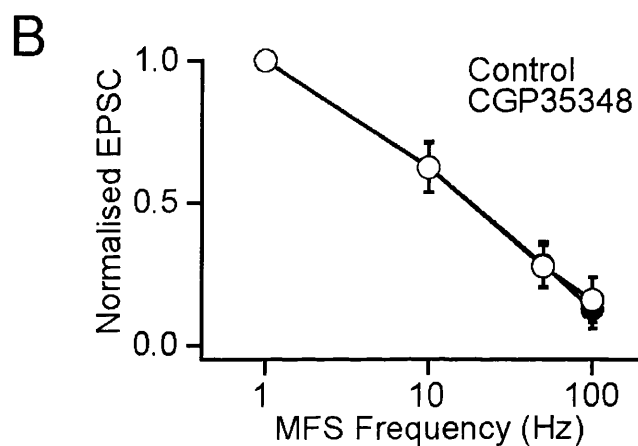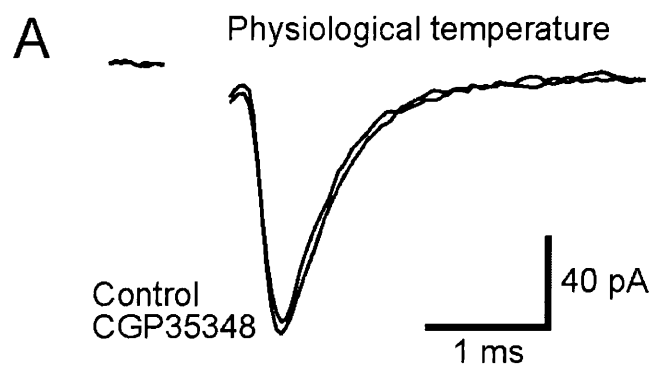
4.3 Tonic GABA release, presynaptic GABA$_B$-R activation, and GABA uptake

In the absence of stimulation, Golgi cells in slices fire spontaneously at 3-6 Hz at

room temperature (Dieudonne, 1998; Misra et al, 2000) and at 8 Hz at 37°C

(Ch. 3; Mitchell and Silver, 2000a), which is comparable to the range of basal

rates observed *in vivo* (8-15 Hz; Edgley and Lidierth, 1987; van Kan et al, 1993;

Vos et al, 1999a). The resulting GABA release contributes to a GABA$_A$ receptor-

mediated tonic leak current in granule cells (Brickley et al, 1996; Tia et al, 1996;

Wall and Usowicz, 1997) and can be detected as spontaneous IPSCs that are

blocked by the GABA$_A$ antagonist bicuculline (data not shown). I sought to

determine whether this spontaneous release of GABA from Golgi cell terminals

could also tonically activate GABA$_B$-Rs on mossy fibres by examining the effect

of a GABA$_B$-R antagonist on the EPSC amplitude. No change in the EPSC

amplitude was observed during application of 500 µM CGP35348 at frequencies

between 1 Hz (97 ± 7% of control, $p = 0.7$, $n = 5$; figure 4.3**A**) and 100 Hz ($p \geq$

0.3, $n = 3$; figure 4.3**B**) at 37°C. These results indicate that GABA$_B$-Rs are not

tonically activated at physiological temperatures.

I investigated whether the lack of tonic activation at the mossy fibre could simply

reflect the recording temperature because tonic activation of GABA$_B$-Rs has been

reported in other preparations at room temperature (Kombian et al, 1996;

Aroniadou-Anderjaska et al, 2000). At room temperature, the GABA$_B$-R

antagonist CGP35348 (500 µM) potentiated EPSCs by 15 ± 3% (1 Hz, $p = 0.01$, n

= 4; figure 4.3**C**, **D**), suggesting that GABA$_B$-Rs tonically depress glutamate

release at this temperature. What mechanism might underlie this difference in
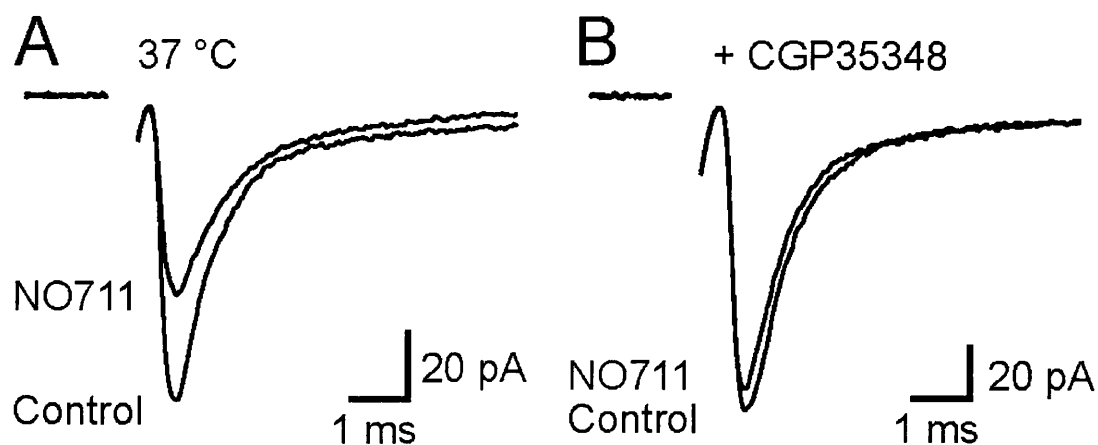
Figure 4.4 - Inhibition of GABA uptake induces tonic activation of GABA$_B$-Rs at physiological temperature. **A**, Averaged EPSCs evoked at 1 Hz in control solution and in the presence of the GABA uptake blocker NO711 (50 μM) at 37°C. **B**, Averaged EPSCs evoked at 1 Hz in the GABA$_B$-R antagonist CGP35348 (500 μM) and in the presence of both 500 μM CGP35348 and 50 μM NO711 at 37°C.
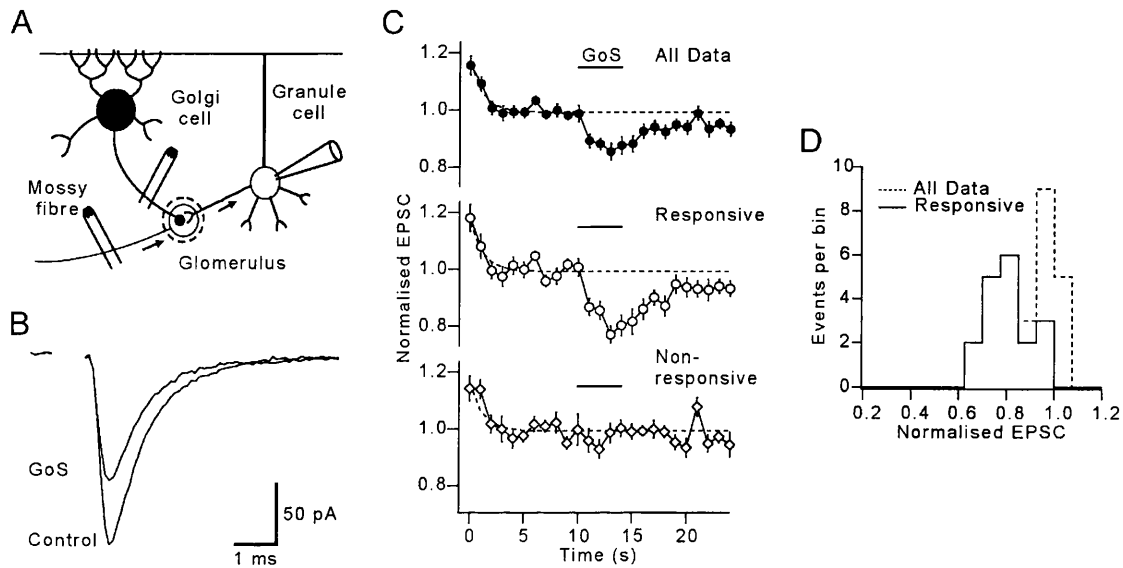
Figure 4.5 - Stimulation of single Golgi cell input suppresses mossy fibre EPSCs. **A**, Recording configuration: whole-cell patch-clamped granule cell and stimulation of independent inhibitory and excitatory inputs. **B**, Average non-NMDA EPSC waveforms from control period and during Golgi cell stimulation (GoS). **C**, Traces show average non-NMDA EPSCs amplitudes (normalised to pre-GoS baseline) evoked by mossy fibre stimulation at 1 Hz in presence of ionotropic GABA_A receptor antagonist. *Bar* shows timing of 5 s burst of GoS at50 Hz. *Dashed lines* show extrapolated single exponential fit to pre-GoS frequency-dependent depression for all data. *Top trace* shows average of all 31 cells. *Middle trace* shows average of 19 cells that responded to GoS (responsive). *Bottom trace* shows average of 12 cells that did not respond to GoS (non-responsive). **D**, *Dashed line* shows distribution of mean EPSC amplitude during GoS for all cells. *Solid line* shows distribution for responsive cells.

GABA$_B$-R activation at high versus low temperature? The most likely candidate is transmitter uptake because transporters have a high Q_{10} (Wadiche and Kavanaugh, 1998; see also Terrian et al, 1987). This possibility was tested by examining whether tonic GABA$_B$-R activation could be induced at physiological temperatures when GABA uptake was blocked. NO711 was used to block GABA uptake because it is not a substrate for uptake (Zeevalk and Nicklas, 1997) and thus does not induce GABA release by heteroexchange. Furthermore, NO711 preferentially blocks the GAT-1 transporter, which is known to be present in cerebellar glomeruli (Itouji et al, 1996). It may also inhibit GAT-3, which is present in the glial sheath that partially surrounds glomeruli at this age (Itouji et al, 1996). Application of 50 µM NO711 produced a tonic depression of the EPSC at physiological temperature (24 ± 5%, p = 0.01, n = 5; figure 4.4**A**) that was blocked by the presence of 500 µM CGP35348 (6 ± 5% reduction, p = 0.22, n = 5; figure 4.4**B**). These results suggest that at physiological temperature uptake maintains the basal GABA concentration below that necessary to activate presynaptic GABA$_B$-Rs.

4.4 Activation of GABA$_B$-Rs on mossy fibres by stimulating single Golgi cell inputs

I examined whether GABA$_B$-Rs on mossy fibre terminals could be activated at physiological temperature when GABA release is increased by stimulating single Golgi axons. Independent mossy fibre and Golgi cell inputs onto a granule cell (illustrated in figure 4.5**A**) were stimulated with minimal stimulation. Care was taken to ensure that stimulation of EPSCs and IPSCs was independent, and that

they originated from single fibres, by checking that PSC amplitude was

independent of stimulation voltage (Silver et al, 1996b) and that there were no

temporally distinct components. Evoked monosynaptic EPSCs and IPSCs were

distinguished by their kinetics and reversal potential (Ch. 3; Mitchell and Silver,

2000a).

The efficacy of the excitatory mossy fibre input was monitored from the amplitude

of evoked non-NMDA receptor-mediated PSCs during a stimulation train

delivered at 1 Hz after block of ionotropic GABA$_A$ receptors with bicuculline. At

the start of the train, the EPSC amplitude declined because of frequency-

dependent depression (figure 4.5C). The depression time course could be well

approximated by a single exponential function (τ = 1.2 s; figure 4.5C, *dashed*

line). Once the EPSC amplitude had stabilised, the inhibitory Golgi cell input was

stimulated for a sustained period at a frequency within the range observed *in vivo*

during limb movement (van Kan et al, 1993), locomotion (Edgley and Lidierth,

1987), and facial stimulation (Vos et al, 1999a). Stimulation of the Golgi cell

input for 5 s at 50 Hz caused a marked depression in the EPSC amplitude (figure

4.5B). Although this depression was present when all experiments were averaged

(figure 4.5C, *top trace*), it is clear from the bimodal distribution of responses

(figure 4.5D) that no EPSC depression occurred in some experiments. Individual

cells were therefore classified into responsive or non-responsive groups by testing

whether the EPSC amplitude was significantly different during Golgi cell

stimulation (GoS), from the prestimulation amplitude (figure 4.5C; single-tailed

t-test). This approach indicated that 61% (19 of 31 cells) of granule cell recordings

Figure 4.6 - Golgi cell-induced suppression of mossy fibre EPSCs is presynaptic. **A**, *Top panel*, normalised EPSC amplitudes for responsive cells during 1 Hz mossy fibre stimulation in presence of ionotropic GABA$_A$ receptor antagonist (same data as figure 4.5**C**; *middle trace*). *Bar* shows timing of 5 s burst of GoS at 50 Hz. *Dashed lines* show time course of frequency-dependent depression from all data (figure 4.5**C**, *top trace*). *Bold line* shows fit of single exponential function to EPSC recovery ($\tau = 3$ s). *Bottom panel*, CV during EPSC depression ($n = 19$). *Dashed line* shows pre-GoS baseline. **B**, Relationship between CV and normalised peak EPSC. Negative correlation (Spearman correlation coefficient, $r = -0.84$) indicates a reduction in release probability during EPSC depression.
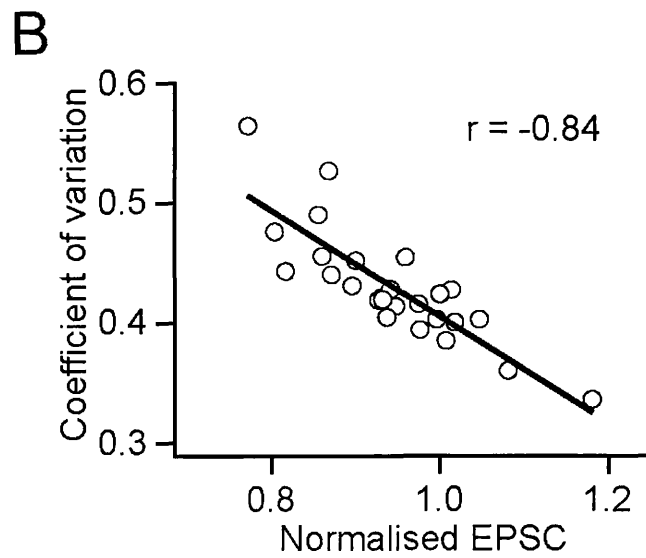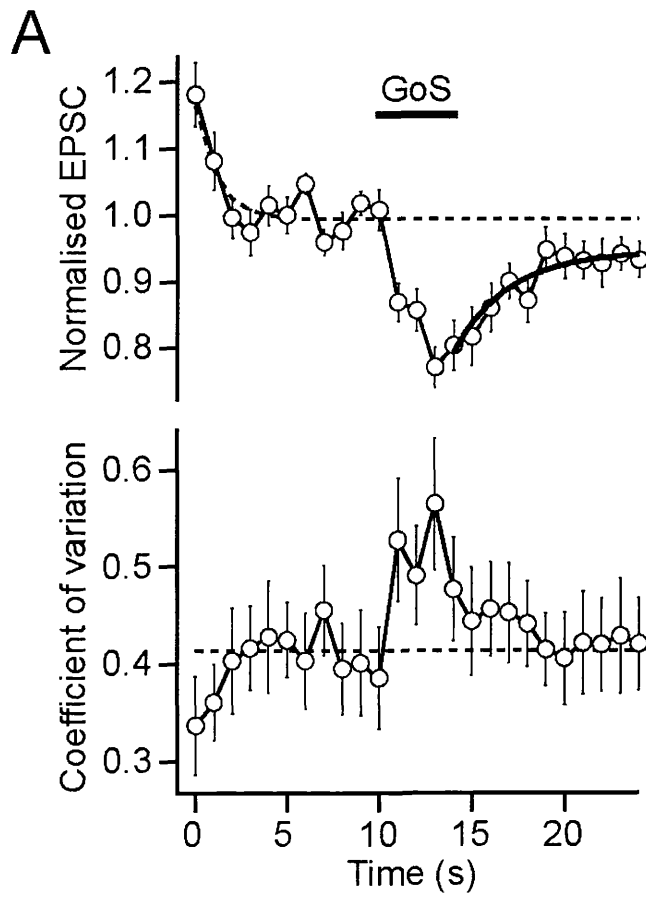
exhibited EPSC depression during GoS (figure 4.5**D**, *solid line*). Averaging the non-responsive cells gave no residual response, confirming that the separation procedure was effective (figure 4.5**C**, *bottom trace*).

The average time course of EPSC depression during GoS was relatively slow with the rising phase detectable after 1 s of Golgi cell stimulation ($p < 0.001$; $n = 19$; figure 4.6**A**). The decay of the EPSC depression could be approximated with a single exponential with a time constant of 3 s which is comparable to GABA$_B$-R-mediated depression of EPSCs and presynaptic calcium currents at other central excitatory synapses (Isaacson et al, 1993; Pfrieger et al, 1994; Dittman and Regehr, 1997). At the peak of the response, the EPSC amplitude was depressed by 24 ± 3% during 5 s GoS at 50 Hz ($p < 0.001$, $n = 19$, responsive cells; figure 4.6**A**). During depression the coefficient of variation of the EPSC increased (0.43 ± 0.05 to 0.58 ± 0.07, $n = 19$, $p = 0.001$; figure 4.6**A, B**), indicating that it was caused by a reduction in probability of glutamate release. I also tested a brief stimulation protocol (80 Hz for 250 ms) that mimicked the duration of Golgi cell activity during joint flexion (van Kan et al, 1993). However, this protocol produced no change in the EPSC amplitude evoked at 1 Hz (101 ±1% of control, $n = 5$, $p = 0.44$).

If the Golgi cell stimulation electrode directly activated the mossy fibre axon, it is possible that the EPSC depression could be caused by depletion of vesicles in the terminal rather than via activation of presynaptic receptors. However, examination

Figure 4.7 - GABA$_B$-Rs mediate Golgi cell stimulation-induced EPSC depression. **A**, Simultaneous 50 Hz Golgi cell stimulation (GoS) and 1 Hz mossy fibre stimulation (MFS) in the presence of GABA$_A$ receptor blockers. EPSCs were evoked by MFS, whereas no currents were associated with the GoS. **B**, Stimulus averaged currents: MFS indicates EPSC evoked at 1 Hz, and GoS shows IPSCs were not evoked during 50 Hz GoS. **C**, Normalised evoked EPSC amplitudes from the same cells before, during, and after 50 Hz GoS for control and in the presence of the GABA$_B$-R antagonist CGP35348 (500 µM; n = 5). *Dashed lines* show time course of frequency-dependent depression from all data (figure 4.5**C**, *top trace*).

A

GoS

MFS

50 pA

200 ms

B

GoS
MFS

50 pA

1 ms

C
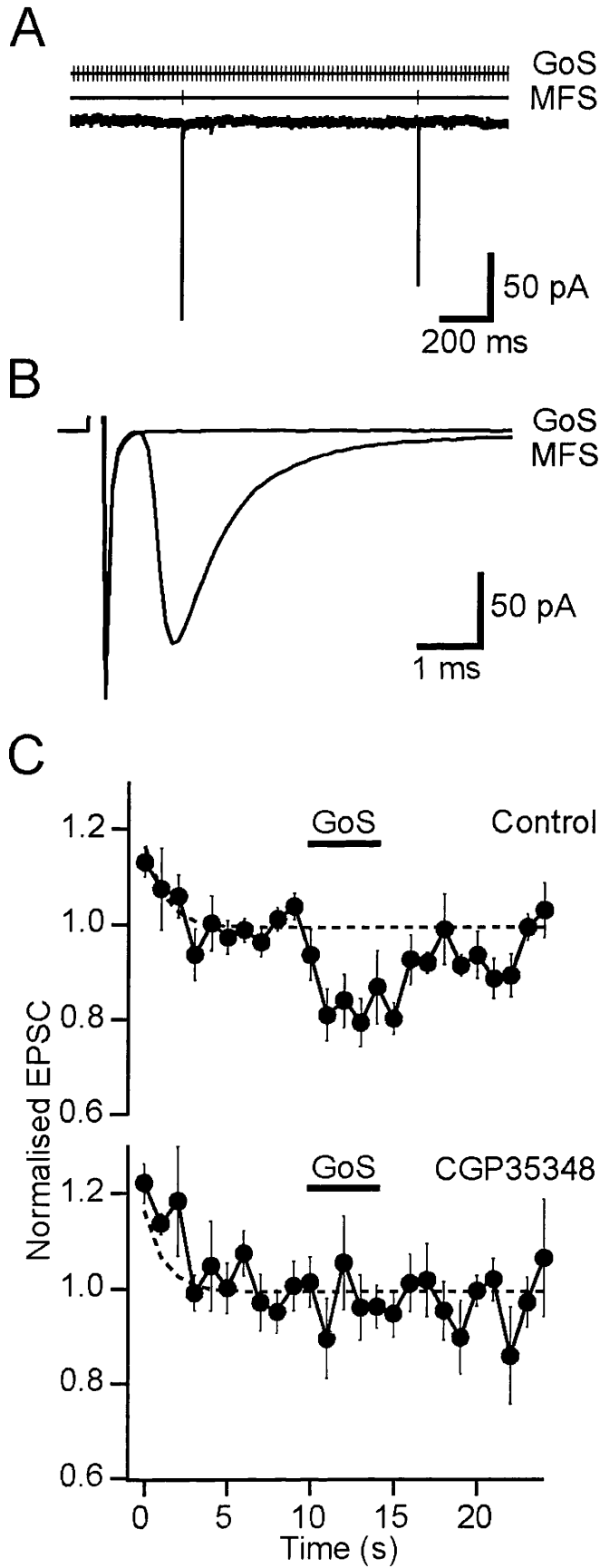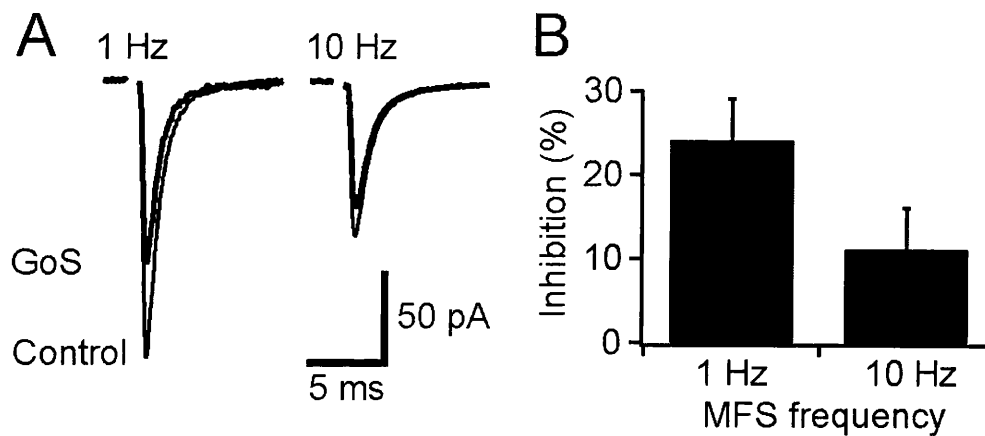
Figure 4.8 - Physiologically activated GABA$_B$-Rs suppress low-frequency excitatory transmission. **A**, Averaged EPSCs from the same cell evoked at 1 and 10 Hz mossy fibre stimulation during 50 Hz Golgi cell stimulation (GoS). GABA$_B$-R mediated EPSC depression was more pronounced at 1 Hz than at 10 Hz. **B**, Histogram of mean EPSC inhibition during GoS for four cells.

of the traces during Golgi cell stimulation showed that no synaptic currents were

evoked in the presence of GABA$_A$ receptor blockers (figure 4.7**A**, **B**), ruling out

this possibility. Furthermore, I tested whether GABA$_B$-Rs were involved in EPSC

depression by examining the effect of sustained 50 Hz GoS in the presence of a

GABA$_B$-R antagonist. In 500 μM CGP35348 the Golgi cell stimulation-induced

depression of the EPSC was completely blocked (98 ± 6% of control, $p = 0.74$,

$n = 5$; figure 4.7**C**), providing direct evidence that depression of glutamate release

from the mossy fibre was caused by GABA$_B$-R activation.

To better understand the physiological role of presynaptic GABA$_B$-Rs and to test

whether the frequency dependence of GABA$_B$-R-mediated depression occurs

during endogenous activation, I examined the effects of Golgi cell stimulation on

EPSCs evoked at two different frequencies. Consistent with the frequency

dependence of pharmacologically activated GABA$_B$-Rs (figure 4.2), inhibition of

EPSCs during Golgi cell stimulation was significantly greater during mossy fibre

stimulation at 1 Hz (22 ± 6%) than during mossy fibre stimulation at 10 Hz

(10 ± 17%, $p = 0.02$, $n = 4$; figure 4.8**A**, **B**). Indeed, EPSCs evoked at 10 Hz

showed no significant depression during sustained Golgi cell stimulation at 50 Hz

($p = 0.30$). These results demonstrate that presynaptic GABA$_B$-Rs selectively

depress low-frequency mossy fibre transmission during activation by synaptically

released GABA at physiological temperature.

4.5 Discussion of Results

In this chapter, I have investigated the role of GABA$_B$-Rs in regulating synaptic

efficacy at the mossy fibre to granule cell synapse. The results show that there are

functional GABA$_B$-Rs on cerebellar mossy fibre terminals, as pharmacological

activation of GABA$_B$-Rs with baclofen depressed the release of glutamate. This is

consistent with immunohistochemical evidence that shows staining for the R1b

splice variant of the GABA$_B$-R in the cerebellar glomerulus (Poorkhalkali et al,

2000). Physiological activation of GABA$_B$-Rs on mossy fibres was induced by

stimulating individual Golgi cells at sustained rates above their basal level at

physiological temperature. This protocol must have induced spillover of GABA

onto the excitatory mossy fibre terminals since no axo-axonal synapses occur in

the cerebellar glomerulus (Jakab and Hámori, 1988). GABA spillover activates

presynaptic GABA$_B$-R heteroreceptors and depresses glutamate release in a

frequency-dependent manner. This suggests that mossy fibres firing at low

frequency are selectively inhibited, whereas high-frequency inputs remain

unaffected.

4.5.1 Locus of depression

An autoradiographic study has indicated that GABA$_B$-Rs are present in granule

cells (Wilkin et al, 1981). Indeed, whole cell recordings from turtle cerebellar

granule cells indicating that GABA released from Golgi cells can physiologically

activate these GABA$_B$-Rs, suggest postsynaptic GABA$_B$-Rs may play a role in

mossy fibre synaptic integration (Jörntell and Midtgaard, 1999). To

pharmacologically block these postsynaptic actions, thereby isolating the

presynaptic actions of GABA$_B$-Rs, a caesium-based internal solution was

employed to block postsynaptic potassium currents, which can be coupled to

GABA_B-Rs (Sodickson and Bean, 1996). Any potential postsynaptic actions of

GABA_B-R activation were not apparent, as application of baclofen did not affect

the input resistance of the granule cell. Indeed, the fact that baclofen application

induced no change in miniature EPSC size, but reduced their frequency, indicated

that GABA_B-R-mediated EPSC depression was mediated entirely by a change in

glutamate release probability.

4.5.2 GABA spillover at physiological temperature

Activation of GABA_B-Rs on mossy fibre terminals by synaptically-released

GABA is likely to be locally restricted within glomeruli because the concentration

of GABA falls rapidly as it diffuses from the release site (for estimates for

glutamate diffusion, see Barbour and Häusser, 1997; Rusakov et al, 1999), GABA

transporters are present in the glomerulus (Itouji et al, 1996), and glomerular

synapses are partially encapsulated by glia at this age (Hámori and Somogyi,

1983). Previous studies indicate that GABA spillover occurs in the cerebellar

glomerulus. The basal level of GABA produces a postsynaptic leak conductance

by tonically activating $\alpha6$-containing GABA_A receptors (Brickley et al, 1996; Tia

et al, 1996; Wall and Usowicz, 1997). These high-affinity receptors, which are

located both synaptically and extrasynaptically (Nusser et al, 1998), also detect

evoked GABA released from neighbouring synapses, generating slow IPSCs

(Rossi and Hamann, 1998). The results showing that presynaptic GABA_B-Rs are

activated tonically at room temperature are consistent with these previous studies

and the observation that GABA_B-Rs are tonically active at excitatory synapses in

rat supraoptic nucleus and olfactory bulb (Kombian et al, 1996; Aroniadou-

Anderjaska et al, 2000). However, presynaptic GABA$_B$-Rs on mossy fibres were

not tonically activated at physiological temperature (~37°C). Several processes

could underlie this temperature dependence, including changes in GABA release,

modulation, or uptake. Reduced GABA release seems unlikely because Golgi cell

firing rate increases with temperature (Dieudonne, 1998; Misra et al, 2000;

Mitchell and Silver, 2000a), and most spontaneous IPSCs in granule cells are

sensitive to tetrodotoxin (Brickley et al, 1996; Wall and Usowicz 1997). A

decrease in the efficacy of the modulatory mechanism is also unlikely because the

degree of inhibition of the EPSC by 100 μM baclofen did not change with

temperature. In contrast, the findings that tonic activation of presynaptic GABA$_B$-

Rs can be revealed at 37°C when uptake is inhibited, suggest that GABA uptake is

likely to underlie this temperature sensitivity. Furthermore, GABA$_B$-Rs can be

activated at physiological temperature when Golgi cell stimulation is sustained for

≥ 1 s, suggesting that uptake can be overcome when the amount of GABA release

is increased. These results suggest that GABA spillover is more restricted at

physiological temperatures than at room temperatures because uptake is more

effective at removing extracellular GABA. Temperature dependence of

heterosynaptic GABA$_B$-R activation has also been observed in hippocampus

(Isaacson et al, 1993), highlighting the importance of uptake when investigating

the physiological role of transmitter spillover.

4.5.3 GABA release from a single Golgi cell input activates heterosynaptic

   GABA$_B$-Rs

Several studies have established that presynaptic GABA$_B$-Rs on excitatory

terminals can be activated by spillover of GABA released from interneurones

(Isaacson et al, 1993; Dittman and Regehr, 1997; Vogt and Nicoll, 1999; Yamada

et al, 1999; Aroniadou-Anderjaska et al, 2000). However, it is unclear whether

GABA release from a single input can activate presynaptic heteroreceptors or

whether synchronous release from many axons is necessary. I have examined this

by stimulating single inhibitory and excitatory inputs onto cerebellar granule cells

at the cerebellar glomerulus. Activation of an individual synaptic input is feasible

with local extracellular stimulation in this preparation (Silver et al, 1996b)

because Golgi cells and mossy fibres are present at a low density in the granule

cell layer (Palay and Chan-Palay, 1974), and one Golgi cell axon is thought to

innervate an individual glomerulus (Eccles et al, 1967; Ito, 1984; Jakab and

Hámori, 1988). Even if more than one Golgi cell axon occasionally innervates

glomeruli, the minimal stimulation method will ensure only one input is activated.

Furthermore, if one of the axons is not synaptically connected to the granule cell

from which I recorded, slow spillover-mediated IPSCs (Rossi and Hamann, 1998)

should be present when the stimulation voltage is lowered to just below the

threshold of the synaptically connected axon. This was not observed. These results

therefore show that GABA$_B$-Rs on excitatory mossy fibre terminals can be

activated by GABA released by stimulating single inhibitory inputs at

physiological temperature and frequencies observed *in vivo* (Edgley and Lidierth,

1987; van Kan et al, 1993; Vos et al, 1999a). The EPSC depression obtained

during physiological activation of $GABA_B$-Rs was significantly smaller than the

depression observed with a high concentration of baclofen. Because GABA and

baclofen are both full agonists (Kaupmann et al, 1997), this result suggests that

$GABA_B$-Rs are only partially occupied by GABA during sustained Golgi cell

firing at 50 Hz. Furthermore, $GABA_B$-R occupancy must approach zero during

transient Golgi cell firing at 80 Hz since no depression occurred during this

protocol. The current model would suggest that uptake impeded the activation of

$GABA_B$-Rs during transient GABA release and that saturation of uptake during

sustained activity permitted diffusion of GABA from its release site to the

presynaptic terminals of mossy fibres. It is possible that the strength of $GABA_B$-R

modulation changes with development because there are considerable changes in

the morphology of the glomerulus between the juvenile animals studied here (P13)

and mature rats (P45; Hámori and Somogyi, 1983).

4.5.4 Frequency dependence of $GABA_B$-R-mediated modulation of the EPSC

Physiological activation of presynaptic $GABA_B$-Rs reduced the EPSC by 24% (at

1 Hz mossy fibre stimulation) during sustained Golgi cell stimulation. At a higher

mossy fibre stimulation frequency of 10 Hz, GABA spillover did not induce

significant EPSC depression, consistent with the frequency dependence observed

with baclofen. Modulation of tonically firing mossy fibres by presynaptic $GABA_B$-

Rs will therefore be restricted to low-frequency inputs. This contrasts with the

behaviour of avian auditory synapses where pharmacological activation of

presynaptic $GABA_B$-Rs causes EPSC depression up to 100 Hz and potentiation at

even high frequencies (Brenowitz et al, 1998). These differences may reflect

functional heterogeneity in GABA$_B$-R-mediated modulation at different central synapses. Characterisation of the steady-state frequency dependence of EPSCs during GABA$_B$-R activation is relevant for understanding transmission at mossy fibre inputs that fire relatively regularly, as observed for "tonic" inputs encoding joint angle (van Kan et al, 1993).

CHAPTER FIVE

MODELLING METHODS

The way in which heterosynaptic modulation of transmitter release in the

cerebellar glomerulus affected synaptic integration was modelled. The somata and

dendrites of granule cells are thought to be electrotonically compact (Silver et al,

1992, 1996c; D'Angelo et al, 1993, 1995; Gabbiani et al, 1994). The DC

electronic length of a granule cell dendrite is 0.02 – 0.05 suggesting that the

granule and are thought to act as a single compartment (Silver et al, 1992).

Moreover the combined filtering of the cell and recording apparatus has a –3 dB

cut-off frequency of ~ 1.9 kHz (Silver et al, 1992). Given that the recording

apparatus, which lies in series with the granule cell has a cut-off of ~ 2.6 kHz, we

can estimate that the cell itself filters with a high bandwidth of ~ 2.7 kHz. The

granule cell was therefore modelled as single compartment integrate-and-fire unit.

5.1 Integrate and fire (I-f) model

The cell membrane has a resistive component (R_m) to the input impedance that lies

in parallel with the membrane capacitance (C_m), and can be modelled by a simple

electronic circuit (figure 5.1**A**). This circuit accumulates charge across the

capacitance when membrane current flows and discharges through the resistance

when the membrane current is reduced. This representation of a cell's behaviour

Figure 5.1 – Classical leaky integrate-and-fire model. **A**, Subthreshold current injections $(I_{inj}(t))$ are passively integrated across a capacitance (C_m), which is set in parallel with a resistance (R_m). When the voltage (V_m) reaches a threshold a spike is produced and integration is shunted for the refractory period, t_{ref}. **B**, Analytical solution for f-I curve of classical integrate–and-fire unit with the properties: $t_{ref} = 0.5$ ms; $R_m = 2.6$ GΩ; $C_m = 3$ pF; $V_{th} = 26$ mV.

A
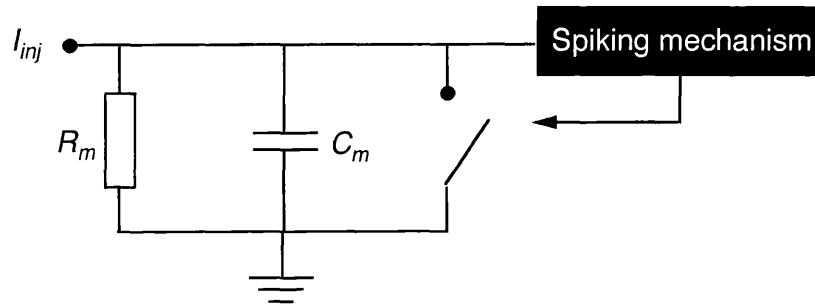
B
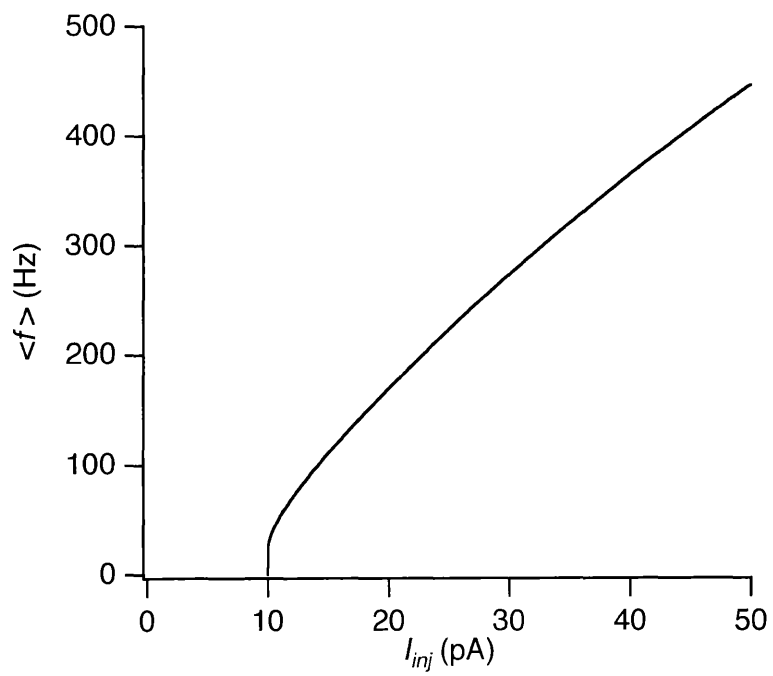
serves to integrate charge in the classic leaky I-f model. The response to a current

injection, $I_{inj}(t)$, is shown in equation 5.1.

$$C_m \frac{dV_m(t)}{dt} + \frac{V_m(t)}{R_m} = I_{inj}(t)$$ (5.1)

where $V_m(t)$ is the membrane voltage as a function of time.

When $V_m(t)$ reaches a threshold (V_{th}) a spiking mechanism is evoked. The

mechanism mimics a real action potential by initially setting $V_m(t)$ to a stereotyped

value >0 mV followed by an afterhyperpolarisation, which is held for a variable

amount of time. During this spike time integration is stopped, thereby imposing a

period during which the cell is refractory; the modelling analogue of the absolute

refractory period (t_{ref}).

The average spiking rate, $<f>$, as a function of current injection (f-I relationship)

can be mathematically derived (Koch, 1999) as,

$$\langle f \rangle = \frac{1}{t_{ref} - R_m \cdot C_m \cdot \ln\left(1 - \frac{V_{th}}{I_{inj} \cdot R_m}\right)}.$$ (5.2)

I have plotted this theoretical f-I relationship is plotted in figure 5.1**B**, where t_{ref} =

0.5 ms; R_m = 2.6 GΩ; C_m = 3 pF; V_{th} = 26 mV.

Figure 5.2 – Conductance-based integrate-and-fire model. **A*i*,** The

basis of this model is the same as the classical integrate-and-fire unit,

with the membrane resistance replaced by a conductance (G_m) in series

with a –70 mV reversal potential. ***ii,*** Linearisation achieved by

introducing a conductance (G_K) with a reversal potential of –90 mV that

is activated by the spiking mechanism. **B,** Computationally derived f-I

curves for conductance-based integrate-and-fire model with and

without linearisation.

A i

Non-linearised

ii

Linearised
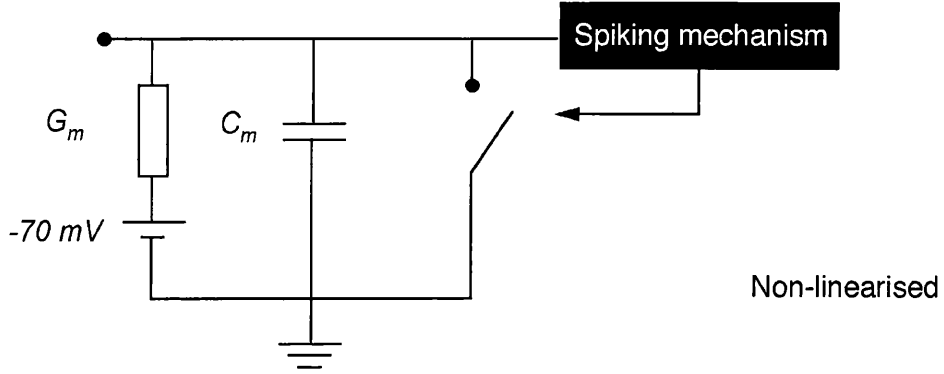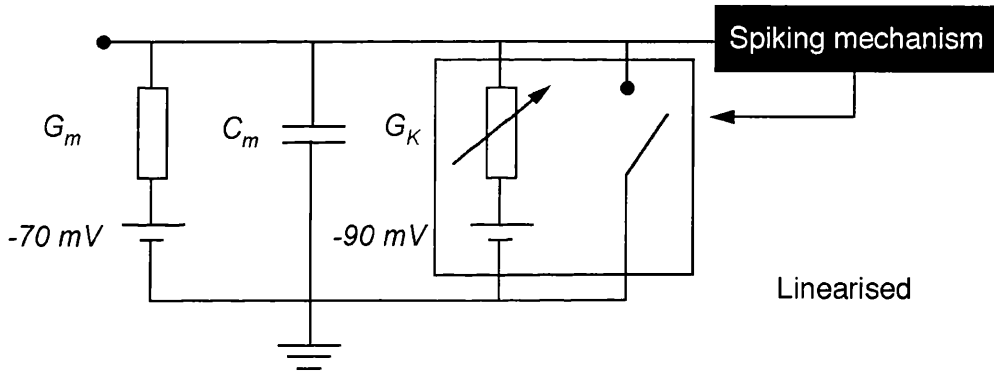
B
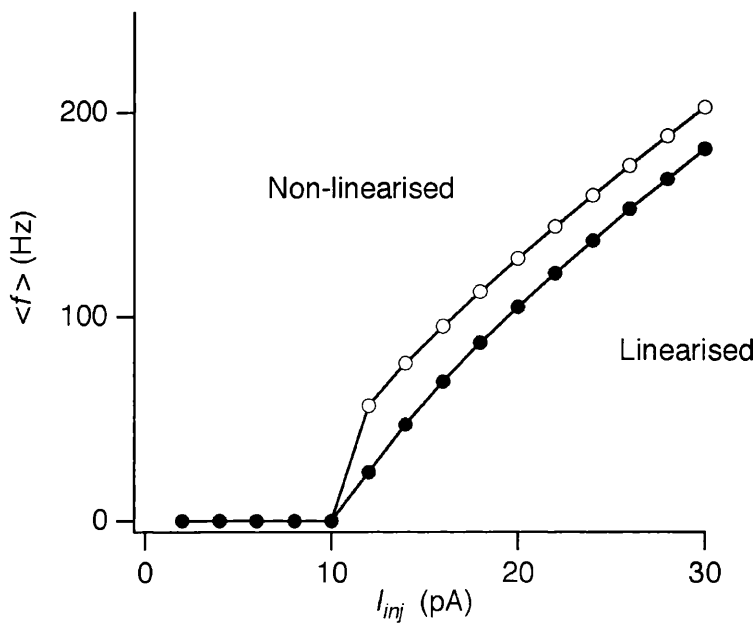
5.2 Specific parameters and optimisation of I-f model

The model implemented here is a variation on the above model where the

membrane resistance is replaced by a membrane conductance with a specific

reversal potential (figure 5.2**Ai**). A conductance passes current (I) according to the

product of its conductance magnitude (G) and its driving force (membrane

potential minus its reversal potential, E_{rev}),

$$I(t) = G(t) \cdot \left(V_m(t) - E_{rev}\right).$$ (5.3)

The voltage derivative is affected by the current associated with G_m (I_{Gm}) can be

calculated using equation 5.1.

$$C_m \frac{dV_m(t)}{dt} = I_{inj}(t) - I_{G_m}(t).$$ (5.4)

This equation can be numerically integrated to obtain $V_m(t)$.

The parameters for the model were set to values that reflected experimentally

derived data. Granule cells exhibit inward rectification with the input resistance

ranging from 0.6 and 5.1 GΩ, at –88 and –55 mV, respectively (D'Angelo, et al,

1995).

This characteristic was not implemented in the model. Instead, the input

conductance was set to the reciprocal of around half the maximal value, at 380 pS

(2.6 GΩ) set in series with a –70 mV battery, setting the resting membrane

potential to –70 mV. The capacitance was set to 3.1 pF (Silver et al, 1992). For

subthreshold current injections the model charges to the voltage, I_{inj}/G_m with a

time constant, C_m/G_m. At a spiking threshold of –44 mV (D'Angelo et al, 1995,

1998), the V_m was set to 10 mV, then to −82 mV, until a refractory period of 0.5

ms had passed. During this refractory period integration is effectively stopped,

analogous to the shunting action of an action potential (Häusser et al, 2001).

The f-I relationship for the model is shown in figure 5.2**B**. The current threshold

(I_{th}) for spiking is equal to $G_m \cdot (V_{th} - E_{Gm}) = 10$ pA, which is within the

physiological range for this cell type (figure 5.2**C**; D'Angelo et al, 1995, 1998).

The relationship exhibited the classic steep slope at I_{th} (compare figure 5.1**B** with

5.2**B**, top trace), which became shallower with increasing I_{inj}. However, since real

granule cells exhibit linear f-I relationships, this characteristic was included in the

model (figure 5.2**C**; D'Angelo et al, 1995, 1998; Brickley et al, 1996). One

method to achieve this is the addition of negative feedback. This can be achieved

by the addition of an adapting conductance that is proportional to the firing rate

(Wehmeier, et al, 1989; Ermentrout, 1998; Wang, 1998). The physiological

correlate of this is the calcium-activated potassium conductance (K_{Ca}; Ermentrout,

1998; Wang, 1998). During spiking, calcium enters via voltage-gated calcium

currents and accumulates proportionally with the firing number and rate (Gamble

and Koch, 1987; Helmchen et al, 1996). This calcium, as well as serving other

purposes, can activate K_{Ca} thereby reducing the excitability of the cell by

decreasing R_m, and reducing the temporal integration of synaptic inputs by

accelerating τ, lowering the firing frequency. This manipulation affects low-

frequency firing more than high-frequencies as the firing rate is inversely

proportional to $t_{ref} - \tau \ln(1 - (V_{th}/I_m R_m))$ (equation 2.6). As I_m grows larger, the firing

rate becomes more dependent on t_{ref}, which is insensitive to the other cellular

parameters. However, K_{Ca} would induce progressive adaptation throughout the

spike train, which is not observed in the granule cell (Gabbiani et al, 1994;

D'Angelo et al, 1995). I have therefore devised method to linearise the f-I curve

without inducing slow adaptation. To achieve this a conductance (G_K) with a

potassium-like reversal potential of –90 mV was introduced to the model (figure

5.2A*ii*). At rest G_K was equal to zero. When a spike was induced, G_K was set to a

maximal level ($G_{max, K}$), and decayed to resting levels with a single exponential

time constant, (τ_K). Since, G_K does not summate with successive spikes, the firing

frequency reaches steady state during the first interpulse interval: that is, no spike

adaptation occurs during the spike train.

The values for $G_{max, K}$ and τ_K were chosen by comparing the f-I curves derived

from models with different G_K parameters to a linear relationship with a slope of

10 Hz.pA^{-1} and a current threshold of 10 pA. The parameters were chosen

according to a sum of squared errors (SSE) minimisation criterion. This analysis

yielded empirically optimal values of 10 pS and 40 ms for $G_{max, K}$ and τ_K,

respectively. The f-I curves for the G_K-optimised and non-optimised models are

shown for comparison in figure 5.2B.

A potassium-like adapting conductance was used to confer specific granule cell

properties. In particular, the widely observed non-adapting spiking response to

current injection and linear f-I characteristics were used to allow the model to act

as a linear detector of excitation. However, a granule cell in a slice expresses

multiple voltage-gated ion channels, which are permeable to sodium, potassium,

calcium that activate/ inactivate on fast and slow timescales. Indeed, a recent

modelling study suggests that the inclusion of a slow potassium conductance can

promote complex firing patterns such as theta-frequency bursting and resonance

(D'Angelo et al, 2001). Therefore, the conclusions derived from the modelling

study presented in this thesis, as from all modelling studies, should be verified in

real neurones.

Table 5.1 Synaptic conductance parameters

Conductance	Parameter					
	τ_{rise} (ms)	τ_1 (ms)	τ_2 (ms)	A_1	k_s	$G_{max,1}$ (pS)
G_{AMPA}[1]	0.17	0.9	8.8	0.870	0.588	661
G_{NMDA}[2]	3.00	39.0	123.0	0.650	0.792	667
G_{GABA}[1]	0.29	4.1	22.5	0.405	0.855	3100

[1] Derived from own data

[2] Derived from D'Angelo et al (1994)

5.3 Synaptic conductances

The time courses of synaptic conductances were modelled with the sum of three

exponential functions (equation 5.5, below) using the parameters shown in table

5.1 for rise time constant (τ_{rise}), fast and slow decay time constants (τ_1 and τ_2,

respectively) and relative amplitude of the fast decay component (A_1), measured

during the voltage-clamp experiments detailed in this thesis. The peak of this

function was normalised to 1 using a constant (k_s) and scaled by the peak

conductance, G_{max}.

$$G(t) = G_{max} \cdot k_s \cdot \left(\left(1 - e^{-t/\tau_{rise}}\right) - A_1 \cdot \left(1 - e^{-t/\tau_1}\right) - \left(1 - A_1\right) \cdot \left(1 - e^{-t/\tau_2}\right) \right) \qquad (5.5)$$

Figure 5.3 – Properties of modelled synaptic conductances. **A**, Non-NMDA conductance. ***i***, Normalised conductance waveform. ***ii***, Peak current-voltage relationship (I-V) for non-NMDA conductance of 661 pS. **B**, NMDA conductance. ***i***, Normalised conductance waveform. ***ii***, Non-linear I-V plot and two linear I-V plots, with g_∞ (g (inf)) calculated at –57 mV (0.17) and –46 mV (0.27), for $G_{max,l}$ of 667 pS (see text for details). **C**, GABA conductance. ***i***, Normalised conductance waveform for phasic inhibition. ***ii***, I-V plots for phasic and tonic inhibition for conductances of 3100 and 100 pS, respectively.

A *i*

non-NMDA

100 ms

ii

Current (pA)
50

-100   -50   50
                    Voltage (mV)

-50

-100

B *i*

NMDA

100 ms

ii

Current (pA)
40

Non-linear

20

g (inf) = 0.27
g (inf) = 0.17

-100   -50   50

Voltage (mV)

-20

C *i*

GABA

100 ms

ii

Current (pA)
400

Phasic

200

Tonic

-100   -50   50

Voltage (mV)

-200
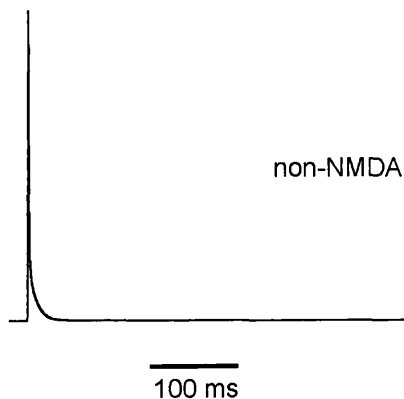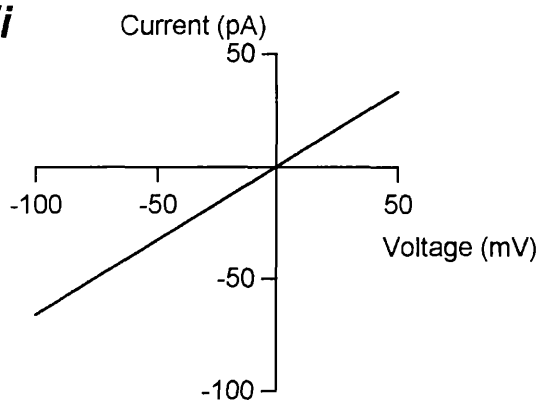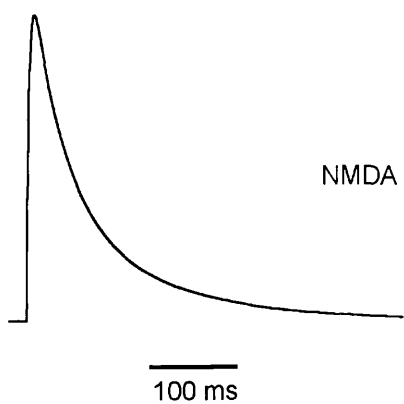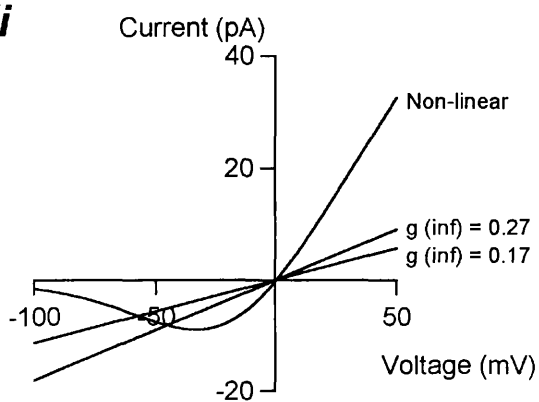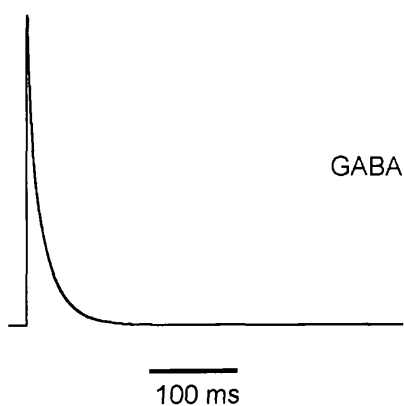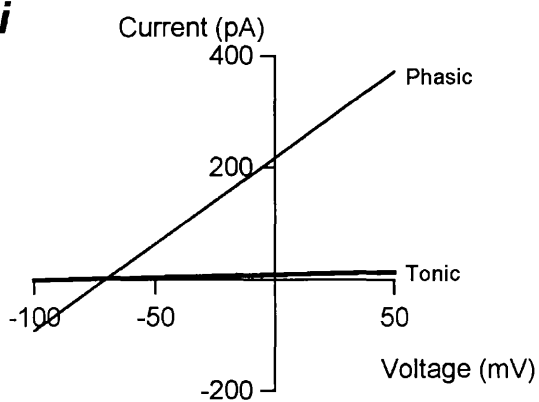
G_{max} is a function of the peak conductance at 1 Hz ($G_{max,1}$), normalised frequency-dependent depression ($F(f)$), normalised frequency-dependent modulation ($M(f)$), normalised modulation as a function of conditioning fibre ($C(f_c)$) and a scaling factor (k_c), which determines the maximal conditioning at 1 Hz as described in section 5.5.

The non-NMDA synaptic waveform ($G_{AMPA}(t)$; figure 5.3**A*i***) was calculated with equation 2.5 using the relevant parameters from table 5.1. The non-NMDA receptor mediated synaptic conductance had a reversal potential of 0 mV and its current-voltage relationship is shown in figure 5.3**A*ii*.**

The NMDA receptor-mediated conductance, $G_{NMDA}(t)$ (figure 5.3**B*i***) was initially modelled in the same way as $G_{AMPA}(t)$. However, the parameters τ_{rise}, τ_1, τ_2 and g_{max} were derived from those reported by D'Angelo et al (1994) at –40 mV (except g_{max} that was derived at 50 mV which is in the near linear region of the NMDA receptor current-voltage relationship). $G_{NMDA}(t)$ was multiplied by a gating factor (Jahr and Stevens, 1990a), $g_\infty(V_m,[Mg^{2+}]_o)$, that characterises the voltage dependence of the magnesium block of the NMDA receptor-linked ion channel as a function of membrane voltage and the external magnesium concentration ($[Mg^{2+}]_o$; Nowak et al, 1984), which was 1 mM,

$$g_\infty(V_m,[Mg^{2+}]_o) = \frac{1}{\left(1 + e^{-\alpha V_m} \cdot \dfrac{[Mg^{2+}]_o}{\beta}\right)},$$
(5.6)

where $\alpha = 0.062$ mV^{-1}, $\beta = 3.57$ mM and [Mg^{2+}]$_o$ = 1 mM. Equation 5.6 is a

simplification of the relationship as it ignores the kinetics of the channel voltage-

dependence (Jahr and Stevens, 1990b; Gabbiani et al, 1994). The NMDA receptor

mediated synaptic conductance had a reversal potential of 0 mV. For control

experiments, the voltage dependence of the NMDA component was removed,

replaced by a fixed g_∞ value that was equal to g_∞(-57 mV, 1 mM) = 0.17 or g_∞(-46

mV, 1 mM) = 0.27. The waveform and current-voltage relationships for the non-

linear and linear NMDA synaptic components are shown in figure 5.3**B***ii*.

GABA inhibition was modelled as two components. Phasic inhibition ($G_{GABA}(t)$)

was modelled in a similar way to G_{AMPA}, using measured parameters, according to

the equation 5.5, using the relevant parameters from table 5.1. The waveform of

phasic inhibition is shown in figure 5.3**C***i*. Tonic GABA-mediated inhibition was

modelled by including a passive conductance of 100 pS (Tia et al, 1996, Brickley

et al, 1996, Wall and Usovicz, 1997). Both phasic and tonic GABA-mediated

conductances had a reversal potential of −70 mV. Their current-voltage

relationships are shown in figure 5.3**C***ii*.

The currents driven by each synaptic conductance ($I_{syn}(t)$) were calculated

according to the product of the driving force and conductance, with the sum of

these currents used to determine the voltage derivative,

$$C_m \frac{dV_m(t)}{dt} = I_{inj}(t) - I_{G_m}(t) - \sum_{syn} I_{syn}(t) \qquad (5.7)$$

where syn = {AMPA; NMDA; GABA}.

Figure 5.4 – Normalised modulation curves for glutamate release (open circles) and GABA release (filled circles). **A**, Dependence of postsynaptic currents on presynaptic fibre firing frequency ($F(f)$), normalised to 1 Hz. Dashed line to right of glutamate curve indicate area of linear extrapolation of this relationship, which was required for some simulations. **B**, Dependence of heterosynaptic modulation on presynaptic fibre firing frequency ($M(f)$), normalised to 1 Hz. **C**, Dependence of heterosynaptic modulation on conditioning fibre firing frequency ($C(f_c)$), normalised to maximum known conditioning fibre firing frequency.

A

B

C
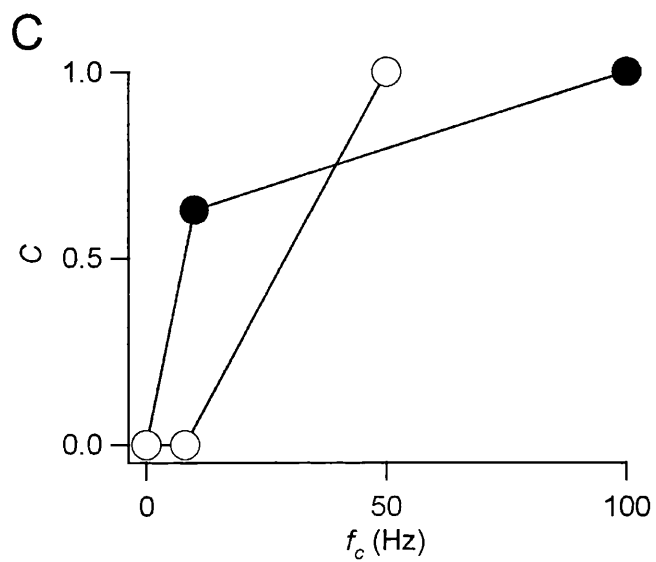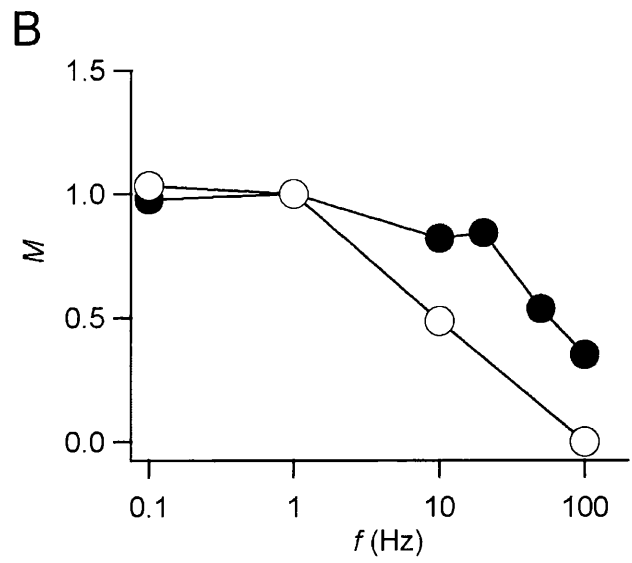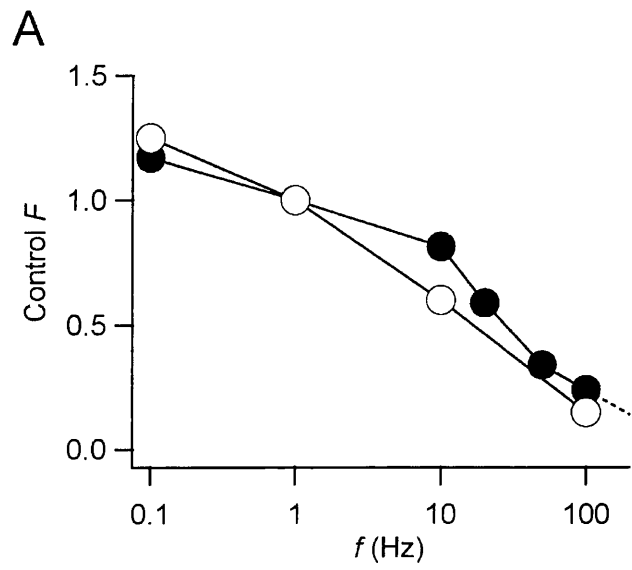
5.4 Synaptic plasticity

The efficacy of synaptic transmission is dependent on the firing frequency of the

presynaptic neurone (Magleby, 1987; Zucker, 1989; Chs 3, 4; Mitchell and Silver,

2000a, 2000b). To emulate this property, the magnitude of the parameter G_{max} for

each conductance was frequency-dependent. For the non-NMDA and phasic

GABA conductances the mean steady-state frequency-dependence of

neurotransmission normalised to 1 Hz (control $F(f)$), was derived from previous

experiments (Chs 3, 4; Mitchell and Silver, 2000a, 2000b). These relationships

were constructed from experiments in which neurotransmission was evoked at 0.1,

1, 10 and 100 Hz (figure 5.4**A**). In simulations where it was necessary to model

transmission at intermediate frequencies, control $F(f)$ was calculated using log-

linear interpolation (figure 5.4**A**). The NMDA-receptor mediated component was

assumed to have the same frequency-dependence as the non-NMDA component.

The onset kinetics of short-term plasticity were not included in this steady-state

model.

5.5 Heterosynaptic modulation

Active mossy fibres inhibit the release of GABA from Golgi cells via mGluRs

(Ch. 3; Mitchell and Silver, 2000a). Conversely, active Golgi cells depress the

release of glutamate from mossy fibres by activating $GABA_B$ receptors (Ch. 4;

Mitchell and Silver, 2000b). For both mechanisms, the degree of inhibition was

dependent on the frequency of both the conditioning and the conditioned fibre.

5.5.1 Modulation depends on firing frequency of conditioned fibre

The steady-state dependence of modulation on the frequency of the conditioned

fibre $(M(f))$, was calculated, and normalised to 1 Hz, according to,

$$M(f) = \left(1 - \frac{\text{modulated } F(f)}{\text{control } F(f)}\right) \Big/ \left(1 - \frac{\text{modulated } G_{max,1}}{\text{control } G_{max,1}}\right), \qquad (5.8)$$

where "modulated" refers to data for the given parameter for excitation or

inhibition in the presence of 100 µM baclofen or 100 µM ACPD, respectively.

The modulated $F(f)$ for the IPSC was corrected for the 8 Hz increase in Golgi cell

firing rate induced by ACPD, which was assumed to be superimposed onto the

stimulation rate at all frequencies. This correction was implemented by evaluating

the degree of frequency-dependent depression induced by a move from frequency

f to $(f+8)$ Hz, by log-linear interpolation, or extrapolation as appropriate, of

control $F(f)$, where $f = \{0.1; 1; 10; 100\}$ Hz. These resulting values were

subtracted from the apparent % inhibition induced by ACPD, to yield the

depression due to a direct action on release. $M(f)$ relationships for release of

GABA and glutamate are shown in figure 5.4**B**.

5.5.2 Modulation depends on firing frequency of conditioning fibre

The dependence of modulation on conditioning-fibre firing frequency $(C(f_c))$ was

based on experimental observations regarding the modulation of

neurotransmission with physiologically released glutamate and GABA (Chs 3, 4;

Mitchell and Silver, 2000a, 2000b). Golgi cells fire spontaneously at 8 Hz at 37

°C, tonically releasing GABA (Tia et al, 1996, Brickley et al, 1996, Wall and

Usovicz, 1997). It was found that tonic GABA release did not activate GABA$_B$

receptors on mossy fibres at physiological temperatures. However, these receptors

can be activated if a single Golgi cell is stimulated at 50 Hz, depressing the EPSC

to 76 % of control. These data were used to model $C(f_c)$ for this effect, which was

normalised to the $f_c = 50$ Hz value (figure 5.4C).

$C(f_c)$ for mGluR-mediated inhibition of GABA release was modelled in a similar

way. Firstly, mossy fibres are not tonically active and ambient levels of glutamate

in the slice are insufficient to induce IPSC depression. Secondly, when a Golgi

cell was stimulated at 5 Hz, conditioning via mossy fibre stimulation at 10 Hz and

100 Hz depressed the IPSC to 66 % and 46 % of control, respectively, with a rapid

onset and sustained efficacy. These data were used to model $C(f_c)$ for this effect,

which was normalised to the $f_c = 100$ Hz value (figure 5.4C). The levels of

conditioning at intermediate frequencies were derived by linear interpolation of

$C(f_c)$. The relationship $C(f_c)$ was scaled by a variable, k_c, to obtain the

relationship for a specific simulation. The parameter, k_c was varied from 0 to 100

% maximal inhibition, respectively.

Frequency-dependent and heterosynaptic depression was implemented by

calculating G_{max} for use with equation 5.5 according to,

$$G_{max} = \text{control}\, G_{max,1} \cdot F(f) \cdot M(f) \cdot \left(1 - k_c \cdot C(f_c)\right) \qquad (5.9)$$

Figure 5.5 – Phasic modulation as represented as tonic. **A*i***, Train (5

Hz) of non-NMDA receptor mediated synaptic conductances. ***ii***, Train

of GABA synaptic conductances at the same frequency and phase as the

excitation. ***iii***, Same as ***ii*** except inhibitory train exactly out of phase

with excitation. **B**, Summation of inhibitory synaptic conductances

simulated at stated frequencies. Dashed line indicates zero level. Bold

lines show equivalent mean level of tonic inhibition.
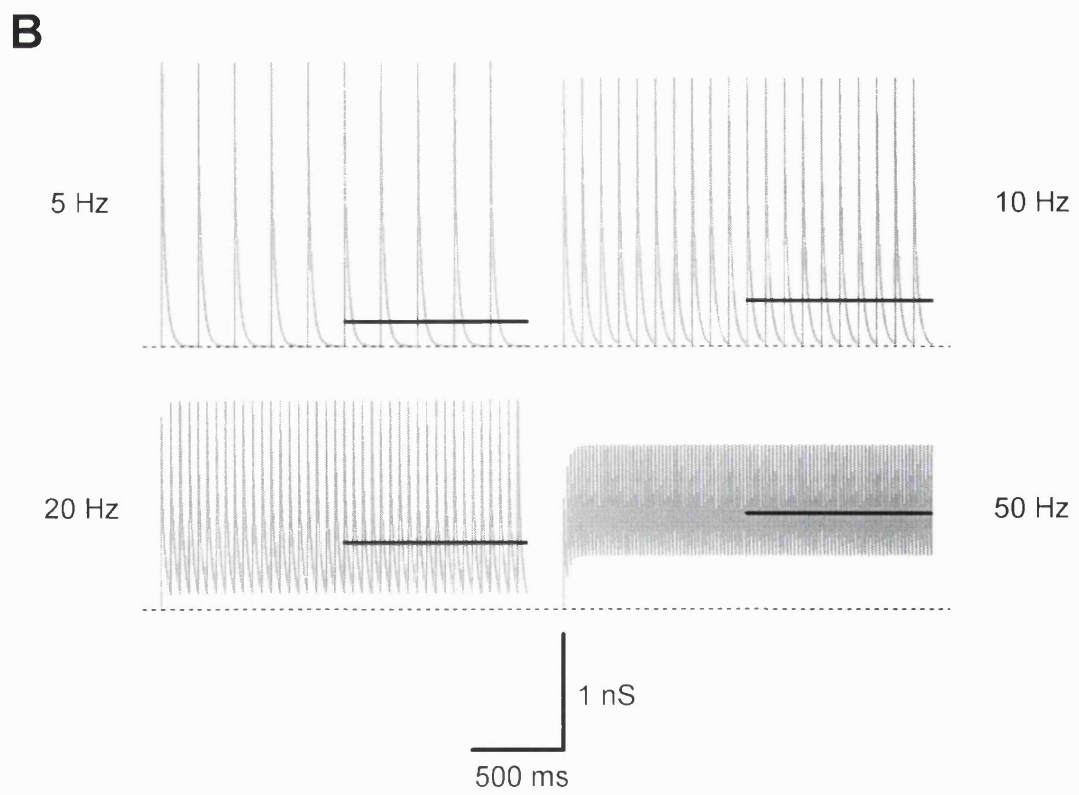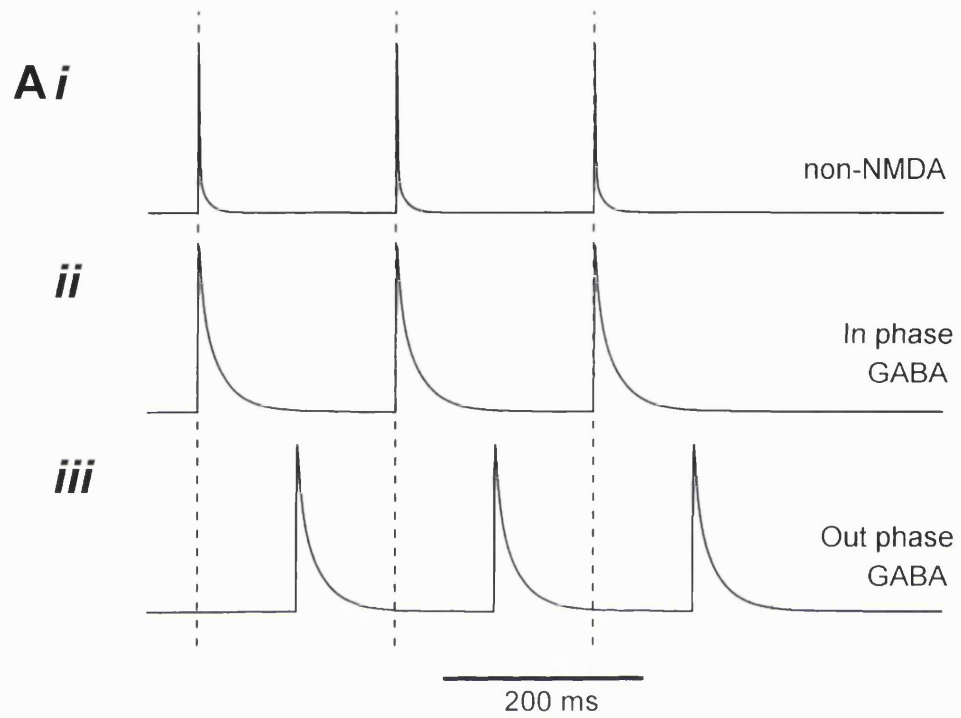
5.6 The reduction of phasic inhibition to tonic

Phasic inhibition will interact with phasic excitation in a complex manner. When

the inhibition is in phase with the excitation (figure 5.5A*i*) its effect will be

maximal. However, when the inhibition is 90° out of phase with the excitation, the

inhibition may have no effect at low frequency (figure 5.5A*ii*). To investigate the

mean effect of a particular level of inhibition, phasic inhibition would have to be

applied at numerous phase positions, with the results averaged. A functionally

equivalent solution was to implement tonic inhibition that captured the features of

phasic response (Gabianni et al, 1994). The level of tonic inhibition was

calculated by first calculating G_{max} for the individual IPSC as described above,

including short-term plastic and modulation properties. Then a train of IPSCs was

made at the appropriate frequency (figure 5.5**B**). Once the level of temporal

summation had reached a steady-state level, the mean level of inhibition was

measured from the stable region (figure 5.5**B**). This figure was implemented as a

tonic shunting conductance, which was added to the unmodulatable tonic GABA

conductance.

5.7 Numerical integration methods

Both models were executed using custom written procedures in Igor Pro 3.1

(Wavemetrics). The differential equations were numerically integrated using an

Euler algorithm (Press et al, 1993), which calculates the next point value

according to,

$$V_m(t + \Delta t) = V_m(t) + \Delta t \cdot \frac{dV_m(t)}{dt}, \qquad\qquad (5.10)$$
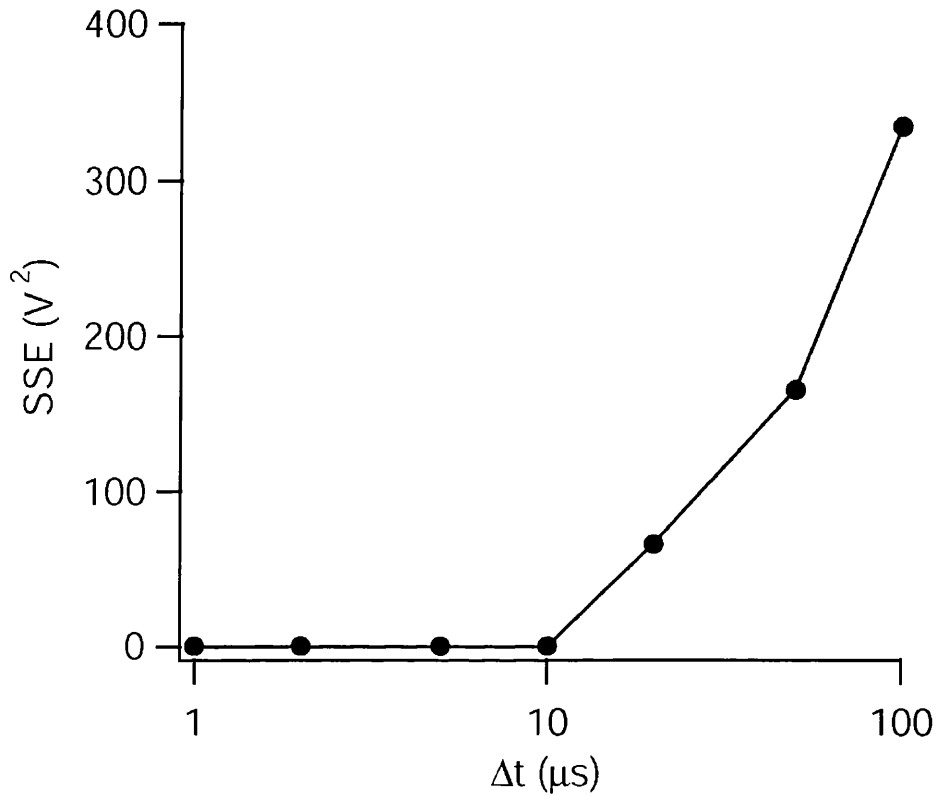
Figure 5.6 – Optimisation of integration time step. Step current
command of 5 pA was applied into single compartment model with
properties: R_m = 500 MΩ; C_m = 3.1 pF. Sum of squared errors between
analytical and computational solutions fro voltage response at various
Δt.

where Δt is the integration time step. The accuracy of this approach is highly

dependent on Δt and therefore needs to be small enough to represent derivative

changes with time adequately. However, computing power is finite, making it

necessary to use the largest value for Δt to obtain an accurate result. In the

integrate and fire model this was assessed by injecting a step current pulse of 5 pA

and comparing the resulting evolution of $V_m(t)$ with the mathematical solution for

a single compartment. The SSE between the computational and analytical

solutions for each Δt is shown in Figure 5.6. The integration time step for this

investigation was set to 10 µs.

5.8 Model analysis

Although the model did not exhibit spike rate adaptation the synaptic

conductances driving the spiking were time dependent. It was therefore necessary

to allow the model to reach steady state before measuring mean firing rate. For

current step-driven spiking the mean interpulse interval was derived from the last

400 ms of the 800 ms step. For synaptic conductance driven spiking, the mean

interpulse interval was derived from the second half of the mossy fibre train.

CHAPTER SIX

THE EFFECT OF HETEROSYNAPTIC MODULATION ON GRANULE CELL SPIKING

6.0 Abstract

Neurones integrate excitatory and inhibitory postsynaptic currents to produce

trains of action potentials. The spiking rate of the cell depends on the balance of

excitation and inhibition, which in turn depends on the firing rate and frequency-

dependent short-term plasticity of the synaptic inputs. Presynaptic modulation of

transmitter release, which can regulate this balance, appears to have a role in the

cerebellar glomerulus since glutamate spillover suppresses Golgi cell-mediated

inhibition of granule cells and GABA spillover inhibits their excitation by mossy

fibres (Chs 3 and 4). To understand how heterosynaptic modulation regulates

spiking in granule cells, I have combined a steady-state model of these processes

with an integrate-and-fire unit. The modelling suggests that mGluR-mediated

suppression of inhibition at 20 Hz GoS boosts spiking during high-frequency

mossy fibre transmission, as previously proposed (Ch. 3). This effect increased the

slope of the relationship between mossy fibre firing rate and granule cell spiking

frequency (f-F relationship). However, two findings were not consistent with the

previous proposals. First, the graded dependence of mGluR activation on mossy

fibre frequency was not essential to change the slope of the f-F relationship, since

reducing the frequency of Golgi cell stimulation mimicked this effect. Second,

even though mGluR-mediated inhibition of GABA release decreased with

increasing Golgi cell firing rate, presynaptic mGluR-mediated boosting of spiking

increased with increasing Golgi cell frequency. Implementation of tonic rather

than phasic excitation removed the ability of mGluR-mediated disinhibition to

change the slope of the f-F relationship. These findings indicate that an interaction

between the non-linear, threshold properties of the excitable model and phasic

excitation is required for the selective boosting of granule cell spiking driven by

high-frequency inputs by mGluRs. $GABA_B$-R-mediated suppression of excitation

attenuated low-frequency mossy fibre transmission, as previously proposed (Ch.

4). This study suggests that activation of presynaptic metabotropic receptors

enhance contrast between granule cells driven by high- and low-frequency mossy

fibres.

6.1 Passive and active properties of the integrate and fire model

The granule cell (GC) is a small cell with short dendrites (Hámori and Somogyi,

1983). Electrophysiological and modelling studies have shown that GC dendrites

and soma act as a single electrical compartment (Silver et al, 1992, 1996c;

D'Angelo et al, 1993, 1995; Gabbiani et al, 1994). I have therefore modelled the

electrical properties of the GC using a linearised integrate-and-fire unit to simulate

the basic synaptic integration and spiking properties of GCs, as described in the

methods. All simulations were performed from a resting potential of –70 mV. The

input resistance of GCs ranges from 0.5 to 5 $G\Omega$, due to inward rectification

(D'Angelo et al, 1995, 1998). This relationship was simplified in the model GC by

implementing a tonic input conductance of 380 pS (2.6 $G\Omega$) in parallel with a 3.1

pF capacitance. Consistent with the predicted electrical properties of the model, a

current injection of 5 pA induced a voltage deflection that rose exponentially to a

Figure 6.1 – Passive and active properties of integrate-and-fire model. **A**, Voltage transients evoked by square current pulses of varying amplitude (timing of pulses indicated by waveform labelled *Current*). *Bold line* shows fit to rising phase using exponential function with time constant of 8 ms. **B**, Voltage-current relationship for steady-state voltage deflection evoked by square current pulse. Linear fit indicated slope of 2.6 GΩ. **C**, Voltage responses to sub and supra threshold current injections at stated amplitudes. **D**, Mean steady-state spiking rate of the model as a function of injected current (f-I relationship).

A

Current

8 ms

-70 mV

4 mV

100 ms

B

Voltage (mV)

2.6 GΩ

Current (pA)

C

Current

-70 mV   30 pA

-70 mV   12 pA

-70 mV   10 pA

10 mV

200 ms

D

Gr <f> (Hz)

Current (pA)
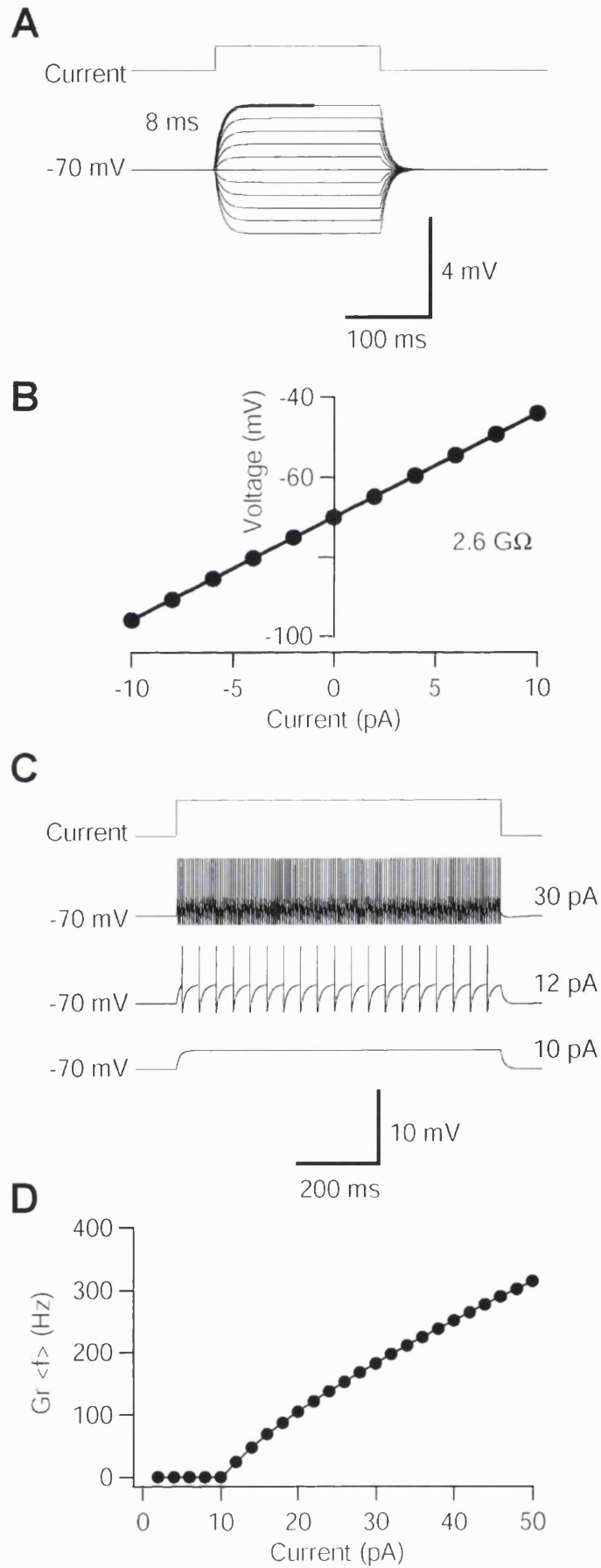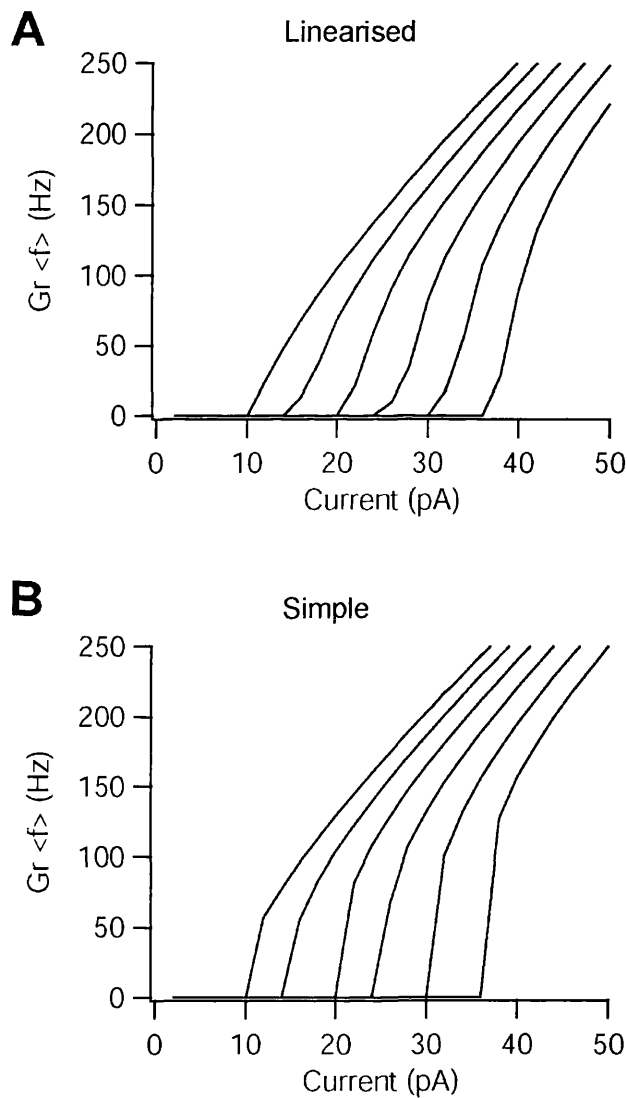
Figure 6.2 – Tonic inhibition shifts f-I relationship to left in linearised
model (i.e. leaky integrate-and-fire model with potassium conductance)
(A) and simple leaky integrate-and-fire models (B). Levels of tonic
inhibition used to generate curves for both models were (in pS; from
left curve to right): 0, 200, 400, 600, 800 and 1000.

steady-state potential of 13 mV with a time constant of 8 ms (figure 6.1**A**). The

amplitude of the voltage transient was linearly related to the amplitude of current

step (figure 6.1**B**). Current steps larger than 10 pA could depolarise the cell

beyond spiking threshold (-44 mV; figure 6.1**C**). The relationship between the

spiking rate and the amplitude of current injection (f-I relationship) was nearly

linear with a slope of ~10 pA/Hz (figure 6.1**D**), as observed in GCs in acute

cerebellar slices (D'Angelo et al, 1995, 1998; Brickley et al, 1996). These data

suggest that the model GC, although highly simplified, shared some properties

with cerebellar GCs in cerebellar slice.

6.2 Tonic inhibition induces a parallel shift in f-I relationship

To investigate how $GABA_A$-R-mediated inhibition affected the integration

properties of GCs, a passive conductance with a reversal potential of –70 mV was

introduced. This made the model less excitable, shifting the f-I relationship to the

right with increasing tonic inhibition (figure 6.2**A**). This behaviour was also

observed with an integrate-and-fire model without linearisation, indicating that

linearisation did not affect the modulation of current integration (figure 6.2**B**).

These data show that tonic inhibition reduces the excitability of the model by

inducing a parallel shift in the f-I relationship, consistent with an earlier slice

experiments (Brickley et al, 1996) and a modelling study (Holt and Koch, 1997).

6.3 Spatial and temporal summation of EPSPs and f-F relationship

The way in which the model granule cell integrated EPSPs was investigated by

simulating phasic excitatory conductances, as described in the methods. Excitation

Figure 6.3 – Spatial and temporal integration of simulated mossy fibre conductances. **A**, EPSPs from a holding potential of –70 mV, with (Control) and without NMDA receptor component (-NMDA), evoked at 0.1 Hz. **B**, Control EPSPs evoked by one or two mossy fibres at 0.1 Hz per fibre. Two fibres elicited spiking. **C**, Temporal summation of EPSPs evoked by one mossy fibre (MF) at stated frequencies. **D**, Temporal summation of EPSPs evoked by two mossy fibres at stated firing frequencies per mossy fibre. **E**, Mean steady-state spiking rate of the model as a function of MFS frequency (f-F relationships) for one to four mossy fibres. *Dashed lines* indicate spiking rates at two multiples of MFS frequency (two EPSPs per spike for *upper trace*; three EPSPs per spike for *lower trace*).
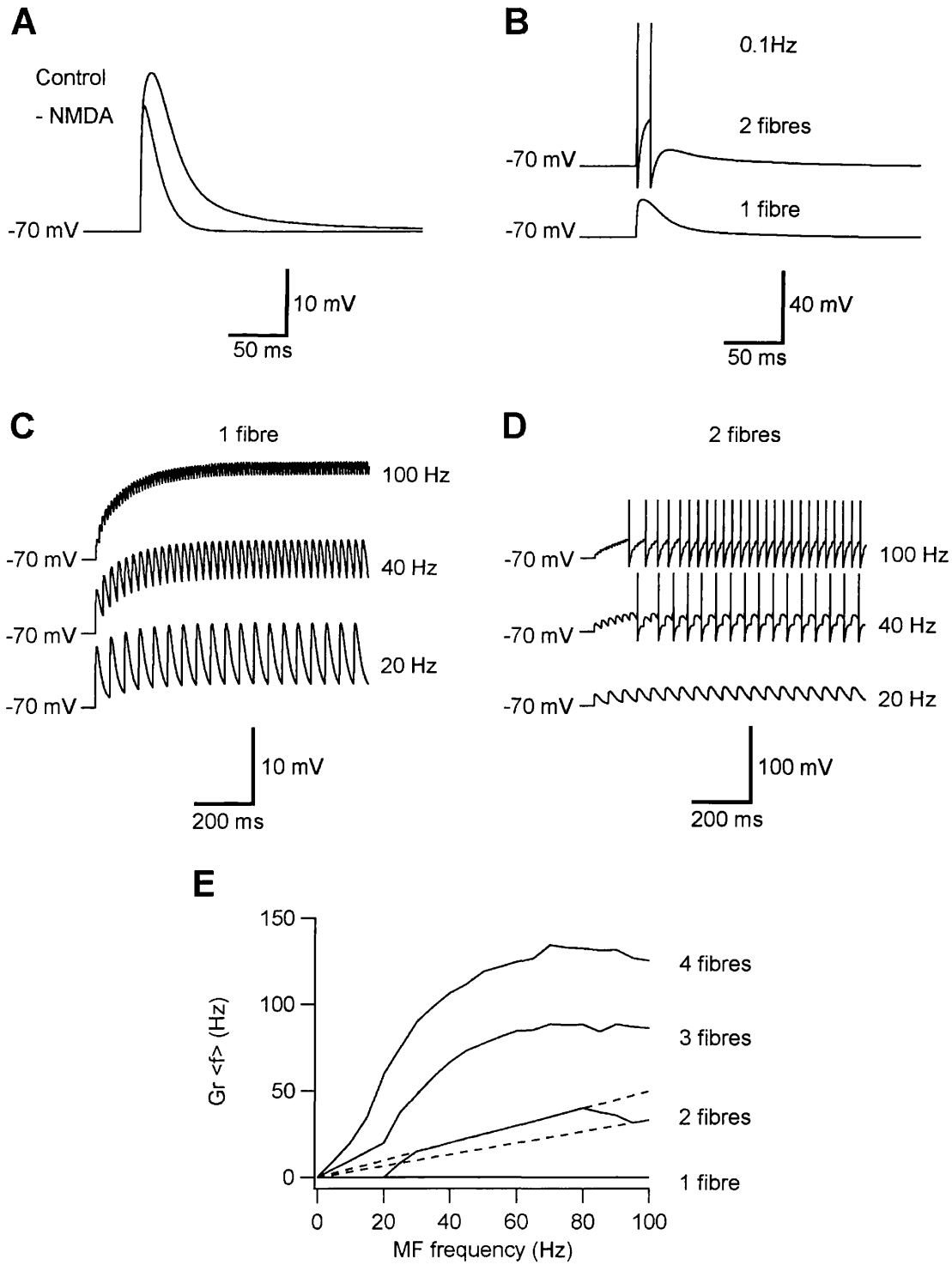
of the model by a single mossy fibre (0.1 Hz) produced subthreshold EPSPs that

decayed more slowly than the membrane time constant (figure 6.3**A**), due to the

prolonged conductance of the NMDA receptor component. The non-NMDA

receptor-mediated EPSP decayed monotonically with decay kinetics limited in

part by the RC time constant (figure 6.3**A**), consistent with the properties of real

GCs (D'Angelo et al, 1995).

The level of excitation required to induce spiking in the model was investigated by

simulating spatial and temporal summation of EPSPs. Summation of

synchronously active mossy fibre inputs (spatial summation) was simulated with

integer multiples of between one and four mossy fibre conductances. EPSPs

generated by two synchronously activated mossy fibres at 0.1 Hz were required to

reach spiking threshold (figure 6.3**B**). Increasing the frequency of mossy fibre

stimulation will invoke two mechanisms with opposing effects on the level of

excitation. The amplitude of the synaptic conductance will decrease, due to

frequency-dependent depression (Ch. 4; Mitchell and Silver, 2000b), while

temporal summation will increase. To investigate how the model integrated

repetitive excitation, conductances from one to four synchronous mossy fibres

were activated at 5 to 100 Hz. Despite the fact that EPSPs evoked by a single

mossy fibre exhibited strong temporal summation, reduction of the underlying

synaptic driving force and strong frequency-dependent depression of the synaptic

conductance limited spiking (figure 6.3**C**). With two mossy fibres, the spiking rate

increased from the threshold at 20 Hz mossy fibre stimulation frequency (MFS)

(figure 6.3**D**, **E**). The spikes were time-locked to the non-NMDA component of

Figure 6.4 – Modelling suppression of inhibition by activation of mGluRs. **A**, Level of $GABA_A$-R-mediated inhibition as a function of MFS rate under three conditions: 100 pS tonic inhibition only (Control); additional phasic inhibition modelled from 20 Hz GoS rate (20 Hz inhibition); 20 Hz GoS with mGluR-mediated inhibition of glutamate release (20 Hz + mGluR). **B**, f-F relationships for model with inhibitory conductances shown in **A**. **C**, Percentage increase in spike rate induced by inclusion of suppression of inhibition (boosting), calculated as ([(frequency with inhibition + mGluR) / (frequency with inhibition)] –1) * 100.

A

B

C
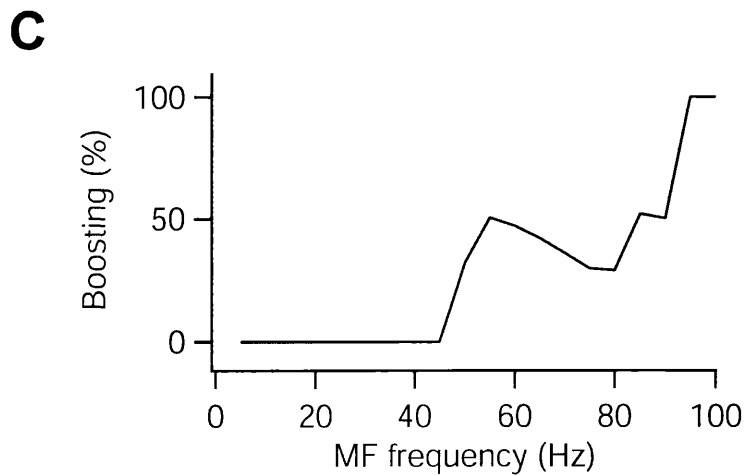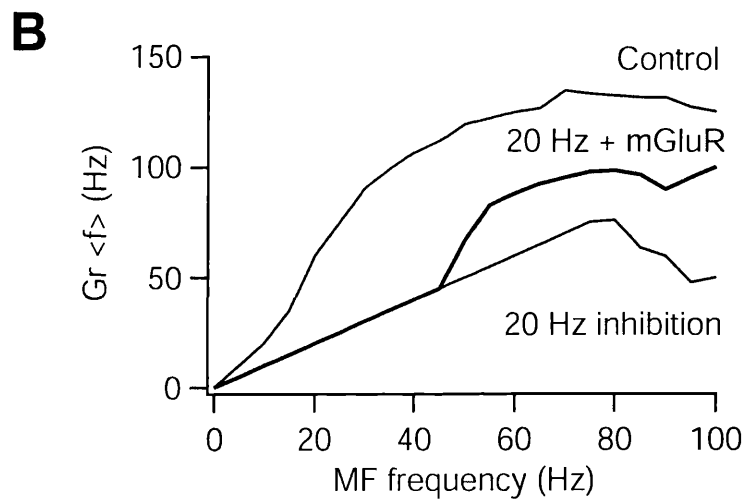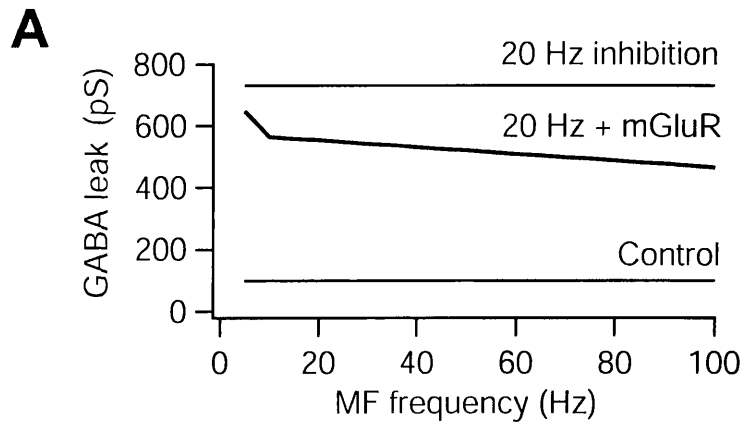
the EPSPs (figure 6.3**D**). The relationship between mossy fibre frequency and

model spike rate (f-F relationship) had a jagged appearance, as the spiking

frequency was driven from one multiple of MFS rate to another (figure 6.3**E**,

dashed lines). The f-F relationship for three and four inputs had a steep slope

around threshold, which reduced as the MFS rate increased towards 100 Hz,

where the spiking rate became independent of excitation frequency (figure 6.3**E**).

6.4 Suppression of inhibition by mGluRs

To investigate the role of mGluR-mediated inhibition of GABA release in

regulating synaptic integration in granule cells, $GABA_A$-R-mediated inhibition

was implemented in the model by calculating the amplitude of the unitary

inhibitory conductance from its dependencies on the firing frequencies of the

Golgi cell and mossy fibre. The mean steady-state inhibitory conductance was

implemented as a tonic leak with a −70 mV reversal potential, set in parallel to the

non-modulated tonic inhibition (100 pS), according to the methods (figure 6.4**A**).

The effects of inhibition of GABA release were investigated by simulating the f-F

relationship for four fibres over a range of Golgi cell stimulation (GoS) rates.

Incorporation of Golgi cell-mediated inhibition at 20 Hz reduced the average

spiking rate of the model at all MFS frequencies compared to control (figure

6.4**B**). Inclusion of mGluR-mediated inhibition of GABA release suppressed
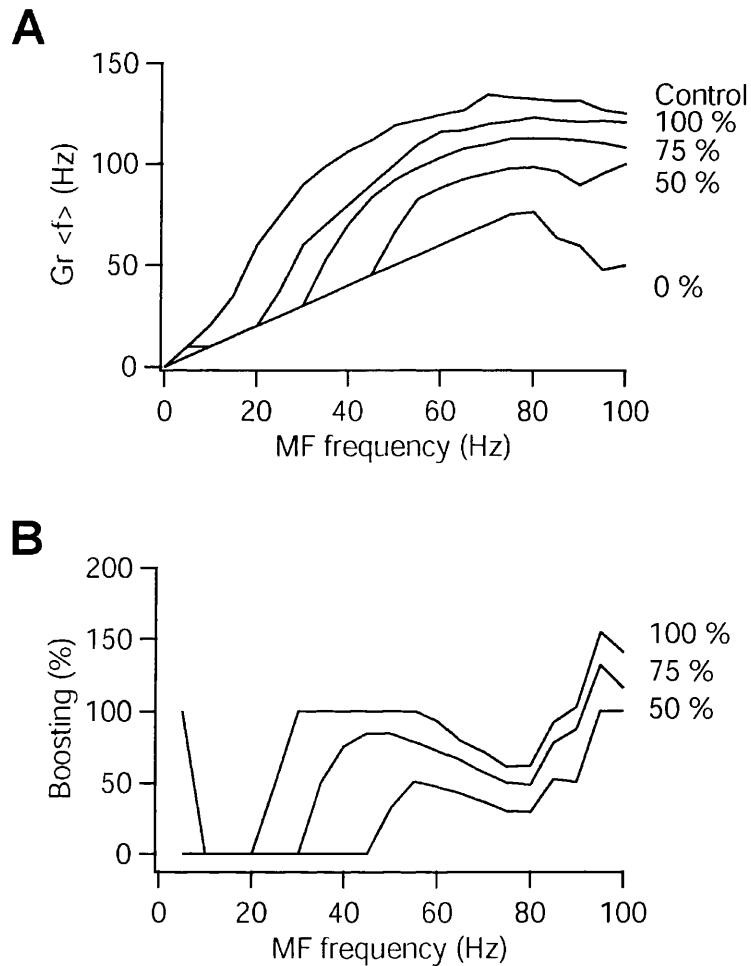
Figure 6.5 – The effect of increasing the level of suppression of inhibition on boosting of spike rate. **A**, f-F relationships for model with inhibition of GABA release at stated maximum possible % inhibition of GABA release. **B**, mGluR-mediated boosting of spike rate at stated efficacies.

inhibition with increasing MFS rate (figure 6.4**A**). This frequency-dependence

suggested that the increase in spike rate might also depend on MFS frequency.

Consistent with this, the spiking rate increased at MFS of 45 Hz and above,

changed the slope of the f-F relationship (figure 6.4**B**). This boosting was

quantified by calculating the percentage increase in spiking rate induced by

presynaptic mGluRs at each MFS frequency. This analysis revealed that mGluR-

mediated suppression of inhibition at 20 Hz GoS increased the spiking rate during

high-frequency MFS (figure 6.4**C**). This effect was also present in a model with

linear NMDA receptor properties (data not shown).

The simulations described so far, were carried out using a level of modulation of

the inhibitory conductance by glutamate spillover similar to that observed *in vitro*

(Ch. 3; Mitchell and Silver, 2000a). Using 20 Hz GoS, increasing the level of the

maximum level of mGluR-mediated inhibition of GABA release had two affects.

First, the magnitude of boosting increased, as expected (figures 5.5**A, B**). Second,

increasing the level of modulation also reduced the frequency of MFS required to

elicit boosting (boosting threshold; figure 6.5).

6.4.1 The relationship between suppression of inhibition and frequency of Golgi
       cell firing

Golgi cells can fire at 5-100 Hz *in vivo* (Edgley and Lidierth, 1987; van Kan et al,

1993). The level of mGluR-mediated modulation of IPSCs decreased with

increasing GoS rate (Ch. 3; Mitchell and Silver, 2000a). This finding led to the

proposal that mGluR-mediated inhibition of GABA release was less important

Figure 6.6 - The effect of increasing the frequency of GoS on boosting

of spiking. **A**, f-F relationships for model with GoS at stated

frequencies. **B**, f-F relationships for model with GoS at stated

frequencies and inhibition of GABA release. **C**, Normalised mGluR-

mediated boosting of spike rate at stated GoS frequencies. *Dashed lines*

indicate measurement window used to derive the mean boosting level

as a function of MFS frequency (**D**).

A

- mGluR

Gr <f> (Hz)

150

100

50

0

Control
5 Hz
10 Hz
20 Hz

30 Hz
40 Hz
50 Hz

0   20   40   60   80   100

MF frequency (Hz)

B

+ mGluR

Gr <f> (Hz)

150

100

50

0

Control
5 Hz
10 Hz
20 Hz
30 Hz
40 Hz
50 Hz

0   20   40   60   80   100

MF frequency (Hz)

C

Boosting (%)

800

600

400

200

0

40 Hz

30 Hz

20 Hz
10 Hz
5 Hz

0   20   40   60   80   100

MF frequency (Hz)

D

Boosting (%)

500

400

300

200

100

0

0   10   20   30   40

Inhibition frequency (Hz)
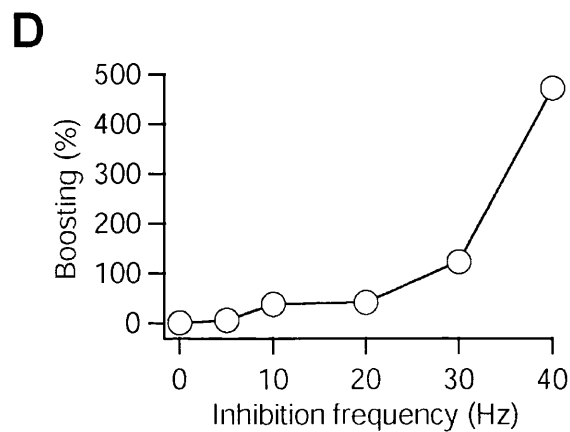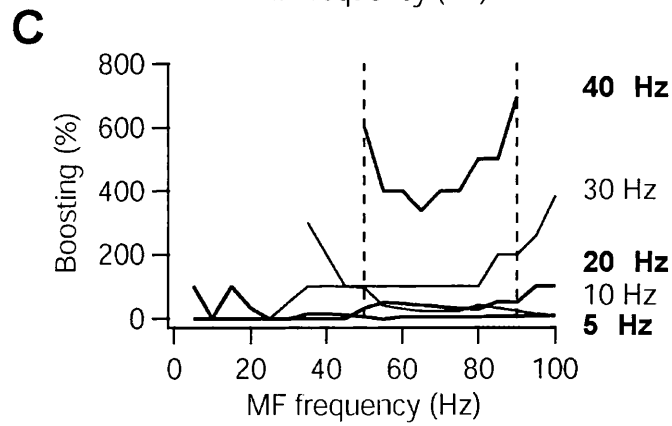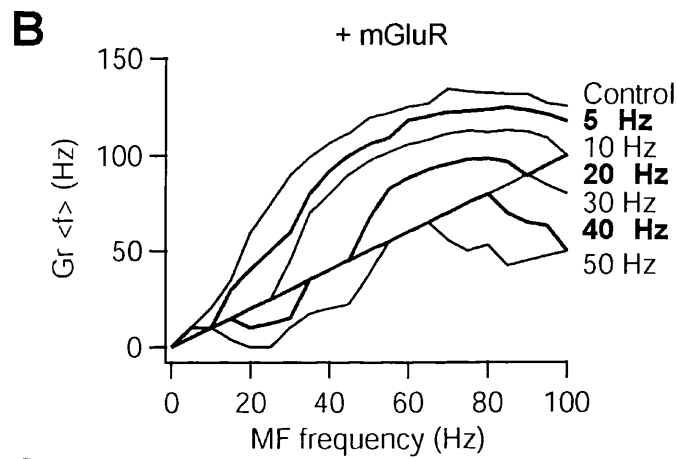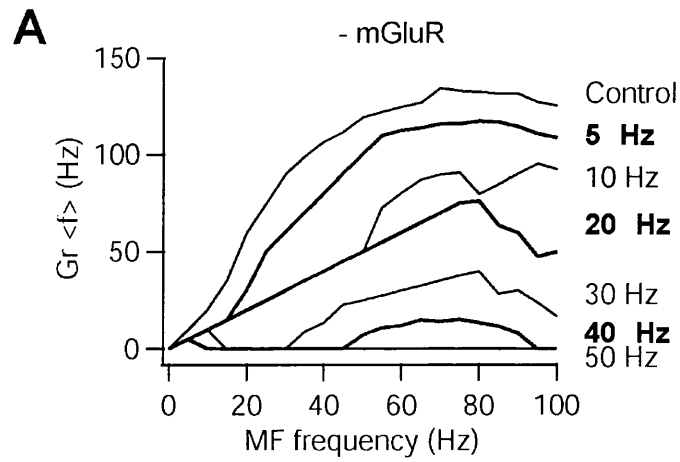
during high-frequency Golgi cell firing. However, the way in which the GC

spiking rate is affected by increasing GoS frequency is difficult to predict since

transmitter release is depressed at higher rates and temporal summation is

enhanced. The relationship between boosting of mossy fibre-driven spiking and

GoS rate was investigated using an mGluR-mediated inhibition of GABA release

level of 50 %.

Increasing GoS rate in the absence of mGluRs reduced the excitability of the

model, suppressing spiking and reducing the slope of the f-F relationship (figure

6.6**A**). Indeed, at GoS frequencies of 30 and 40 Hz the cell failed to spike at some

MFS frequencies, and at 50 Hz GoS rate firing was observed only at 5 Hz MFS

rate (figure 6.6**A**). Inclusion of mGluR-mediated inhibition of GABA release

increased the spiking rate at all GoS rates, and increased the slope of the f-F

relationship with GoS rates of 10-50 Hz (figure 6.6**B**). The level of boosting

reflected this effect (figure 6.6**C**). In cases where suppression of inhibition had

reinstated spiking that had been completely depressed by GoS alone (e.g. with 50

Hz GoS; figures 5.6**B, C**), the boosting level was infinite. Surprisingly, the mean

boosting level (measured between dashed lines of figure 6.6**C**) had a steep

supralinear relationship between GoS frequency and boosting level (figures 5.6**D**).

These simulations suggest that the boosting of excitatory inputs via mGluRs

increases with GoS rate, contrary to earlier predictions (Ch. 3; Mitchell and Silver,

2000a), and that changing the level of inhibition both via presynaptic mGluRs on

Golgi cells and by changing the GoS rate could change the slope of the f-F

relationship.

Figure 6.7 – Frequency-dependent inhibition of GABA release is not required for the selective boosting of high-frequency mossy fibres. **A**, A reduction in inhibition rate to 10 Hz from 20 Hz induces a similar decrease in the mean inhibition as including presynaptic mGluRs with an level of 50 %. A small frequency-dependence in suppression of inhibition is evident with mGluRs. **B**, f-F relationships for model with levels of GABA leak shown in **A**. **C**, A reduction in inhibition rate to 5 Hz from 20 Hz induces a similar reduction in the mean inhibition as including presynaptic mGluRs with a maximum level of inhibition of 100 %. A strong frequency-dependence in suppression of inhibition is evident with mGluRs at this level. **D**, f-F relationships for model with levels of GABA leak shown in **C**.

A

B

C

D
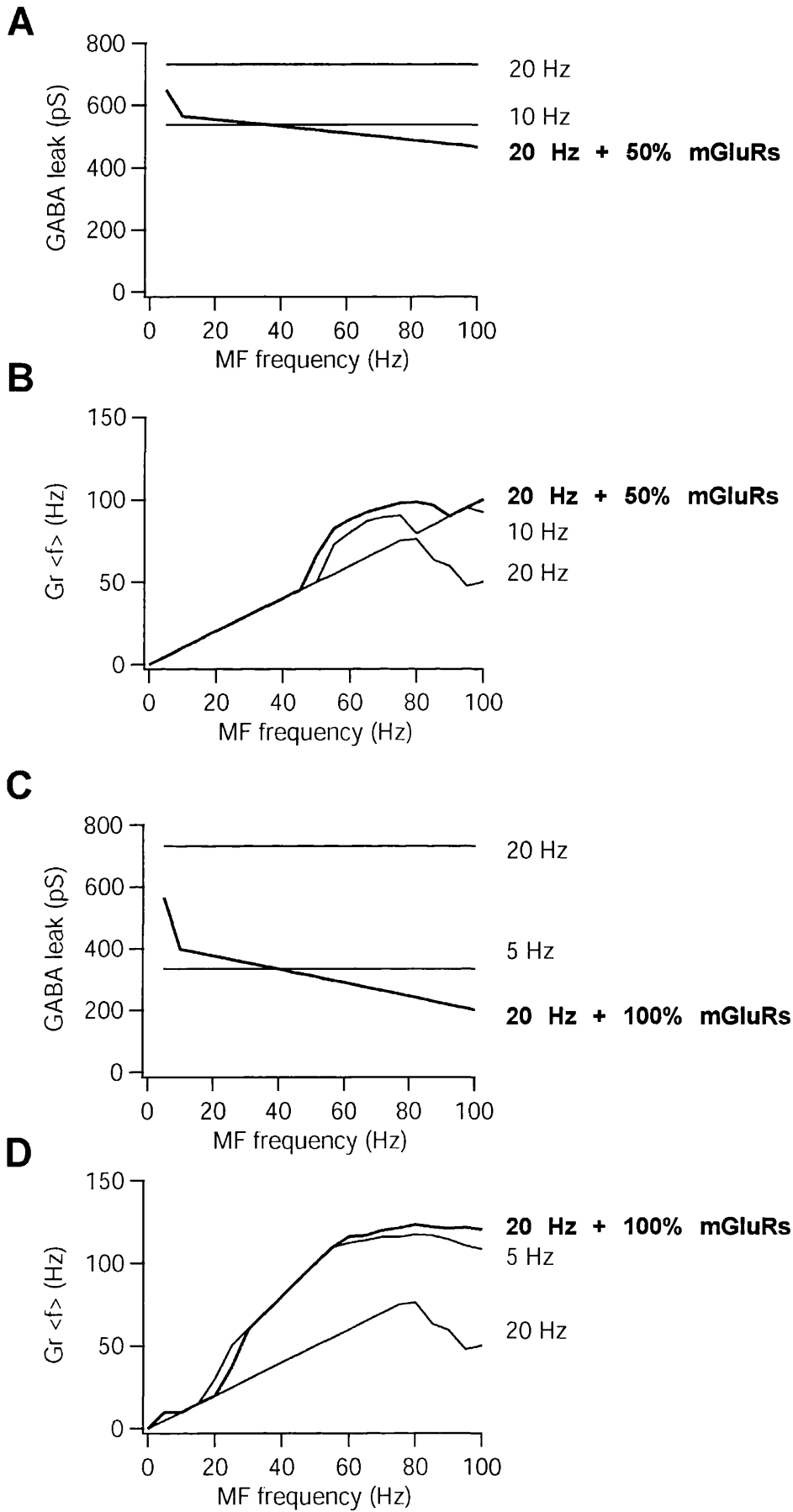
6.4.2 Frequency-dependence of modulation of GABA release is not necessary to boost spiking

Experimental data indicated that suppression of inhibition via mGluRs is dependent on MFS rate, inducing a mean inhibition of evoked IPSC of 34 and 54%, at 10 and 100 Hz MFS frequency, respectively (Ch. 3; Mitchell and Silver, 2000a). These findings led to the proposal that the frequency-dependence of mGluR activation might produce MFS frequency-dependent boosting of spiking. To evaluate the importance of the relationship between MFS rate and spike rate boosting, I investigated the effects of removing this frequency-dependence. For these simulations, 20 Hz GoS-mediated inhibition was reduced by the two mechanisms of frequency-dependent mGluR-mediated inhibition of GABA release and frequency-independent reduction of the GoS rate. The mean reduction in GABA leak, across MFS rates, induced by maximum level of GABA release modulation of 50%, was equal to that induced by a reduction to 10 Hz GoS rate (figure 6.7**A**). The f-F relationships obtained for each condition both showed boosting of spiking during high-frequency MFS, although the f-F curves differed quantitatively (figure 6.7**B**). Increasing the level of the mGluR mechanism to 100% not only induced a more pronounced suppression of inhibition, but also clearly increased the slope of the f-F relationship (figure 6.7**C**; thick trace). However, this boosting of spiking was mimicked by reducing the GoS rate to 5 Hz, which had a similar mean inhibition level across MFS frequencies (figure 6.7**C, D**). Comparison of figures 5.7**B** and **D** also clearly shows that increasing the level of $GABA_A$-R-mediated inhibition shifts the frequency threshold for boosting towards higher frequencies. These results suggest that the frequency-dependence of mGluR-mediated modulation of IPSCs is not important to boost spiking and

Figure 6.8 – f-F relationships for model driven by tonic excitation. **A**, Level of $GABA_A$-R-mediated inhibition as a function of MFS rate under three conditions: 100 pS tonic inhibition only (Control); additional phasic inhibition modelled from 20 Hz GoS rate (20 Hz inhibition); 20 Hz GoS with mGluR-mediated inhibition of glutamate release (20 Hz + mGluR). **B**, Level of non-NMDA receptor-mediated excitation as a function of MFS rate. The NMDA receptor conductance had the same frequency-dependence not including the voltage-dependent properties. **C**, f-F relationships for model with inhibitory conductances shown in **A**.

A

GABA leak (pS)

20 Hz -mGluRs

20 Hz +mGluRs

Control

MF frequency (Hz)

B

non-NMDA conductnace (pS)

MF frequency (Hz)

C

Gr <f> (Hz)

Control
20 Hz +mGluRs

20 Hz -mGluRs

MF frequency (Hz)
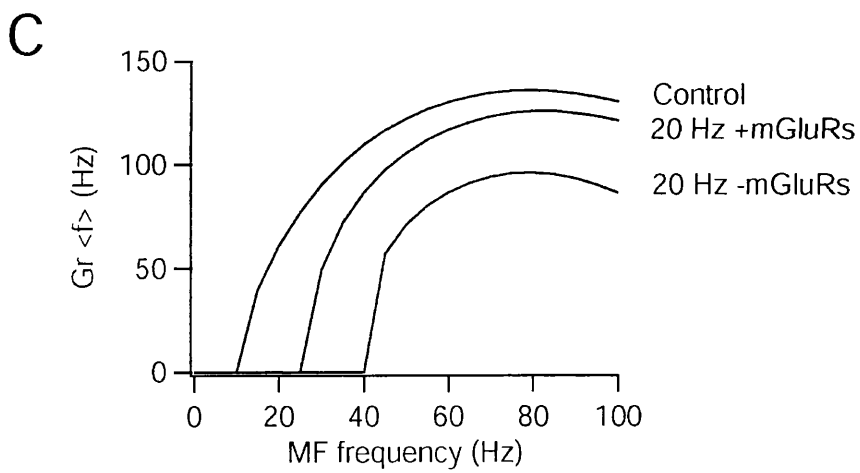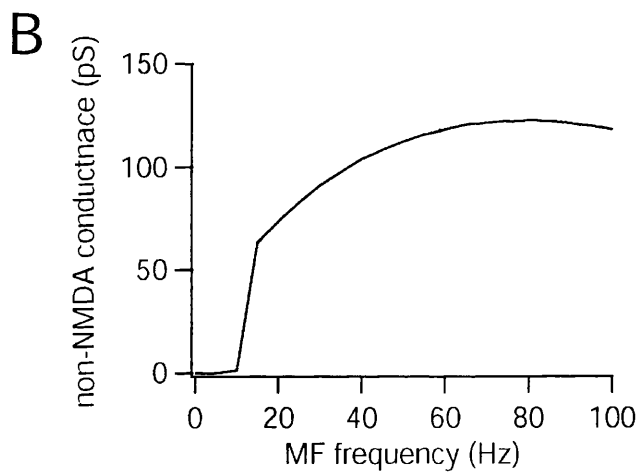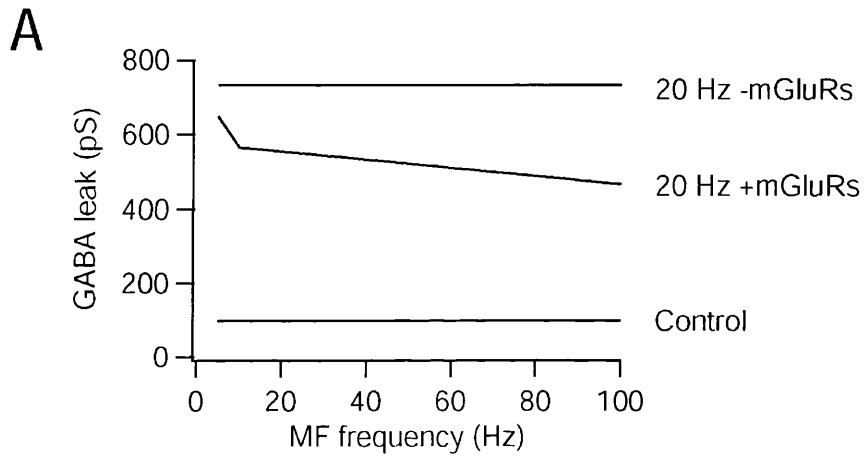
generate a change in f-F relationship slope at 20 Hz GoS, contrary to a previous

proposal (Ch. 3; Mitchell and Silver, 2000a).

6.4.3 Phasic nature of excitation underlies change in slope of f-F relationship

Spiking driven by four mossy fibres was locked to the timing of the EPSPs (figure

6.3**E**). The changes in f-F relationship slope observed during mGluR-mediated

inhibition of GABA release at 20 Hz GoS tended to equate to changes in multiples

of MFS timing. It is therefore possible that this change in slope is only possible

when excitation is phasic. This possibility was investigated by implementing

NMDA and non-NMDA receptor-mediated excitation as tonic conductances. The

level of tonic excitation was calculated by a similar method as for the conversion

of phasic to tonic inhibition (figure 6.8**A**, **B**), as detailed in the methods. At a GoS

rate of 20 Hz, without inhibition of GABA release, application of tonic excitation

elicits spiking above 40 Hz (figure 6.8**C**), in contrast with phasic excitation that

elicits spiking throughout the MFS range. This shift in the f-F relationship arises

because the peaks of the phasic excitatory conductances, which normally drive the

model beyond threshold, are no longer present. Inclusion of inhibition of GABA

release shifted the spiking threshold to 25 Hz, which was also the boosting

threshold frequency (figure 6.8**C**). The shift in the f-F relationship to the left was

approximately parallel, consistent with a reduction of tonic inhibition on the f-I

relationship (figure 6.2). Although, there is some indication of frequency-

dependence of spike boosting towards 100 Hz MFS rate (figure 6.8**C**). This

simulation suggests phasic inputs (mainly non-NMDA receptor component)

Figure 6.9 – GABA$_B$-R-mediated suppression of excitation with synchronous mossy fibres. **A**, f-F relationships for model with GoS at stated frequencies. **B**, f-F relationships for model with GoS at stated frequencies and GABA$_B$-R-mediated inhibition of glutamate release. **C**, Percentage decrease in firing rate induced by inclusion of inhibition of excitation (attenuation). **D**, Voltage traces taken at a MFS and GoS rate of 20 Hz. Inclusion of GABA$_B$-R-mediated inhibition of glutamate release halved the spike rate of the model at these frequencies.
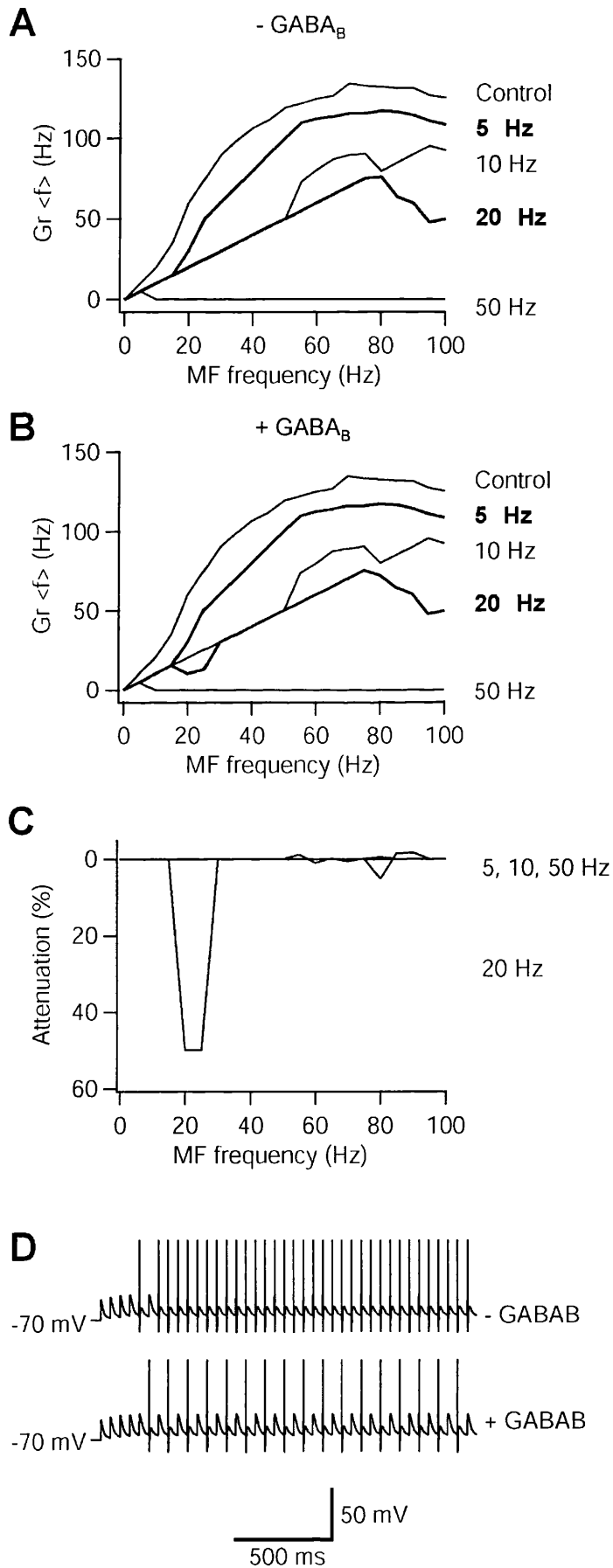
interact with changes in inhibition to induce an alteration in f-F relationship slope

by constraining the spiking rate to multiples of the input frequency.

6.5 Suppression of excitation via GABA$_B$-Rs

6.5.1 GABA$_B$-R-mediated inhibition of synchronous inputs firing at same rate

Experimental data indicates that spillover-mediated activation of GABA$_B$-Rs on

mossy fibres mediates an inhibition of EPSCs that decreased with increasing MFS

(Ch. 4; Mitchell and Silver, 2000b). Indeed, at 10 Hz MFS the variability of the

response was such that that the small magnitude of the inhibition was not

statistically significant. To investigate how GABA$_B$-R-mediated inhibition of

EPSCs affected synaptically driven spiking in granule cells, a steady-state model

of these modulation properties was combined with the integrate-and-fire unit,

without presynaptic mGluRs on Golgi cells. It should be noted that the

experimentally measured magnitude of EPSC inhibition at 10 Hz MFS was

included despite not being statistically significant (see methods; Ch 4; Mitchell

and Silver, 2000b). The effects of varying GABA$_A$-R-mediated inhibition on the f-

F relationship alone are shown in figure 6.9**A**. Inclusion of the GABA$_B$

mechanism had no effect on the f-F curves simulated at most of the GoS

frequencies tested (figure 6.9**B**). However, analysis of the percentage attenuation

in spiking rate induced by GABA$_B$-Rs revealed that spiking was potently

attenuated during low-frequency MFS (20 and 25 Hz) selectively, only at a GoS

frequency of 20 Hz (figure 6.9**C**, **D**).

Figure 6.10 - $GABA_B$-R-mediated inhibition of excitation with two

sets of two mossy fibres, each set is stimulated with ratio of rates of

2:5. **A**, Relationship between mean MFS rate and mean spike rate of the

model, with GoS at stated frequencies. **B**, Similar plots as **A** for model

with GoS at stated frequencies and inhibition of glutamate release. **C**,

$GABA_B$-R-mediated attenuation of firing frequency at stated GoS

frequencies.

A

- GABA$_B$

B

+ GABA$_B$

C
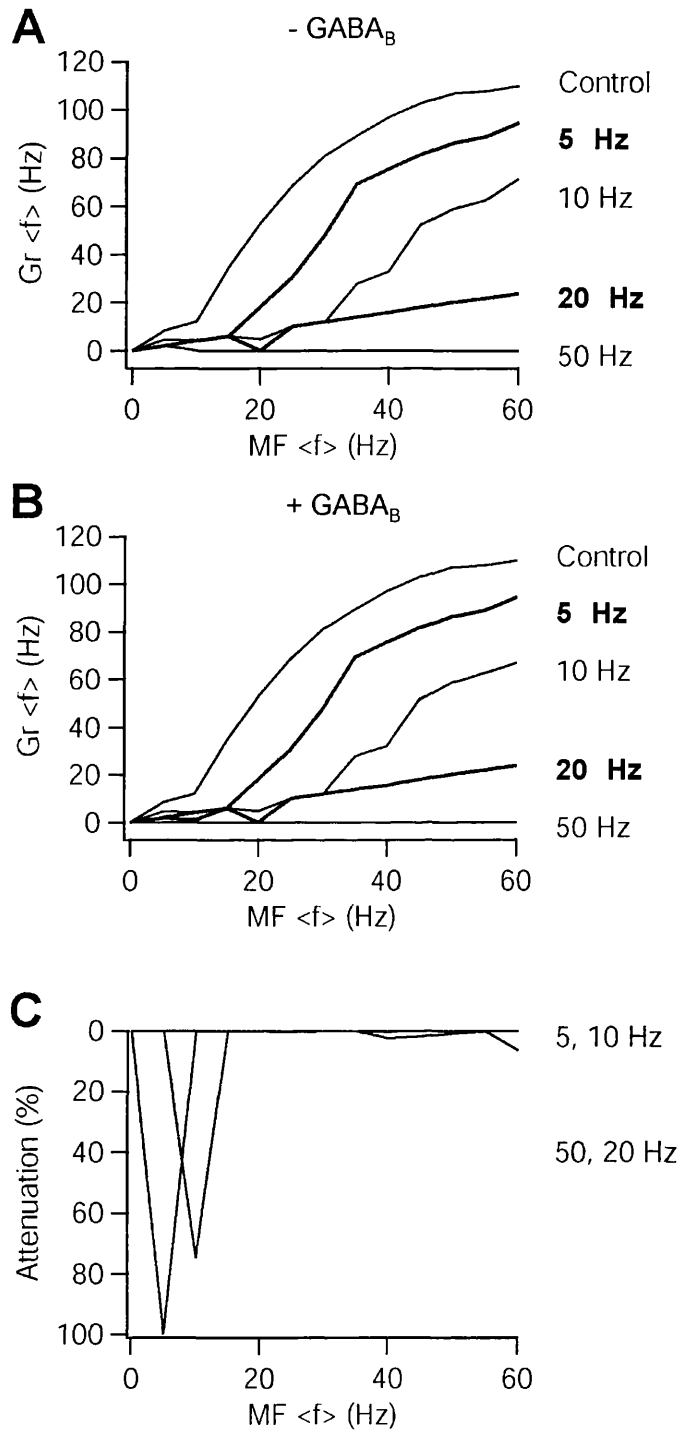
6.5.2 GABA$_B$-R-mediated inhibition of inputs firing at different rates

GABA$_B$-R-mediate inhibition of glutamate release is maximal at subthreshold

MFS frequencies (<10 Hz). I therefore, examined the effect of implementing

excitation at a range of MFS frequencies, to combine greater excitation with

reduced GABA$_B$-R-mediated modulation of the lower-frequency inputs and

increased spiking driven by the high-frequency inputs. The four mossy fibres were

split into two groups, each firing at a different frequency in a ratio of 2:5. This was

possible as the model permitted calculation of synaptic short-term plasticity and

modulation for each individual input. The spiking rate was simulated at mean

MFS frequencies between 5 and 60 Hz, for a range of GoS levels. Here, as with

the synchronous inputs, inclusion of GABA$_B$-R mediated inhibition of glutamate

had no effect at high-frequency MFS (figure 6.10**A**, **B**). However, in the

simulation with mossy fibres stimulated at different rates, GABA$_B$-R-mediated

inhibition of glutamate release attenuated the spiking rate at the lower MFS rates

of 5 and 10 Hz, at GoS frequencies of 50 and 20 Hz, respectively (figure 6.10**C**).

These results suggest that the properties of attenuation of excitation via GABA$_B$-

Rs are likely to be important when there is greater excitation due to a non-uniform

distribution of input frequencies or the spiking threshold is lower.

6.6 Discussion of results

I have investigated how heterosynaptic inhibition of glutamate and GABA release

affects synaptic integration in granule cells. A steady-state integrate-and-fire

model of the regulation of transmission from Golgi cell axons and mossy fibres

was constructed from electrophysiological data (Chs 3 and 4, Mitchell and Silver,

2000a, 2000b). Modelling suggested that mGluR-mediated suppression of GABA

release boosts granule cell spiking during high-frequency mossy fibre frequencies,

under some conditions of inhibition. GABA$_B$-R-mediated suppression of

excitation attenuated spiking driven by low-frequency mossy fibres.

6.6.1 Modelling granule cell excitability with an integrate-and-fire unit

A steady-state model of the frequency-dependence of neurotransmission from

Golgi cell axons and mossy fibres was combined with a simple postsynaptic

model, an integrate-and-fire unit, since the soma and dendrites of granule cells

behave as a single electrical compartment (Silver et al, 1992, 1996c; D'Angelo et

al, 1993, 1995; Gabbiani et al, 1994). Adding an action potential-dependent

conductance to mimic voltage-activated potassium conductances made the f-I

relationship of the model more linear, consistent with properties of granule cells in

vitro (D'Angelo et al, 1995, 1998; Brickley et al, 1996). Unlike adapting integrate-

and-fire models that also exhibit a linear f-I relationship due to a calcium-

dependent potassium conductance (Koch, 1999), the linearised model does not

exhibit adaptation in interspike interval throughout a train, to mimic another

characteristic feature of granule cells (D'Angelo et al, 1995, 1998). Increasing

levels of tonic inhibition induced a parallel shift in f-I relationship of the model, as

previously shown: with cerebellar granule cells in vitro (Brickley et al, 1996); in a

detailed compartmental model of a granule cell with many ionic conductances

(Gabbiani et al 1994); and in another modelling study, which used both a detailed

compartmental model of a pyramidal cell and a simple integrate-and-fire unit

(Holt and Koch, 1997).

Synapses in the model were implemented as time-varying conductances with experimentally derived properties (Chs 3 and 4). The implementation of realistic synaptic conductances resulted in an f-F relationship that shared some features with *in vitro* granule cells (D'angelo et al, 1995). First, more than one mossy fibre input was required to make the model fire in the absence of inhibition. Second, the spiking frequency of the model increased with increasing MFS rate. It was not possible to compare temporal summation with previous studies, since earlier computation studies have not implemented synaptic depression (Gabbiani et al 1994; see Ch. 4 or Mitchell and Silver, 2000b for mossy fibre synaptic depression). These findings indicate that the present model captured some important features of synaptic integration in the cerebellar granule cell.

6.6.2 Suppression of inhibition boosts spiking

Phasic inhibition was modelled as a tonic conductance to remove phase-dependent interactions between excitation and inhibition (see methods), as used previously (Gabbiani et al, 1994). As expected, GoS level at 20 Hz reduced the spiking rate of the model at each MFS frequency. Activation of mGluRs on Golgi cells preferentially inhibits GABA release at high MFS rates (Ch. 3; Mitchell & Silver, 2000a), suggesting that the mechanism should preferentially boost spiking driven by high-frequency MFS. Consistent with this hypothesis, mGluR-mediated suppression of inhibition increased the slope of the f-F relationship, with 20 Hz GoS. However, the properties of boosting of spiking could be similarly induced by both frequency-dependent mGluR activation and reducing the rate of GoS, which

reduces inhibition equally at all MFS rates. This finding suggests that the

frequency-dependence of suppression of inhibition via mGluRs above 10 Hz (i.e.

above model spiking threshold) did not significantly contribute to the change in f-

F relationship slope. Given this fact, it is unlikely that active mossy fibres firing at

a distribution of frequencies above 10 Hz will exhibit significantly different

boosting properties to synchronously active mossy fibres, stimulated at the mean

frequency. Despite the fact that mGluR-mediated inhibition of GABA release only

expressed at active glomeruli on an individual granule cell, the mechanism will

not selectively enhance the transmission of information from high-frequency

mossy fibres to an individual granule cell. Instead, inhibition of GABA release via

mGluRs might enhance contrast between granule cells innervated by high- and

low-frequency mossy fibres by changing their excitability.

Why can a reduction in tonic GABA conductance mediate a change in slope of the

f-F relationship, but not the f-I curve? Synaptic excitation phase locked spiking to

a multiple of the non-NMDA component frequency. To investigate whether phase

locking contributed to the change in f-F relationship slope with varying tonic

inhibition, the effects of suppression of inhibition with tonic excitation were

investigated. Suppression of inhibition induced a parallel shift in the f-F

relationship with tonic excitation, consistent with the effects of tonic inhibition on

the f-I curve (figure 6.2; Holt and Koch, 1997). These data suggest that the phase-

locking behaviour of the EPSP is essential to induce the increase in f-F

relationship slope mediated by a reduction in inhibition. It therefore seems likely

that the properties of spike boosting by mGluRs are generated by an interaction

between phasic excitation and the non-linear, threshold properties of spike

generation of the integrate-and-fire model. This mechanism might be particularly

important in neurones with rapid time course EPSPs. Cerebellar granule cells

might be well suited for this purpose since evoked EPSPs produce a large and

rapid depolarisation (figure 6.3; D'Angelo et al, 1993, 1995). This is possible

because the underlying EPSCs charge a high input resistance on a submillisecond

timescale, and are not significantly filtered due to the compact morphology of the

cell granule cells (Silver et al, 1992, 1996c). Rapid time course excitation can also

be found at the calyx of Held in neurones of the medial nucleus of the trapezoid

body (Barnes-Davies and Forsythe, 1995), between principle and inhibitory

interneurones of the hippocampal dentate gyrus (Geiger et al, 1997), in non-

Pyramidal neurones in the visual cortex (Stern et al, 1992) and in the spinal cord

(Finkel and Redman, 1983; Nelson et al, 1986). However, electrophysiological

data suggests that granule cells, as well as other cell types, express a wide range of

voltage-activated conductances (summarised in Gabbiani at el, 1994), which will

tend to shape the temporal profile of temporal summation and thus mGluR-

mediated boosting. Although, the model used here does not directly consider the

contribution of these conductances, this chapter demonstrates a general principle

that can be tested *in vitro*.

Recordings from granule cells in slice showed that the magnitude of suppression

of inhibition decreased with increasing Golgi cell stimulation frequency (Ch. 3,

Mitchell and Silver, 2000a). This led to the hypothesis that suppression of

inhibition becomes less important with increasing rates of GoS. However, the

modelling revealed that the level of boosting increased as the GoS rate increased,

inconsistent with this hypothesis. Therefore, suppression of inhibition is most

important in areas innervated by high-frequency Golgi cells.

Voltage-clamp recordings showed that the IPSC, evoked by stimulation of an

individual Golgi cell axon at 5 Hz, was depressed by an average of ~50 % during

single mossy fibre stimulation at 100 Hz (Ch. 3; Mitchell and Silver, 2000a). The

simplest interpretation of this result is that at an individual glomerulus, GABA

release was inhibited by 50 %, assuming the IPSC amplitude is linearly related to

GABA release. However, the Golgi cell axon is highly arbourised, suggesting the

possibility that one Golgi cell axon might innervate more than one glomerulus per

granule cell. Indeed, my data indicating a ~48% probability of inhibition of GABA

release (Ch. 3; Mitchell and Silver, 2000a) suggests that a Golgi cell innervates

two of the four glomeruli associated with a granule cell (Jakab and Hamori, 1988),

under slice conditions. It is therefore possible that the reported 50 % inhibition

level is a lower limit, reflecting the suppression of inhibition by a single mossy

fibre at one of the two glomeruli that the Golgi cell innervates. When all glomeruli

contain an active mossy fibre and Golgi cell axon, the upper limit for suppression

of inhibition could be 100 %, with complete suppression of low-frequency GoS-

mediated inhibition at a MFS frequency of 100 Hz. The simulations performed

here, in which all four glomeruli received an equally weighted mossy fibre and

Golgi cell input, revealed that as the level of mGluR-mediated boosting increased

and the threshold for boosting moved towards lower mossy fibre frequencies.

Therefore, the level of suppression of inhibition is a key parameter in setting its

dependence on MFS frequency. If only a subset of mossy fibres that innervate a

granule cell are active, the level of suppression of inhibition will be reduced where

a glomerulus containing an active Golgi cell is not excited. However, this granule

cell might also experience less feed forward inhibition, which is also dependent on

the number of active mossy fibres in the region. Indeed, modelling indicated that

boosting of spiking during high-frequency MFS could be achieved by reducing

GoS rate. Furthermore, should the GoS rate remain high, the ability of mGluR-

mediate inhibition of GABA release to boost spiking rate is enhanced, which

might partly compensate for a reduced level of activation of mGluRs on Golgi

cells.

6.6.3 Suppression of excitation selectively attenuates spiking during low-frequency mossy fibre transmission

Activation of presynaptic $GABA_B$-Rs preferentially inhibits mossy fibre

transmission below 10 Hz (Ch. 4; Mitchell & Silver, 2000b). Modelling, which

included the finite level of inhibition measured at 10 Hz MFS, revealed that

attenuation of spike rate by $GABA_B$-Rs in granules cells driven by synchronous

inputs occurred only at MFS rates of 20-25 Hz, during GoS-mediated inhibition

rate of 20 Hz. Below these MFS rates the EPSP amplitude is sufficiently above

threshold to still drive spiking when modulated. The EPSP amplitude was reduced

towards threshold by frequency-dependent depression as the input rate increases to

20-25 Hz allowing even a small amount of modulation to depress spiking. As the

MFS frequency increased further, $GABA_B$-R-mediated modulation reduces to zero

(Ch. 4; Mitchell & Silver, 2000b). Spike rate modulation does not occur at 5 or 10

Hz GoS frequencies since $GABA_B$-Rs are not activated (Ch. 4; Mitchell and

Silver, 2000b). At GoS frequency of 50 Hz the model is already completely

inhibited over most of the MFS frequency range, occluding $GABA_B$-R-mediated

attenuation of spiking.

$GABA_B$-R-mediate inhibition of glutamate release is maximal at subthreshold

MFS frequencies (<10 Hz). Therefore, if excitation is supplied as a distribution of

firing rates around a mean, then the combination reduced $GABA_B$-R-mediated

modulation of the lower-frequency inputs and increased spiking driven by the

high-frequency inputs might reduce the mean MFS rate necessary to precipitate

attenuation of spiking. To test this, I investigated heterosynaptic inhibition in the

model driven by two populations of mossy fibres, each firing at a different rate.

This revealed that $GABA_B$-R-mediated inhibition of glutamate release attenuated

the spiking rate at the lower MFS rates of 5 and 10 Hz, at GoS frequencies of 50

and 20 Hz, respectively. This finding suggests that the enhanced excitation by the

high frequency mossy fibres shifted the range of MFS frequencies over which

$GABA_B$-Rs can modulate granule cell spiking. A similar result might be obtained

with synchronous inputs in real granule cells, if they are more excitable than the

model.

6.6.4 Conclusions

A simplified model of synaptic integration in granule cells suggests that as

expected, mGluR-mediated suppression of inhibition boosted spiking during high-

frequency mossy fibres. It was found that the subtle frequency-dependence of

mGluR activation between 10 and 100 Hz was not necessary to produce this

change in slope. Simulations using tonic excitation exhibited a near-parallel shift

in f-F relationship, as with the f-I relationship. It is therefore likely that an

interaction between the non-linear, threshold properties of the excitable model and

the phasic nature of synaptic excitation generated the frequency-dependent

properties of boosting of spiking. The level of boosting increased with increasing

Golgi cell-mediated inhibition, contrary to previous predictions (Ch. 3; Mitchell

and Silver, 2000a). Inversely, $GABA_B$-R-mediated attenuation of excitation

suppressed firing during low-frequency MFS, consistent with earlier predictions

(Ch. 4; Mitchell and Silver, 2000b). Like mGluR-mediated boosting of spiking,

$GABA_B$-R-mediated inhibition is enhanced at higher GoS frequencies. Therefore,

the contrast between granule cells will be enhanced on the basis of how many

active mossy fibres innervate them, in areas innervated by high-frequency Golgi

cells.

CHAPTER SEVEN

DISCUSSION

7.0 Summary of experimental findings

Electrophysiological and computational approaches were used to investigate

heterosynaptic modulation in the cerebellar glomerulus. In chapter 3, I

demonstrated that mGluRs located on presynaptic terminals of Golgi cells (Ohishi

et al, 1994) are functional by showing that pharmacolgical activation induced

inhibition of GABA release. The level of modulation decreased as the frequency

of Golgi cell firing increased. For these pharmacological findings to have

physiological relevance it was necessary to demonstrate that the mGluRs could be

activated by synaptically-released glutamate at physiological temperatures. This

requirement was met by the observation that spillover of glutamate, induced by the

stimulation of mossy fibres, could inhibit GABA release from Golgi cells at 37°C.

Furthermore, the magnitude of disinhibition was dependent on the frequency and

duration of mossy fibre stimulation.

In chapter 4, I used a similar approach to investigate heterosynaptic activation of

$GABA_B$-Rs on mossy fibres. Application of a $GABA_B$-R agonist depressed

glutamate release from mossy fibres in a frequency-dependent manner.

Physiologically-released GABA from spontaneously active Golgi cells depressed

the evoked EPSC at room temperature but not at 37°C, highlighting the

importance of carrying out investigations of transmitter spillover at physiological

temperatures. However, when the activity of a single Golgi cell axon was

increased by stimulation, the EPSC was depressed at 37°C. Spillover- and agonist-

mediated modulation of glutamate release had the same frequency-dependence.

7.1 Development of the cells of the cerebellar glomerulus

The presented study was carried out in immature rats (~P13), an age at which

much development has taken place and further changes will occur. It is therefore

possible that the conclusions presented here may not hold for younger or older/

adult animals. Indeed, every neuron in the network studied exhibits dramatic

changes at this development window. Granule cells migrate from the outer

granular layer to their final position (the inner granular layer) by moving in direct

apposition to radially oriented glial cells (Gregory et al, 1988). Data from mouse

suggests that this migration peaks at P8-12 and active migration slows at P13-20

(Grovas and O'Shea, 1984). Granule cells within the inner granule cell layer also

exhibit a distinct developmental profile. The resting membrane potential granule

cells is more depolarised in P7 than P18 rats (-59 vs -71 mV; Brickley et al,

1996). In P14 mouse, two populations of granule cell can be found with resting

membrane potentials of -54 and -72 mV, which seems to correspond well with

'immature' and 'mature' granule cells (Brickley et al, 2001). In the same cells a

change in input conductance can be measured between immature and mature

granule cells (0.2 and 0.6 nS, respectively). Between P7 and P21 a tonic GABA$_A$

conductance develops (Brickley et al, 1996; Usovicz et al, 1996), while

spontaneous phasic GABAergic IPSCs reduce in amplitude and decay kinetic time

constant over a similar time frame (Brickley et al, 1996; Tia et al, 1996). This

change in properties has been attributed to the inclusion of the α6 subunit in the

GABAA receptors in granule cells (Tia et al, 1996; Brickley et al, 2001). This

switch in receptor type may also underlie the observation of long-lasting spillover-

mediated IPSCs in more mature rats (Rossi and Hamann, 1998). This shift

towards tonic inhibition has been shown to affect the excitability of granule cells

(Brickley et al, 1996, 2001).

Mossy fibres also continue to develop during the second postnatal week. In

mouse, branching patterns and boutons of mossy fibres are identifiable at p5, and

growth cones innervate granule cells, making typical glomerular synapses (Mason

and Gregory, 1984). However, some immature mossy fibres have a branching

profile in the upper granule cell layer that resembles young climbing fibres

between p7 and 14. It is unclear whether these fibres make functional synapses

with granule cells. During the first growth stage of development of the glomerulus

(P6-15) the mossy fibre rosette rapidly enlarges in parallel with an intense

proliferation of granule cell dendrites (Hamori and Somogyi, 1983). Both, the size

of mossy fibre rosettes and the proportion of rosette membrane area occupied by

synaptic junctions reaches steady state at P15, roughly the age at which this study

was carried out. Thus, a relatively stable period of development occurs after the

second postnatal week. During the second stabilisation phase (P15-45), the

number of granule cell dendrites in the glomerulus increases, likely increasing the

tortuosity of the intersynaptic extracellular space. However, the proportion of

mossy fibre membrane area occupied by synaptic junctions remains constant. Over

the same period, the glial sheath that surrounds the mature glomerulus develops

(Hamori and Somogyi, 1983).

The way in which glutamate released from mossy fibres mediates excitation

changes with development as the subunit composition of ionotropic glutamate

receptors on granule cell switches. Throughout the growth stage of the

glomerulus, cerebellar granule cells switch their expression of the AMPA receptor

GluRD subunit from mainly flip to predominantly flop, conferring faster

desensitisation kinetics (Mosbacher, et al, 1994). The first growth stage of

development also sees an increase in the ratio of NMDA to non-NMDA

component of the EPSC, with a concomitant reduction in the weighted tau of the

NMDA component (Cathala et al, 2000). These changes are consistent with a

switch from NR2B containing receptors to NR2A. However, during the

stabilisation period of development this trend in kinetics and NMDA/non-NMDA

ratio is reversed with the inclusion of the NR2C subunit, which additionally

confers a reduction in magnesium concentration sensitivity.

Anecdotal evidence suggests that experimentation with slices from older animals

is more difficult than from younger animals. First, it can be more difficult to make

good quality slices since the tissue seems less resilient to the mechanical and

metabolic stress involved. Second, visualisation of cells in slices from older

animals is compromised due to increased levels of scattering of illumination light

as it passes through the tissue. It is unclear why this should be the case, but it may

be due to more densely packed axonal and dendritic processes that proliferate with

development. This problem can be allayed with the use of infrared differential

interference contrast microscopy (Stuart et al, 1993) and image contrast

enhancement electronics. However, only the former was available to me during

this study. Third, due to the reduced tissue resilience, cells within of slices from

older animals have impaired longevity, reducing the experimental time window

for a successfully patched cell. The experimental protocols described in this thesis

were challenging, with some experiments yielding less than 10 per cent success

rate (see section 3.3.1). Therefore, the competing pressures to push the

developmental stage further and the practical difficulties involved in doing so

necessitated a compromise to maximise productivity and reproducibility. It was

therefore decided to perform the study on P13 rats.

7.2 Mechanisms underlying frequency-dependence of modulation

Inhibition of GABA release via mGluRs decreased as the frequency of Golgi cell

stimulation (GoS) increased, such that the degree of modulation at 100 Hz GoS

was ~40% of that at 0.1 Hz (Ch. 3). Similarly, inhibition of glutamate release via

$GABA_B$-Rs decreased as the frequency of mossy fibre stimulation (MFS)

increased, becoming statistically insignificant at 10 Hz and above (Ch. 4). What is

the molecular basis for the dependence of modulation on frequency and for the

differences in frequency-dependence between Golgi cell axons and mossy fibres?

$GABA_B$-Rs and mGluRs are thought to inhibit transmitter release mainly via G-

protein-mediated downregulation of presynaptic calcium currents (Dittman and

Regehr, 1996; Takahashi et al, 1996, 1998; Isaacson, 1998) and of the release

process (Capogna et al, 1996a, 1996b; Dittman and Regehr, 1996; Schrader and

Tasker, 1997). If metabotropic receptors simply modulate the initial release

probability, then the frequency dependence might arise from the release process

itself. Simple vesicular depletion models predict that as stimulation frequency is

increased, the steady-state release probability becomes dependent on the rate of

recovery of the readily releasable pool and independent of the vesicle fusion rate

and thus the initial release probability (Abbott et al, 1997; Tsodyks and Markram,

1997; Matveev and Wang, 2000). This has been proposed to underlie the changes

in synaptic properties after cortical long-term plasticity (Markram and Tsodyks,

1996). If the above mechanism contributes to other forms of presynaptic

modulation, differences in the frequency dependence of $GABA_B$-R-mediated

modulation of excitatory mossy fibres and mGluR-mediated modulation of

inhibitory Golgi cells could simply reflect different values of initial release

probability and rates of recovery of the release sites at these two synapses.

Other mechanisms might underlie the frequency dependence of presynaptic

inhibition. The first possibility is voltage-dependent relief of G-protein inhibition

(Bean, 1989; Brody et al, 1997; Dolphin, 1998) at higher fibre firing frequencies,

since bursts of action potential waveforms relieve inhibition of P/Q-type calcium

current by M2 acetylcholine receptors in human embryonic kidney 293 cells

(Brody et al, 1997). The finding that both mossy fibre and Golgi cell transmission

is mediated by P/Q-type, as well as N-type calcium channels (Shen et al, 2000) is

consistent with voltage-dependent relief of G-protein inhibition in the glomerulus.

Second, activation of mGluRs on the Golgi cell terminals during mossy fibre

stimulation might also influence frequency dependence of physiologically

activated GABA$_B$-R-mediated EPSC depression by reducing GABA release at

higher mossy fibre stimulation frequencies. However, this mechanism is not likely

to be limiting because the frequency dependence of EPSC depression observed

with GABA spillover and baclofen was similar. Inversely, activation of GABA$_B$-

Rs on the mossy fibres might influence the frequency dependence of the efficacy

of mGluR-mediated IPSC depression by reducing glutamate release at higher

Golgi cell stimulation frequencies. However, this is unlikely since mossy fibres

are not spontaneously active in the slice and during the physiological activation of

mGluR experiments the GoS rate was 5 Hz, below the frequency required to

activate GABA$_B$-Rs on mossy fibres. Third, if the mechanisms underlying auto-

and heteroreceptor signal transduction are similar in terms of molecular cascade

and/or calcium channel inhibition, mGluR- and GABA$_B$-R heteroreceptor-

mediated depression could be occluded by autoreceptor-mediated IPSC or EPSC

depression, if present, which is also likely to be frequency-dependent. Such an

interaction between auto- and heteroreceptor mediated inhibition has been

observed in noradrenergic neurones (Schlicker and Göthert, 1998). However, it is

not clear to what extent autoreceptors contribute to activity-dependent synaptic

depression at these synapses. Last, an interaction between release probability and

frequency-dependent postsynaptic non-NMDA receptor desensitisation might

underlie the frequency-dependence of GABA$_B$-R-mediated non-NMDA receptor

inhibition, as is the case for AMPA receptors at an endbulb synapse in the chick

cochlear nucleus (Brenowitz et al, 1998; Brenowitz and Trussell, 2001). If this

interaction existed at the mossy fibre to granule cell synapse, baclofen and

synaptically-released GABA induced depression should have different frequency

dependences because each produces a different fractional reduction in release

probability, and thus desensitisation. However, the ratio of EPSC depression for

10 and 100 Hz MFS frequency was similar for baclofen and synaptically activated

$GABA_B$-Rs. The role of desensitisation could be directly tested using

cyclothiazide to inhibit desensitisation. Investigation of the precise mechanisms

underlying the frequency dependence of metabotropic receptor-mediated

depression in the cerebellar glomerulus would require detailed knowledge of the

mechanisms underlying homosynaptic depression at the mossy fibre and Golgi to

granule cell synapses, which was beyond the scope of this study. The steady-state

data from the present study provides the basis for a detailed investigation of the

effects of metabotropic receptor-mediated modulation on short-term plasticity by

determining the level of metabotropic receptor activation under physiological

conditions.

7.3 Bidirectional spillover of transmitter in the glomerulus

Spillover of GABA onto $GABA_B$-Rs on mossy fibre terminals mirrors glutamate

spillover onto mGluRs on Golgi cell axon terminals. The two components of these

bidirectional spillover-mediated processes have opposite effects, yet might be

complementary in terms of information processing. Activation of mGluRs on

Golgi cell terminals has an excitatory action by suppressing GABA release onto

granule cells. Because the degree of modulation depends on the firing frequency

of the excitatory input, mGluR activation might be expected to boost the

postsynaptic effects of mossy fibres firing at higher rates and compensate for

frequency-dependent depression of the EPSC. In contrast, activation of $GABA_B$-

Rs on mossy fibres by GABA spillover depresses low-frequency excitatory inputs,

making these inputs less effective. The voltage-clamp studies suggest that these

two spillover-mediated presynaptic mechanisms could be effective under different

network conditions: the mGluR system might be most effective when the Golgi

cell firing rate is low, whereas the GABA$_B$-R system will be most effective when

it is high.

7.4 Modulation of transmitter release affects synaptic integration in model granule cells

How bidirectional spillover affected mossy fibre driven spiking was investigated

using a simplified model of synaptic integration in granule cells. The modelling in

chapter 7 suggested that, as expected, mGluR-mediated suppression of inhibition

boosted spiking during high-frequency mossy fibre activity, by changing the slope

of the relationship between MFS rate and granule cell spiking frequency.

However, it was found that the subtle frequency-dependence of mGluR activation

between 10 and 100 Hz was not necessary to produce the dependence of spike rate

boosting on mossy fibre frequency, inconsistent with a previous proposal (Ch. 3;

Mitchell and Silver, 2000a). Instead, it is likely that an interaction between

mGluR-mediated disinhibition, the non-linear threshold properties of the model

and phasic excitation were responsible for boosting of high-frequency inputs. An

important finding is that the level of boosting increased with increasing Golgi cell-

mediated inhibition, since this is contrary to predictions based on voltage-clamp

data (Ch. 3; Mitchell and Silver, 2000a). This finding suggests that both mGluR-

and GABA$_B$-R-mediated heterosynaptic inhibition could be important when Golgi

cells are firing at relatively high frequencies. $GAB A_B$-R-mediated attenuation of

excitation suppressed low-frequency mossy fibres, consistent with earlier

predictions (Ch. 4; Mitchell and Silver, 2000b). This study has provided a

predictive framework which can be used to direct an *in vitro* current-clamp study

into the modulation of mossy fibre spiking in granule cells by heterosynaptic

inhibition in the cerebellar glomerulus.

7.5 The physiological role of heterosynaptic modulation at the cerebellar glomerulus

7.5.1 Heterosynaptic inhibition in an associative network

A classical theoretical model of information processing suggests that the

cerebellar cortex acts as an associative network, which stores learned movements

as patterns of input activity (parallel fibres) and output activity (Purkinje cells)

(Marr, 1969; Tyrrell and Willshaw, 1992). During learning, the synaptic weights

are increased between conjunctively active parallel fibres and Purkinje cells.

When the same input pattern is subsequently presented, the potentiated synapses

will evoke the learned pattern of firing in Purkinje cells. The ability of the network

to discriminate between input firing patterns is determined by the level of pattern

overlap. A greater number of non-overlapping patterns are possible when each

pattern is made up of fewer active inputs. "Sparse coding" requires that as few

active granule cells as possible should represent a movement. Feedback inhibition,

via Golgi cells ensures that granule cell excitability is reduced as more granule

cells fire action potentials. Increasing the level of tonic inhibition also increases

the spiking threshold of the granule cell (Brickley et al, 1996; Holt and Koch,

1997), allowing only higher-frequency mossy fibres to elicit spiking in granule

cells. The activation of feedforward Golgi cell-mediated inhibition by mossy

fibres will also tend to reduce the number of active granule cells. This mechanism

promotes a form of "predictive spiking threshold control". In addition to shifting

the firing threshold, the modelling results suggest that an interaction between tonic

inhibition and phasic excitation might decrease the slope of the f-F relationship

(Ch. 6), further decreasing granule cell spiking during even high-frequency mossy

fibre transmission. This property has not been observed in real granule cells to

date.

The spatial distribution of $GABA_B$-R-mediated inhibition of the EPSC, like

$GABA_A$-R-mediated inhibition, is set by the Golgi cell axonal arbour, which

contacts ~5000 granule cells in the region (Ito, 1984). However, $GABA_B$-R-

mediated presynaptic inhibition will only be active during high-frequency

inhibition, to suppress less active mossy fibres (Ch. 4; Mitchell and Silver,

2000b). When active, $GABA_B$-R-mediated presynaptic inhibition will complement

the effects of tonic and phasic postsynaptic $GABA_A$-R-mediated inhibition (Rossi

and Hamann, 1998), by reducing the efficacy of mossy fibres firing a low rates.

Metabotropic glutamate receptor-mediated Golgi cell disinhibition is activated at a

mossy fibre firing threshold at 10 Hz or below (Ch. 4; Mitchell and Silver, 2000b),

and is set by the distribution of the ~20 glomeruli per folium associated with an

individual active mossy fibre (Eccles et al, 1967; Ito, 1984). In granule cells that

receive concurrent active mossy fibre and high-frequency Golgi cell transmission,

mGluR-mediated disinhibition will locally promote spiking, and increase the slope

of the relationship between MFS rate and granule cell spiking frequency,

increasing the synaptic gain. This will, in turn, increase the overall excitation of

Purkinje cells. To balance this, enhanced granule cell spiking will activate

feedback inhibition via ascending dendrites of Golgi cells. Feedback inhibition

will increase the level of inhibition in the granule cells and decrease excitation of

granule cells by low frequency mossy fibres via $GABA_B$-Rs, as discussed. By

enhancing transmission in granule cells with active mossy fibres and promoting

feedback inhibition via Golgi cells mGluR-mediated heterosynaptic inhibition will

also exaggerate differences in spiking rate between granule cells experiencing

different levels of excitation.

The modelling results in chapter 6 suggested that the change slope of the

relationship between MFS rate and granule cell spiking frequency via mGluR-

mediated disinhibition could be mimicked by simply reducing the GoS frequency,

since the frequency-dependence of mGluR activation was shallow between 10 and

100 Hz MFS (Chs 3 and 5). This suggests the possibility that disinhibition could

simply be mediated via feedforward and feedback inhibition between Golgi cells

(Dieudonne, 1995). However, this mechanism would not preserve the ability of

mGluRs to suppress inhibition locally, since reducing the GoS frequency would

tend to disinhibit all granule cells in the region. The glomerulus-specific nature of

mGluR-mediated inhibition of GABA release allows the level of disinhibition to a

particular granule cell to be determined by how many mossy fibres, firing at >10

Hz, innervate that cell. Thus, granule cell spiking driven by two mossy fibres will

be more sensitive to changes in the level of Golgi cell-mediated inhibition than a

cell driven by four mossy fibres, assuming all dendrites receive an equal level of

inhibition. This process would therefore enhance the contrast between granule

cells.

7.5.2 Heterosynaptic inhibition in temporal encoding of spatial firing patterns

A more recent model of the cerebellar cortex suggests that it is a temporal encoder

(Maex and De Schutter, 1998; Vos et al, 1999b). It has been proposed that parallel

fibre-mediated feedback via Golgi cells may control the timing of granule cell

spiking, promoting synchronised activity along the ventral axis of the cerebellar

cortex (Maex and De Schutter, 1998; Vos et al, 1999b). By synchronisation of

granule cell firing, the spatial information encoded in patterns of mossy fibre

activity can be transformed into a temporal code (Hopfield, 1995), recognised by

the Purkinje cell. By locally changing the slope of the relationship between MFS

rate and granule cell spiking frequency and altering mossy fibre plasticity during

periods of Golgi cell activity, heterosynaptic modulation might be expected to

have an important role in shaping this temporal pattern.

7.5.3 Heterosynaptic inhibition induces periods of altered synaptic plasticity

Heterosynaptic modulation shown in this study persisted for hundreds to

thousands of milliseconds after the cessation of receptor activation. These kinetics

will create a time window of modulated transmission onto granule cells. During

this period, mGluR-mediated disinhibition might favour the induction of LTP at

mossy fibre inputs onto granule cells with many active mossy fibres, since

experimental studies indicate that LTP cannot be induced at this synapse in the

absence of a GABA$_A$-R antagonist (Armano et al, 2000), consistent with the

finding that reduced inhibition also facilitates LTP induction in the hippocampus

(Davies et al, 1991). Also, GABA$_B$-R-mediated inhibition of glutamate release

will induce periods of altered short-term plasticity of mossy fibre transmission, as

for the steady-state case.

7.6 Spillover-mediated heterosynaptic modulation in other systems

Presynaptic GABA$_B$-Rs on cerebellar mossy fibres provide a mechanism to reduce

the density of excitation through the inhibition of glutamate release. This might

also be the case at other central synapses. At the granule to Purkinje cell synapse

feedforward inhibition by molecular layer inhibitory interneurones is

supplemented by the inhibition of glutamate release via the activation GABA$_B$-Rs

on parallel fibre terminals (Dittman and Regehr, 1997). Theoretical studies of the

hippocampus (reviewed in Skaggs and McNaughton, 1992) indicate that sparse

coding enhances the capacity of the CA3 associative network, as in the cerebellum

(Marr, 1969). Sparse coding in the hippocampus might be favoured by inhibition

mediated by presynaptic GABA$_B$-Rs (Vogt and Nicoll, 1999). Further downstream

in the hippocampus, at CA1, inhibition via GABA$_B$-Rs is also evident (Isaacson et

al, 1993).

In the cerebellum, contrast between excitation pathways might be enhanced by

mGluR-mediated disinhibition (Chs 3 and 6). A similar mechanism might occur at

the CA1 region of the hippocampus, where activation of presynaptic kainate

receptors on inhibitory interneurones inhibits GABA release onto principle

neurones (Min et al, 1999). However, the role of presynaptic mGluRs on

inhibitory interneurones of CA1 appears to be different. Glutamate spillover

inhibits GABA release onto other interneurones but not principle neurones

(Semyanov and Kullman, 2000). Thus, activation of presynaptic mGluRs in CA1

might enhance inhibition that might be important in controlling epilepsy

(Semyanov and Kullmann, 2000). However, the heterosynaptic actions of

glutamate appear to be absent at physiological temperature (Min et al, 1999; Vogt

and Nicoll, 1999; Semyanov and Kullman, 2000). Input specificity of

heterosynaptic inhibition has not been established in CA1, an area where the

diffuse actions of transmitter have been proposed (Isaacson et al, 1993; Rusakov

et al, 1999). It is likely that heterosynaptic inhibition at the cerebellar glomerulus

is input specific, since the glial sheath that surrounds the synaptic complex might

impede lateral diffusion of transmitter (Jakab and Hamori, 1988). Although I have

provided indirect evidence for the input specificity in this thesis (Ch. 3), this

feature is yet to be directly shown.

In conclusion, mGluRs and GABA$_B$-Rs mediate heterosynaptic modulation at the

cerebellar glomerulus. Metabotropic glutamate receptors might promote excitation

of granule cells with more active mossy fibres by suppressing inhibition, while

GABA$_B$-Rs decrease the excitation of granule cells by mossy fibres firing at low

frequencies. Heterosynaptic modulation is likely to locally enhance contrast

between different granule cells with different numbers of active mossy fibres,

thereby shaping the way sensory information carried by mossy fibres is processed

in the cerebellar cortex.

REFERENCES

Abbott LF (1999) Lapicque's introduction of the integrate-and-fire model neuron

(1907). *Brain Res. Bull.* **50**: 303–304.

Abbott LF, Varela JA, Sen K, Nelson SB (1997) Synaptic depression and cortical

gain control. *Science* **275**: 220–224.

Abe T, Sugihara H, Nawa H, Shigemoto R, Mizuno N, Nakanishi S (1992)

Molecular characterization of a novel metabotropic glutamate receptor

mGluR5 coupled to inositol phosphate/Ca2+ signal transduction. *J. Biol.*

Chem. **267**: 13361–13368.

Albus, JS (1971) A theory of cerebellar function. *Math. Biosci.* **10**: 25-61

Andrade R, Malenka RC, Nicoll RA (1986) A G protein couples serotonin and

GABAB receptors to the same channels in hippocampus. *Science* **234**:

1261–1265.

Andreu R, Barrett EF (1980) Calcium dependence of evoked transmitter release at

very low quantal contents at the frog neuromuscular junction. *J. Physiol.*

(*Lond.*) **308**: 79-97.

Aoki E, Semba R, Kashiwamata S (1986) New candidates for GABAergic

neurons in the rat cerebellum: an immunocytochemical study with anti-

GABA antibody. *Neurosci. Lett.* **68**: 267-271.

Arai A, Lynch G (1998) AMPA receptor desensitization modulates synaptic responses induced by repetitive afferent stimulation in hippocampal slices. *Brain Res.* **799**: 235–242.

Armano S, Rossi P, Taglietti V, D'Angelo E (2000) Long-term potentiation of intrinsic excitability at the mossy fiber-granule cell synapse of rat cerebellum. *J. Neurosci.* **20**: 5208–5216.

Aroniadou-Anderjaska V, Zhou FM, Priest CA, Ennis M, Shipley MT (2000) Tonic and synaptically evoked presynaptic inhibition of sensory input to the rat olfactory bulb via GABA(B) heteroreceptors. *J. Neurophysiol.* **84**: 1194–1203.

Atluri PP, Regehr WG (1996) Determinants of the time course of facilitation at the granule cell to Purkinje cell synapse. *J. Neurosci.* **16**: 5661–5671.

Augustine GJ, Charlton MP, Smith SJ (1985) Calcium entry and transmitter release at voltage-clamped nerve terminals of squid. *J. Physiol. (Lond.)* **369**: 163–181.

Augustine GJ, Adler EM, Charlton MP (1991) The calcium signal for transmitter secretion from presynaptic nerve terminals. *Ann. N. Y. Acad. Sci.* **635**: 365–381.

Barbour B, Häusser M (1997) Intersynaptic diffusion of neurotransmitter. *Trends Neurosci.* **20**: 377–384.

Barker JL, Nicoll RA (1972) Gamma-aminobutyric acid: role in primary afferent depolarization. *Science* **176**: 1043-1045.

Barnes-Davies M, Forsythe ID (1995) Pre- and postsynaptic glutamate receptors at

a giant excitatory synapse in rat auditory brainstem slices. *J. Physiol.*

(Lond.) **488**: 387–406.

Batchelor AM, Garthwaite J (1997) Frequency detection and temporally dispersed

synaptic signal association through a metabotropic glutamate receptor

pathway. *Nature* **385**: 74–77.

Baude A, Nusser Z, Roberts JD, Mulvihill E, McIlhinney RA, Somogyi P (1993)

The metabotropic glutamate receptor (mGluR1α) is concentrated at

perisynaptic membrane of neuronal subpopulations as detected by

immunogold reaction. *Neuron* **11**: 771–787.

Bean BP (1989) Neurotransmitter inhibition of neuronal calcium currents by

changes in channel voltage dependence. *Nature* **340**: 153–156.

Bekkers JM, Stevens CF (1989) NMDA and non-NMDA receptors are colocalized

at individual excitatory synapses in cultured rat hippocampus. *Nature* **341**:

230–233.

Bennett MK (1997) Ca2+ and the regulation of neurotransmitter secretion. *Curr.*

Opin. Neurobiol. **7**: 316-322.

Blackman JG, Ginsborg BL, Ray C (1963) Synaptic transmission in the

sympathetic ganglion of the frog. *J. Physiol. (Lond.)* **267**: 355-373

Bliss TV, Collingridge GL (1993) A synaptic model of memory: long-term

potentiation in the hippocampus. *Nature* **361**: 31–39.

Bliss TV, Lømo T (1973) Long-lasting potentiation of synaptic transmission in the

dentate area of the anaesthetized rabbit following stimulation of the

perforant path. *J. Physiol. (Lond.)* **232**: 331–56.

Bollmann JH, Sakmann B, Borst JG (2000) Calcium sensitivity of glutamate

release in a calyx-type terminal. *Science* **289**: 953-957.

Bonci A, Grillner P, Siniscalchi A, Mercuri NB, Bernardi G (1997) Glutamate

metabotropic receptor agonists depress excitatory and inhibitory

transmission on rat mesencephalic principal neurons. *Eur. J. Neurosci.* **9**:

2359–2369.

Borst JG, Sakmann B (1996) Calcium influx and transmitter release in a fast CNS

synapse. *Nature* **383**: 431–434.

Bowery NG (1993) GABAB receptor pharmacology. *Annu. Rev. Pharmacol.*

Toxicol. **33**: 109–147.

Brailoiu E, Miyamoto MD (2000) Inositol trisphosphate and cyclic adenosine

diphosphate-ribose increase quantal transmitter release at frog motor nerve

terminals: possible involvement of smooth endoplasmic reticulum.

Neuroscience **95**: 927–931.

Brenowitz S, David J, Trussell L (1998) Enhancement of synaptic efficacy by

presynaptic GABA(B) receptors. *Neuron* **20**: 135–141.

Brenowitz S, Trussell LO (2001) Minimizing synaptic depression by control of

release probability. *J. Neurosci.* **21**: 1857-1867.

Brickley SG, Cull-Candy SG, Farrant M (1996) Development of a tonic form of synaptic inhibition in rat cerebellar granule cells resulting from persistent activation of GABAA receptors. *J. Physiol. (Lond.)* **497**: 753–759.

Brickley SG, Revilla V, Cull-Candy SG, Wisden W, Farrant M (2001) Adaptive regulation of neuronal excitability by a voltage-independent potassium conductance. *Nature* **409**: 88-92.

Brock LG, Coombs JS, Eccles JC (1952) The recording of potentials from motoneurones with an intracellular electrode. *J. Physiol. (Lond.)* **117**: 431-460.

Brody DL, Patil PG, Mulle JG, Snutch TP, Yue DT (1997) Bursts of action potential waveforms relieve G-protien inhibition of recombinant P/Q-type Ca2+ channels in HEK 293 cells. *J. Physiol. (Lond.)* **499**: 637–644.

Brody DL, Yue DT (2000) Relief of G-protein inhibition of calcium channels and short-term synaptic facilitation in cultured hippocampal neurons. *J. Neurosci.* **20**: 889–898.

Brooks PA, Glaum SR, Miller RJ, Spyer KM (1992) The actions of baclofen on neurones and synaptic transmission in the nucleus tractus solitarii of the rat *in vitro. J. Physiol. (Lond.)* **457**: 115–129.

Cajal, SR (1911). *Histologie du Système Nerveux de l'Homme et des Vertébrés*. L. Azoulay, trans. Maloine: Paris.

Capogna M, Gahwiler BH, Thompson SM (1996a) Presynaptic inhibition of calcium-dependent and -independent release elicited with ionomycin, gadolinium, and alpha-latrotoxin in the hippocampus. *J. Neurophysiol.* **75**: 2017–2028.

Capogna M, Gahwiler BH, Thompson SM (1996b) Calcium-independent actions of alpha-latrotoxin on spontaneous and evoked synaptic transmission in the hippocampus. *J. Neurophysiol.* **76**: 3149–3158.

Castillo PE, Malenka RC, Nicoll RA (1997) Kainate receptors mediate a slow postsynaptic current in hippocampal CA3 neurons. *Nature* **388**: 182–186.

Cathala L, Misra C, Cull-Candy SG (2000) Developmental profile of the changing properties of NMDA receptors at cerebellar mossy fiber-granule cell synapses. *J. Neurosci.* **20**: 5899-5905.

Ceccarelli B, Hurlbut WP, Mauro A (1972) Depletion of vesicles from frog neuromuscular junctions by prolonged tetanic stimulation. *J. Cell. Biol.* **54**: 30-38.

Charlton MP, Smith SJ, Zucker RS (1982) Role of presynaptic calcium ions and channels in synaptic facilitation and depression at the squid giant synapse. *J. Physiol. (Lond.)* **323**: 173-193.

Clements JD, Bekkers JM (1997) Detection of spontaneous synaptic events with an optimally scaled template. *Biophys. J.* **73**: 220–229.

Clements JD, Silver RA (2000) Unveiling synaptic plasticity: a new graphical and analytical approach. *Trends Neurosci.* **23**: 105–113 .

Cochilla AJ, Alford S (1998) Metabotropic glutamate receptor-mediated control of neurotransmitter release. *Neuron* **20**: 1007–1016.

Conn PJ, Pin J-P (1997) Pharmacology and functions of metabotropic glutamate receptors. *Annu. Rev. Pharmacol. Toxicol.* **37**: 205–237.

Cull-Candy SG, Ogden DC (1985) Ion channels activated by L-glutamate and GABA in cultured cerebellar neurons of the rat. *Proc. R. Soc. Lond. B Biol. Sci.* **224**: 367-373.

Curtis DR, Duggan AW, Felix D, Johnston GA (1970a) GABA, bicuculline and central inhibition. *Nature* **226**: 1222-1224.

Curtis DR, Duggan AW, Felix D, Johnston GA (1970b) Bicuculline and central GABA receptors. *Nature* **228**:676-677.

Curtis DR, Phillis JW, Watkins JC (1959) Chemical excitation of spinal neurons. *Nature* **183**: 611

Curtis DR, Phillis JW, Watkins JC (1960) The chemical excitation of spinal neurones by certain acidic amino acids. *J. Physiol. (Lond.)* **150**: 656-682

D'Angelo E, De Filippi G, Rossi P, Taglietti V (1995) Synaptic excitation of individual rat cerebellar granule cells in situ: evidence for the role of NMDA receptors. *J. Physiol. (Lond.)* **484**: 397–413.

D'Angelo E, De Filippi G, Rossi P, Taglietti V (1998) Ionic mechanism of electroresponsiveness in cerebellar granule cells implicates the action of a persistent sodium current. *J. Neurophysiol.* **80**: 493–503.

D'Angelo E, Nieus T, Maffei A, Armano S, Rossi P, Taglietti V, Fontana A, Naldi

G (2001) Theta-frequency bursting and resonance in cerebellar granule

cells: experimental evidence and modeling of a slow K+-dependent

mechanism. *J. Neurosci.* **21**: 759-770.

D'Angelo E, Rossi P, Garthwaite J (1990) Dual-component NMDA receptor

currents at a single central synapse. *Nature* **346**: 467-470.

D'Angelo E, Rossi P, Taglietti V (1993) Different proportions of N-methyl-D-

aspartate and non-N-methyl-D-aspartate receptor currents at the mossy

fibre-granule cell synapse of developing rat cerebellum. *Neuroscience* **53**:

121–130.

D'Angelo E, Rossi P, Taglietti V (1994) Voltage-dependent kinetics of N-methyl-

D-aspartate synaptic currents in rat cerebellar granule cells. *Eur. J.*

Neurosci. **6**: 640–645.

Dale HH (1935) Pharmacology and nerve endings. *Proc. R. Soc. Lond. Med.* **28**:

319-332.

Davidoff RA (1972) Gamma-aminobutyric acid antagonism and presynaptic

inhibition in the frog spinal cord. *Science* **175**: 331-333.

Davies CH, Collingridge GL (1993) The physiological regulation of synaptic

inhibition by GABAB autoreceptors in rat hippocampus. *J. Physiol.*

(Lond.) **472**: 245–265.

Davies CH, Starkey SJ, Pozza MF, Collingridge GL (1991) GABA autoreceptors

regulate the induction of LTP. *Nature* **349**: 609–611

de Robertis E, Bennett HS (1954) Submicroscopic vesicular components in the synapse. *Fed. Proc.* **13**: 35.

de Robertis E, Bennett HS (1955) Some features of sub-microscopic morphology of synapses in frog and earthworm. *J. Biophys. Biochem. Cytol.* **1**: 47-58.

De Waard M, Liu H, Walker D, Scott VE, Gurnett CA, Campbell KP (1997) Direct binding of G-protein betagamma complex to voltage-dependent calcium channels. *Nature* **385**: 446–450.

del Castillo J, Katz B (1954) Quantal components of the end-plate potential. *J. Physiol. (Lond.)* **124**: 560–573.

del Castillo, Katz (1956) Biophysical aspects neuromuscular transmission. *Prog. Biophys. Biophys Chem.* **6**: 121-170.

del Castillo J, Stark L (1952) The effect of calcium ions on the motor end-plate potentials. *J. Physiol. (Lond.)* **116**: 507-515.

Demeneix BA, Taleb O, Loeffler JP, Feltz P (1986) $GABA_A$ and $GABA_B$ receptors on porcine pars intermedia cells in primary culture: functional role in modulating peptide release. *Neuroscience* **17**: 1275–1285.

Diamond JS, Jahr CE (1997) Transporters buffer synaptically released glutamate on a submillisecond time scale. *J. Neurosci.* **17**: 4672–4687.

Dieudonne S (1995) Glycinergic synaptic currents in Golgi cells of the rat cerebellum. *Proc. Natl Acad. Sci. USA* **92**: 1441–1445.

Dieudonne S (1998) Submillisecond kinetics and low efficacy of parallel fibre-Golgi cell synaptic currents in the rat cerebellum. *J. Physiol. (Lond.)* **510**: 845–866.

Dittman JS, Kreitzer AC, Regehr WG (2000) Interplay between facilitation, depression, and residual calcium at three presynaptic terminals. *J. Neurosci.* **20**: 1374–1385.

Dittman JS, Regehr WD (1996) Contributions of calcium-dependent and calcium-independent mechanisms to presynaptic inhibition at a cerebellar synapse. *J. Neurosci.* **16**: 1623–1633.

Dittman JS, Regehr WD (1997) Mechanisms and kinetics of heterosynaptic depression at a cerebellar synapse. *J. Neurosci.* **17**:9048–9059.

Dittman JS, Regehr WD (1998) Calcium dependence and recovery kinetics of presynaptic depression at the climbing fiber to Purkinje cell synapse. *J. Neurosci.* **18**: 6147–6162.

Dodge FA Jr, Rahamimoff R (1967) Co-operative action a calcium ions in transmitter release at the neuromuscular junction. *J. Physiol. (Lond.)* **193**: 419–432.

Dolphin AC (1998) Mechanisms of modulation of voltage-dependent calcium channels by G-proteins. *J. Physiol. (Lond.)* **506**: 3–11.

Dolphin AC, Scott RH (1987) Calcium channel currents and their inhibition by (-)-baclofen in rat sensory neurones: modulation by guanine nucleotides. *J. Physiol. (Lond.)* **386**: 1–17.

Duncan D, Morales R (1978) Relative numbers of several types of synaptic connections in the substantia gelatinosa of the cat spinal cord. *J. Comp. Neurol.* **182**: 601–610.

Dutar P, Nicoll RA (1988) A physiological role for GABAB receptors in the central nervous system. *Nature* **332**: 156–158.

Dutar P, Petrozzino JJ, Vu HM, Schmidt MF, Perkel DJ (2000) Slow synaptic inhibition mediated by metabotropic glutamate receptor activation of GIRK channels. *J. Neurophysiol.* **84**: 2284–2290.

Eccles JC, Eccles RM, Magni F (1961) Central inhibitory action attributable to presynaptic depolarization produced by muscle afferent volleys. *J. Physiol. (Lond.)* **159**: 147-166.

Eccles JC, Fatt P, Koketsu K (1954) Cholinergic and inhibitory synapses in a pathway from motor-axon collaterals to motoneurones. *J. Physiol. (Lond.)* **126**: 275-291.

Eccles JC, Ito M, Szentagothia J (1967) *The cerebellum as a neuronal machine.* Springer-Verlag, Berlin.

Edgley SA, Lidierth M (1987) The discharges of cerebellar Golgi cells during locomotion in the cat. *J. Physiol. (Lond.)* **392**: 315–332.

Edwards FA, Konnerth A, Sakmann B, Takahashi T (1989) A thin slice preparation for patch clamp recordings from neurones of the mammalian central nervous system. *Pflugers Arch.* **414**: 600-612.

Elmquist D, Quastel D (1965) A quantitative study of end-plate potentials in isolated human muscle. *J. Physiol. (Lond.)* **178**: 505–529.

Ermentrout B (1998) Linearization of f-I curves by adaptation. *Neural Comput.* **10**: 1721–1729.

Fatt P, Katz B (1951) An analysis of the end-plate potential recorded with an intra-cellular electrode. *J. Physiol. (Lond.)* **115**: 320-370.

Feng TP (1936) Studies on the neuromuscular junction. II. The universal antagonism between calcium and curarizing agencies. *Ch. J. Physiol.* **10**, 513-528.

Finkel AS, Redman SJ (1983) The synaptic current evoked in cat spinal motoneurones by impulses in single group 1a axons. *J. Physiol. (Lond.)* **342**: 615–632.

Forsythe ID, Tsujimoto T, Barnes-Davies M, Cuttle MF, Takahashi, T (1998) Inactivation of presynaptic calcium current contributes to synaptic depression at a fast central synapse. *Neuron* **20**: 797–807.

Foster M (1897) *A textbook of physiology*, 7th Ed. Macmillan, New York.

Frank K, Fuortes MGF (1957) Presynaptic and post-synaptic inhibition of monosynaptic reflexes. *Fed.. Proc.* **16**: 39-40.

Gabbiani F, Midtgaard J, Knopfel T (1994) Synaptic integration in a model of cerebellar granule cells. *J. Neurophysiol.* **72**: 999–1009.

Gabbott PL, Somogyi J, Stewart MG, Hamori J (1986) GABA-immunoreactive neurons in the rat cerebellum: a light and electron microscope study. *J. Comp. Neurol.* **251**: 474-490.

Galarreta M, Hestrin S (1998) Frequency-dependent synaptic depression and the balance of excitation and inhibition in the neocortex. *Nature Neurosci.* **1**: 587–594.

Gamble E, Koch C (1987) The dynamics of free calcium in dendritic spines in response to repetitive synaptic input. *Science* **236**: 1311–1315.

Garthwaite J, Brodbelt AR (1989) Synaptic activation of N-methyl-D-aspartate and non-N-methyl-D-aspartate receptors in the mossy fibre pathway in adult and immature rat cerebellar slices. *Neuroscience* **29**: 401-412.

Geiger JR, Lubke J, Roth A, Frotscher M, Jonas P (1997) Submillisecond AMPA receptor-mediated signaling at a principal neuron-interneuron synapse. *Neuron* **18**: 1009–1023.

Gereau RW 4th, Conn PJ (1995) Multiple presynaptic metabotropic glutamate receptors modulate excitatory and inhibitory synaptic transmission in hippocampal area CA1. *J. Neurosci.* **15**: 6879–6889.

Ghirardi M, Braha O, Hochner B, Montarolo PG, Kandel ER, Dale N (1992) Roles of PKA and PKC in facilitation of evoked and spontaneous transmitter release at depressed and nondepressed synapses in Aplysia sensory neurons. *Neuron* **9**: 479–489.

Gil Z, Conners BW, Amitai Y (1997) Differential regulation of neocortical synapses by neuromodulators and activity. *Neuron* **19**: 679–686.

Gilbert CD (1983) Microcircuitry of the visual cortex. *Annu. Rev. Neurosci.* **6**: 217-247.

Glitsch M, Llano I, Marty A, Morishita W (1996) Glutamate as a candidate retrograde messenger at interneurone-Purkinje cell synapses of rat cerebellum. *J. Physiol. (Lond.)* **497**: 531–537.

Gray EG (1962) A morphological basis for presynaptic inhibition? *Nature* **193**: 82-83.

Gregory WA, Edmondson JC, Hatten ME, Mason CA (1988) Cytology and neuron-glial apposition of migrating cerebellar granule cells in vitro. *J. Neurosci.* **8**: 1728-1738.

Grovas AC, O'Shea KS (1984) An SEM examination of granule cell migration in the mouse cerebellum. *J. Neurosci. Res.* **12**: 1-14.

Hamill OP, Marty A, Neher E, Sakmann B, Sigworth FJ (1981) Improved patch-clamp techniques for high-resolution current recording from cells and cell-free membrane patches. *Pflugers Arch.* **391**: 85–100.

Hamori J, Somogyi J (1983) Differentiation of cerebellar mossy fiber synapses in the rat: a quantitative electron microscope study. *J. Comp. Neurol.* **220**: 365–377 .

Häusser M, Major G, Stuart GJ (2001) Differential shunting of EPSPs by action potentials. *Science* **291**: 138-141.

Hayashi T (1954) Effects of sodium glutamate on the nervous system. *Keio J. Med.* **3**: 183-192.

Hayashi Y, Momiyama A, Takahashi T, Ohishi H, Ogawa-Meguro R, Shigemoto R, Mizuno N, Nakanishi S (1993) Role of a metabotropic glutamate receptor in synaptic modulation in the accessory olfactory bulb. *Nature* **366**: 687–690.

Helmchen F, Imoto K, Sakmann B (1996) Ca2+ buffering and action potential-evoked Ca2+ signaling in dendrites of pyramidal neurons. *Biophys. J.* **70**: 1069–1081.

Hendrickson AE, Ogren MP, Vaughn JE, Barber RP, Wu JY (1983) Light and electron microscopic immunocytochemical localization of glutamic acid decarboxylase in monkey geniculate complex: evidence for gabaergic neurons and synapses. *J. Neurosci.* **3**: 1245-1262.

Herlitze S, Garcia DE, Mackie K, Hille B, Scheuer T, Catterall WA (1996) Modulation of Ca2+ channels by G-protein beta gamma subunits. *Nature* **380**: 258–262.

Heuser JE, Reese TS (1973) Evidence for recycling of synaptic vesicle membrane during transmitter release at the frog neuromuscular junction. *J. Cell Biol.* **57**: 315-344.

Heuser JE, Reese TS, Dennis MJ, Jan Y, Jan L, Evans L (1979) Synaptic vesicle exocytosis captured by quick freezing and correlated with quantal transmitter release. *J. Cell Biol.* **81**: 275-300.

Heuser JE, Reese TS, Landis DM (1974) Functional changes in frog neuromuscular junctions studied with freeze-fracture. J. *Neurocytol.* **3**: 109–131.

Heuser JE (1989) Review of electron microscopic evidence favouring vesicle exocytosis as the structural basis for quantal release during synaptic transmission. *Q. J. Exp. Physiol.* **74**: 1051-1069.

Hille B (1994) Modulation of ion-channel function by G-protein-coupled receptors. *Trends Neurosci.* **17**: 531-536.

Hille, B (1992) Potassium channels and chloride channels. In: *Ionic channels of excitable membranes*. 2nd edition. Ch 5. Sinauer Associates, Inc., Sunderland, Massachusetts.

Hodgkin AL, Huxley AF (1952) A quantitative description of membrane current and its application to conduction and excitation in nerve. *J. Physiol. (Lond.)* **117**: 500-544.

Hollmann M, Heinemann S (1994) Cloned glutamate receptors. *Annu. Rev. Neurosci.* **17**: 31-108.

Holt GR, Koch C (1997) Shunting inhibition does not have a divisive effect on firing rates. *Neural Comput.* **9**: 1001-1013.

Hopfield JJ (1995) Pattern recognition computation using action potential timing for stimulus representation. *Nature* **376**: 33-6.

Huang CL, Slesinger PA, Casey PJ, Jan YN, Jan LY (1995) Evidence that direct binding of G beta gamma to the GIRK1 G protein-gated inwardly rectifying K+ channel is important for channel activation. *Neuron* **15**: 1133-1143.

Ikeda SR (1996) Voltage-dependent modulation of N-type calcium channels by G-protein beta gamma subunits. *Nature* **380**: 255–258.

Inukai T (1928) On the loss of Purkinje cells, with advancing age, from the cerebellar cortex of the albino rat. *J. Comp. Neurol.* **45**: 1-31.

Isaacson JS (1998) GABAB-R-mediated modulation of presynaptic currents and excitatory transmission at a fast central synapse. *J. Neurophysiol.* **80**:1571–1576.

Isaacson JS (1999) Glutamate spillover mediates excitatory transmission in the rat olfactory bulb. *Neuron* **23**: 377–384.

Isaacson JS, Solis JM, Nicoll RA (1993) Local and diffuse synaptic actions of GABA in the hippocampus. *Neuron* **10**: 165–175.

Ito M (1984) In: *The Cerebellum and Neural Control*. Raven, New York.

Ito M, Sakurai M, Tongroach P (1982) Climbing fibre induced depression of both mossy fibre responsiveness and glutamate sensitivity of cerebellar Purkinje cells. *J. Physiol. (Lond.)* **324**: 113–134.

Itouji A, Sakai N, Tanaka C, Saito N (1996) Neuronal and glial localization of two GABA transporters (GAT1 and OAT3) in the rat cerebellum. *Brain Res. Mol. Brain. Res.* **37**: 309–316.

Jaarsma D, Dino MR, Ohishi H, Shigemoto R, Mugnaini E (1998) Metabotropic glutamate receptors are associated with non-synaptic appendages of unipolar brush cells in rat cerebellar cortex and cochlear nuclear complex. *J. Neurocytol.* **27**: 303–327.

Jack JJB, Noble D, Tsien R (1983) *Electrical current flow in excitable cells.*

Revised paperback edition OUP: Oxford.

Jahr CE, Stevens CF (1990a) Voltage dependence of NMDA-activated

macroscopic conductances predicted by single-channel kinetics. *J.*

Neurosci. **10**: 3178–3182.

Jahr CE, Stevens CF (1990b) A quantitative description of NMDA receptor-

channel kinetic behavior. *J. Neurosci.* **10**: 1830–1837.

Jakab RL, Hámori J (1988) Quantitative morphology and synaptology of

cerebellar glomeruli in the rat. *Anat. Embryol.* **179**: 81–88.

Jan LY, Jan YN (1976) L-glutamate as an excitatory transmitter at the Drosophila

larval neuromuscular junction. *J. Physiol. (Lond.)* **262**: 215-236.

Ji ZQ, Aas JE, Laake J, Walberg F, Ottersen OP (1991) An electron microscopic,

immunogold analysis of glutamate and glutamine in terminals of rat

spinocerebellar fibers. *J. Comp. Neurol.* **307**: 296-310.

Jiang ZG, Allen CN, North RA (1995) Presynaptic inhibition by baclofen of

retinohypothalamic excitatory synaptic transmission in rat suprachiasmatic

nucleus. *Neuroscience* **64**: 813–819.

Johnston GA (1996) GABAC receptors: relatively simple transmitter-gated ion

channels? *Trends Pharmacol. Sci.* **17**: 319–329.

Jörntell H, Midtgaard J (1999) Inhibitory control of mossy fibre input in turtle

cerebellar granule cells by $GABA_A$ and $GABA_B$ responses. *Society for*

Neuroscience Abstracts **25**: 566.13.

Kaneda M, Farrant M, Cull-Candy SG (1995) Whole-cell and single-channel

currents activated by GABA and glycine in granule cells of the rat

cerebellum. *J. Physiol. (Lond.)* **485**: 419-435.

Kaneko T, Itoh K, Shigemoto R, Mizuno N (1989) Glutaminase-like

immunoreactivity in the lower brainstem and cerebellum of the adult rat.

Neuroscience **32**: 79-98.

Katz B (1962) The transmission of impulses from nerve to muscle and the

subcellular unit of synaptic action. *Proc. R. Soc. Lond. B Biol. Sci.* **155**:

455-477.

Katz B (1969) *The release of neural transmitter substances*. Liverpool: Liverpool

University Press.

Katz B, Miledi R (1968) The role of calcium in neuromuscular facilitation. *J.

Physiol. (Lond.)* **195**: 481–492.

Kaupmann K, Huggel K, Heid J, Flor PJ, Bischoff S, Mickel SJ, McMaster G,

Angst C, Bittiger H, Froestl W, Bettler B (1997) Expression cloning of

GABA(B) receptors uncovers similarity to metabotropic glutamate

receptors. *Nature* **386**: 239–246.

Kim U, Sanchez-Vives MV, McCormick DA (1997) Functional dynamics of

GABAergic inhibition in the thalamus. *Science* **278**: 130–134.

Kirischuk S, Veselovsky N, Grantyn R (1999) Relationship between presynaptic

calcium transients and postsynaptic currents at single gamma-aminobutyric

acid (GABA)ergic boutons. *Proc. Natl. Acad. Sci. USA.* **96**: 7520-7525.

Knoflach F, Kemp JA (1998) Metabotropic glutamate group II receptors activate a

G protein-coupled inwardly rectifying K+ current in neurones of the rat

cerebellum. *J. Physiol. (Lond.)* **509**: 347–354.

Knoflach F, Woltering T, Adam G, Mutel V, Kemp JA (2001) Pharmacological

properties of native metabotropic glutamate receptors in freshly dissociated

Golgi cells of the rat cerebellum. *Neuropharmacology* **40**: 163-169.

Koch C (1999) *Biophysics of computation*. Oxford University Press, New York.

Kombian SB, Zidichouski IA, Pittman QJ (1996) $GABA_B$ receptors

presynaptically modulate excitatory synaptic transmission in the rat su-

praoptic nucleus in vitro. *J. Neurophysiol.* **76**: 1166–1179.

Kreitzer AC, Regehr WG (2000) Modulation of transmission during trains at a

cerebellar synapse. *J. Neurosci.* **20**: 1348–1357.

Kusano K, Landau EM (1975). Depression and recovery of transmission at the

squid giant synapse. *J. Physiol. (Lond.)* **245**: 13–22.

Lam DM, Ayoub GS (1983) Biochemical and biophysical studies of isolated

horizontal cells from the teleost retina. *Vision Res.* **23**: 433-444.

Lapicque, L (1907) Recherches quantitatifs sur l'excitation electrique des nerfs

traitée comme une polarisation, *J. Physiol. (Paris)* **9**: 620–635.

Llano I, Marty A (1995) Presynaptic metabotropic glutamatergic regulation of

inhibitory synapses in rat cerebellar slices. *J. Physiol. (Lond.)* **486**: 163–

176.

Llinas R, Blinks JR, Nicholson C (1972) Calcium transient in presynaptic terminal of squid giant synapse: detection with aequorin. *Science* **176**: 1127-1129.

Llinas R, Steinberg IZ, Walton K (1981) Relationship between presynaptic calcium current and postsynaptic potential in squid giant synapse. *Biophys. J.* **33**: 323-351.

Luscher C, Jan LY, Stoffel M, Malenka RC, Nicoll RA (1997) G protein-coupled inwardly rectifying K+ channels (GIRKs) mediate postsynaptic but not presynaptic transmitter actions in hippocampal neurons. *Neuron* **19**: 687–695.

MacDonald RL, Olsen RW (1994) GABAA receptor channels. *Annu. Rev. Neurosci.* **17**: 569–602.

Maex R, De Schutter ED (1998) Synchronization of golgi and granule cell firing in a detailed network model of the cerebellar granule cell layer. *J. Neurophysiol.* **80**: 2521–2537.

Magleby KL (1987) Short-term changes in synaptic efficacy. In: *Synaptic Function.* Edelman GM, Gall WE, Cowan WM, eds, John Wiley & Sons: New York.

Markram H., Tsodyks M (1996). Redistribution of synaptic efficacy between neocortical pyramidal neurons. *Nature* **382**: 807–810.

Marr D (1969) A theory of cerebellar cortex. *J. Physiol. (Lond.)* **202**: 437-470.

Marshall FH, Jones KA, Kaupmann K, Bettler B (1999) GABAB receptors - the first 7TM heterodimers. *Trends Pharmacol. Sci.* **20**: 396–399.

Martin R, Miledi R (1978) A structural study of the squid synapse after

intraaxonal injection of calcium. *Proc. R. Soc. Lond. B Biol. Sci.* **201**: 317-

333.

Martin AR, Patel V, Faille L, Mallart A (1989) Presynaptic calcium currents

recorded from calyciform nerve terminals in the lizard ciliary ganglion.

Neurosci. Lett. **105**: 14-18.

Mason A, Ilinsky IA, Beck S, Kultas-Ilinsky K (1996) Reevaluation of synaptic

relationships of cerebellar terminals in the ventral lateral nucleus of the

rhesus monkey thalamus based on serial section analysis and three-

dimensional reconstruction. *Exp. Brain Res.* **109**: 219–239.

Mason CA, Gregory E (1984) Postnatal maturation of cerebellar mossy and

climbing fibers: transient expression of dual features on single axons. *J.

Neurosci.* **4**: 1715-1735.

Matveev V, Wang XJ (2000) Implications of all-or-none synaptic transmission

and short-term depression beyond vesicle depletion: a computational

study. *J. Neurosci.* **20**: 1575–1588.

McGlade-McCulloh E, Yamamoto H, Tan S-E, Brickey DA, Soderling TR (1993)

Phosphorylation and regulation of glutamate receptors by

calcium/calmodulin-dependent protein kinase II. *Nature* **362**: 640–642.

Miledi R, Slater CR (1966) The action of calcium on neuronal synapses in the

squid. *J. Physiol. (Lond.)* **184**: 473-498.

Miledi R (1973) Transmitter release induced by injection of calcium ions into

nerve terminals. *Proc. R. Soc. Lond. B Biol. Sci.* **183**: 421-425.

Min MY, Melyan Z, Kullmann DM (1999) Synaptically released glutamate

reduces gamma-aminobutyric acid (GABA)ergic inhibition in the

hippocampus via kainate receptors. *Proc. Natl Acad. Sci. USA* **96**: 9932–

9937.

Mintz IM, Bean BP (1993) GABAB receptor inhibition of P-type Ca2+ channels

in central neurons. *Neuron* **10**: 889–898.

Mintz IM, Sabatini BL, Regehr WG (1995) Calcium control of transmitter release

at a cerebellar synapse. *Neuron* **15**: 675-688.

Misra C, Brickley SG, Farrant M, Cull-Candy SG (2000) Identification of subunits

contributing to synaptic and extrasynaptic NMDA receptors in Golgi cells

of the rat cerebellum. *J. Physiol. (Lond.)* **524**: 147–162.

Mitchell SJ, Silver RA (2000a) Glutamate spillover suppresses inhibition by

activating presynaptic mGluRs. *Nature* **404**: 498–502.

Mitchell SJ, Silver RA (2000b) GABA spillover from single inhibitory axons

suppresses low frequency excitatory transmission at the cerebellar

glomerulus. *J. Neurosci.* **20**: 8651–8658.

Morishita W, Kirov SA, Alger BE (1998) Evidence for metabotropic glutamate

receptor activation in the induction of depolarization-induced suppression

of inhibition in hippocampal CA1. *J. Neurosci.* **18**: 4870–4882.

Morishita W, Sastry BR (1994) Presynaptic actions of GABA and baclofen in

CA1 region of the guinea-pig hippocampus *in vitro*. *Neuroscience* **61**:

447–455.

Mosbacher J, Schoepfer R, Monyer H, Burnashev N, Seeburg PH, Ruppersberg JP

(1994) A molecular determinant for submillisecond desensitization in

glutamate receptors. *Science* **266**: 1059-1062.

Nachshen DA, Sanchez-Armass S (1987) Co-operative action of calcium ions in

dopamine release from rat brain synaptosomes. *J. Physiol. (Lond.)* **387**:

415-423.

Neki A, Ohishi H, Kaneko T, Shigemoto R, Nakanishi S, Mizuno N (1996)

Metabotropic glutamate receptors mGluR2 and mGluR5 are expressed in

two non-overlapping populations of Golgi cells in the rat cerebellum.

Neuroscience **75**: 815–826.

Nelson PG, Pun RY, Westbrook GL (1986) Synaptic excitation in cultures of

mouse spinal cord neurones: receptor pharmacology and behaviour of

synaptic currents. *J. Physiol. (Lond.)* **372**: 169–190.

Nicoll RA (1988) The coupling of neurotransmitter receptors to ion channels in

the brain. *Science* **241**: 545-551.

Nisenbaum ES, Berger TW, Grace AA (1992) Presynaptic modulation by GABAB

receptors of glutamatergic excitation and GABAergic inhibition of

neostriatal neurons. *J. Neurophysiol.* **67**: 477–481.

Nowak L, Bregestovski P, Ascher P, Herbet A, Prochiantz A (1984) Magnesium

gates glutamate-activated channels in mouse central neurones. *Nature* **307**:

462–465.

Nusser Z, Sieghart W, Somogyi P (1998) Segregation of different GABA$_A$

receptors to synaptic and extrasynaptic membranes of cerebellar granule

cells. *J. Neurosci.* **18**:1693–1703.

O'Connor V, El Far O, Bofill-Cardona E, Nanoff C, Freissmuth M, Karschin A,

Airas JM, Betz H, Boehm S (1999) Calmodulin dependence of presynaptic

metabotropic glutamate receptor signaling. *Science* **286**: 1180–1184.

Obata K, Takeda K, Shinozaki H (1970) Further study on pharmacological

properties of the cerebellar-induced inhibition of Deiters neurones. *Exp.*

Brain. Res. **11**: 327-342.

Obata K, Takeda K (1969) Release of gamma-aminobutyric acid into the fourth

ventricle induced by stimulation of the cat's cerebellum. *J. Neurochem.* **16**:

1043-1047.

Ohishi H, Ogawa-Meguro R, Shigemoto R, Kaneko T, Nakanishi S, Mizuno N

(1994) Immunohistochemical localization of metabotropic glutamate

receptors, mGluR2 and mGluR3, in rat cerebellar cortex. Neuron **13**: 55–

66.

Ohishi H, Shigemoto R, Nakanishi S, Mizuno N (1993) Distribution of the mRNA

for a metabotropic glutamate receptor (mGluR3) in the rat brain: an in situ

hybridization study. *J. Comp. Neurol.* **335**: 252–266.

Olney JW (1990) Excitotoxic amino acids and neuropsychiatric disorders. *Annu.*

Rev. Pharmacol. Toxicol. **30**: 47–71.

Otis TS, Zhang S, Trussell LO (1996). Direct measurement of AMPA receptor

desensitization induced by glutamatergic synaptic transmission. *J.

Neurosci.* **16**: 7496–7504.

Otsuka M, Obata K, Miyata Y, Tanaka Y (1971) Measurement of gamma-

aminobutyric acid in isolated nerve cells of cat central nervous system. *J.

Neurochem.* **18**: 287-295.

Overstreet LS, Kinney GA, Liu YB, Billups D, Slater NT (1999) Glutamate

transporters contribute to the time course of synaptic transmission in

cerebellar granule cells. *J. Neurosci.* **19**: 9663–9673.

Palade GE (1954) Electron microscope observations of interneuronal and

neuromuscular synapses. *Anatomical record* **118**: 335-6.

Palay SL (1954) Electron microscope study of the cytoplasm of neurons.

Anatomical record **118**: 336.

Palay SL, Chan-Palay V (1974) *Cerebellar cortex cytology and organization.*

Berlin: Springer.

Peng YY, Frank E (1989a) Activation of GABAB receptors causes presynaptic

inhibition at synapses between muscle spindle afferents and motoneurons

in the spinal cord of bullfrogs. *J. Neurosci.* **9**: 1502-1515.

Peng YY, Frank E (1989b) Activation of GABAA receptors causes presynaptic

and postsynaptic inhibition at synapses between muscle spindle afferents

and motoneurons in the spinal cord of bullfrogs. *J. Neurosci.* **9**: 1516-

1522.

Pfrieger FW, Gottmann K, Lux HD (1994) Kinetics of GABA$_B$ receptor-mediated inhibition of calcium currents and excitatory synaptic transmission in hippocampal neurones *in vitro. Neuron* **12**: 97–107.

Poncer JC, Shinozaki H, Miles R (1995) Dual modulation of synaptic inhibition by distinct metabotropic glutamate receptors in the rat hippocampus. *J. Physiol. (Lond.)* **485**: 121–134.

Poorkhalkali N, Juneblad K, Jonsson AC, Lindberg M, Karlsson O, Wallbrandt P, Ekstrand J, Lehmann A (2000) Immunocytochemical distribution of the GABA(B) receptor splice variants GABA(B) Rla and Rlb in the rat CNS and dorsal root ganglia. *Anat. Embryol. (Berl.)* **201**: 1–13.

Press WH, Teukolsky SA, Vetterling WT, Flannery BP (1993) Integration of ordinary differential equations. In: *Numerical Recipes in C*, 2nd edition. Ch. 16 Cambridge University Press, Cambridge, UK.

Purves D, et al. (2001) *Neuroscience*, 2nd Ed. Sinauer, Sunderland, Massachusetts.

Redman S (1990) Quantal analysis of synaptic potentials in neurons of the central nervous system. *Physiol. Rev.* **70**: 165–198.

Reid CA, Bekkers JM, Clements JD (1998) N- and P/Q-type Ca2+ channels mediate transmitter release with a similar cooperativity at rat hippocampal autapses. *J. Neurosci.* **18**: 2849-2855.

Reid CA, Clements JD (1999) Postsynaptic expression of long-term potentiation in the rat dentate gyrus demonstrated by variance-mean analysis. *J. Physiol. (Lond.)* **518**: 121–130.

Reuveny E, Slesinger PA, Inglese J, Morales JM, Iniguez-Lluhi JA, Lefkowitz RJ,

Bourne HR, Jan YN, Jan LY (1994) Activation of the cloned muscarinic

potassium channel by G protein beta gamma subunits. *Nature* **370**: 143–

146.

Rosenmund C, Carr DW, Bergeson SE, Nilaver G, Scott JD, Westbrook GL

(1994) Anchoring of protein kinase A is required for modulation of

AMPA/kainate receptors on hippocampal neurons. *Nature* **368**: 853–856.

Rosenmund C, Stevens CF (1996) Definition of the readily releasable pool of

vesicles at hippocampal synapses. *Neuron* **16**: 1197–1207.

Rossi DJ, Hamann M (1998) Spillover-mediated transmission at inhibitory

synapses promoted by high affinity alpha6 subunit GABAA receptors and

glomerular geometry. *Neuron* **20**: 783–795.

Rossi DJ, Oshima T, Attwell D (2000) Glutamate release in severe brain

ischaemia is mainly by reversed uptake. *Nature* **403**: 316–321.

Rusakov DA, Kullmann DM, Stewart MG (1999) Hippocampal synapses: do they

talk to their neighbours? *Trends Neurosci.* **22**: 382–388.

Sabatini BL, Regehr WG (1996) Timing of neurotransmission at fast synapses in

the mammalian brain. *Nature* **384**: 170–172.

Salt TE, Eaton SA (1995) Distinct presynaptic metabotropic receptors for L-AP4

and CCG1 on GABAergic terminals: pharmacological evidence using

novel alpha-methyl derivative mGluR antagonists, MAP4 and MCCG, in

the rat thalamus in vivo. *Neuroscience* **65**: 5-13.

Satake S, Saitow F, Yamada J, Konishi S (2000) Synaptic activation of AMPA receptors inhibits GABA release from cerebellar interneurons. *Nat. Neurosci.* **3**: 551–558.

Saugstad JA, Segerson TP, Westbrook GL (1996) Metabotropic glutamate receptors activate G-protein-coupled inwardly rectifying potassium channels in Xenopus oocytes. *J. Neurosci.* **16**: 5979–5985.

Saxena NC, MacDonald RC (1996) Properties of putative cerebellar γ-aminobutyric acid A receptor isoforms. *Mol. Pharmacol.* **49**: 567–579.

Scanziani M, Salin PA, Vogt KE, Malenka RC, Nicoll RA (1997) Use-dependent increases in glutamate concentration activate presynaptic metabotropic glutamate receptors. *Nature* **385**: 630–634.

Schäfer EA (1900) *Text-book of physiology.* Young J Pentland, London

Schneggenburger R, Neher E (2000) Intracellular calcium dependence of transmitter release rates at a fast central synapse. *Nature* **406**: 889–893.

Scholz KP, Miller RJ (1991) GABAB receptor-mediated inhibition of Ca2+ currents and synaptic transmission in cultured rat hippocampal neurones. *J. Physiol. (Lond.)* **444**: 669–686.

Schrader LA, Tasker JG (1997) Presynaptic modulation by metabotropic glutamate receptors of excitatory and inhibitory synaptic inputs to hypothalamic magnocellular neurons. *J. Neurophysiol.* **77**: 527–536.

Seabrook GR, Adams DJ (1989) Inhibition of neurally-evoked transmitter release by calcium channel antagonists in rat parasympathetic ganglia. *Br. J. Pharmacol.* **97**: 1125-1136.

Semyanov A, Kullmann DM (2000) Modulation of GABAergic signaling among interneurons by metabotropic glutamate receptors. *Neuron* **25**: 663–672.

Shekter LR, Taussig R, Gillard SE, Miller RJ (1997) Regulation of human neuronal calcium channels by G protein betagamma subunits expressed in human embryonic kidney 293 cells. *Mol. Pharmacol.* **52**: 282–291.

Shen KZ, Johnson SW (1997) Presynaptic GABA$_B$ and adenosine A1 receptors regulate synaptic transmission to rat substantia nigra reticulata neurones. *J. Physiol. (Lond.)* **505**: 153–163.

Shepherd, GM (1972) Synaptic organisation of the mammalian olfactory bulb. *Physiol. Rev.* **52**: 864–917.

Sherrington, S. C (1947). *The integrative action of the nervous system.* Cambridge University Press.

Shigemoto R, Nakanishi S, Mizuno N (1992) Distribution of the mRNA for a metabotropic glutamate receptor (mGluR1) in the central nervous system: an in situ hybridization study in adult and developing rat. *J. Comp. Neurol.* **322**: 121–135.

Sigworth FJ (1980) The variance of sodium current fluctuations at the node of Ranvier. *J. Physiol. (Lond.)* **307**: 97–129.

Silver RA, Colquhoun D, Cull-Candy SG, Edmonds B (1996a) Deactivation and

desensitization of non-NMDA receptors in patches and the time course of

EPSCs in rat cerebellar granule cells. *J. Physiol. (Lond.)* **493**: 167-173.

Silver RA, Cull-Candy SG & Takahashi T (1996b) Non-NMDA glutamate

receptor occupancy and open probability at a rat cerebellar synapse with

single and multiple release sites. *J. Physiol. (Lond.)* **494**: 231–250.

Silver, R.A., Farrant, M. and Cull-Candy, S.G (1996c). Filtering of synaptic

currents estimated from the time course of NMDA channel opening at the

rat cerebellar mossy fibre-granule cell synapse. *J. Physiol. (Lond.)* **494.P**:

85P.

Silver RA, Momiyama A & Cull-Candy SG (1998) Locus of frequency-dependent

depression identified with multiple-probability fluctuation analysis at rat

climbing fibre-Purkinje cell synapses. *J. Physiol. (Lond.)* **510**: 881-902.

Silver RA, Traynelis SF, Cull-Candy SG (1992) Rapid-time-course miniature and

evoked excitatory currents at cerebellar synapses *in situ. Nature* **355**: 163–

166.

Skaggs WE, McNaughton BL (1992) Computational approaches to hippocampal

function. *Curr. Opin. Neurobiol.* **2**: 209–211.

Sodickson DL, Bean BP (1996) GABAB receptor-activated inwardly rectifying

potassium current in dissociated hippocampal CA3 neurons. *J. Neurosci.*

16: 6374–6385.

Soejima M, Noma A (1984) Mode of regulation of the ACh-sensitive K-channel by the muscarinic receptor in rabbit atrial cells. *Pflugers Arch.* **400**: 424–431.

Somogyi P, Halasy K, Somogyi J, Storm-Mathisen J, Ottersen OP (1986) Quantification of immunogold labelling reveals enrichment of glutamate in mossy and parallel fibre terminals in cat cerebellum. *Neuroscience* **19**: 1045-1050.

Stanley EF (1986) Decline in calcium cooperativity as the basis of facilitation at the-P9 squid giant synapse. *J. Neurosci.* **6**: 782-789.

Stanley EF (1989) Calcium currents in a vertebrate presynaptic nerve terminal: the chick ciliary ganglion calyx. *Brain Res.* **505**: 341-345.

Sterling P (1983) Microcircuitry of the cat retina. *Annu. Rev. Neurosci.* **6**: 149-185.

Stern P, Edwards FA, Sakmann B (1992) Fast and slow components of unitary EPSCs on stellate cells elicited by focal stimulation in slices of rat visual cortex. *J. Physiol. (Lond.)* **449**: 247–278.

Stuart GJ, Dodt HU, Sakmann B (1993) Patch-clamp recordings from the soma and dendrites of neurons in brain slices using infrared video microscopy. *Pflugers Arch.* **423**: 511–518.

Stuart GJ, Redman SJ (1992) The role of GABAA and GABAB receptors in presynaptic inhibition of Ia EPSPs in cat spinal motoneurones. *J. Physiol. (Lond.)* **447**: 675-692.

Sultan F (2001) Distribution of mossy fibre rosettes in the cerebellum of cat and mice: evidence for a parasagittal organization at the single fibre level. *Eur. J. Neurosci.* **13**: 2123-2130.

Tachibana M, Okada T, Arimura T, Kobayashi K, Piccolino M (1993) Dihydropyridine-sensitive calcium current mediates neurotransmitter release from bipolar cells of the goldfish retina. *J. Neurosci.* **13**: 2898-2909.

Takahashi T, Forsythe ID, Tsujimoto T, Barnes-Davies M, Onodera K (1996) Presynaptic calcium current modulation by a metabotropic glutamate receptor. *Science* **274**: 594–597.

Takahashi T, Hori T, Kajikawa Y, Tsujimoto T (2000) The role of GTP-binding protein activity in fast central synaptic transmission. *Science* **289**: 460–463.

Takahashi T, Kajikawa Y, Tsujimoto T (1998) G-Protein-coupled modulation of presynaptic calcium currents and transmitter release by a $GABA_B$ receptor. *J. Neurosci.* **18**: 3138–3146.

Tanabe Y, Nomura A, Masu M, Shigemoto R, Mizuno N, Nakanishi S (1993) Signal transduction, pharmacological properties, and expression patterns of two rat metabotropic glutamate receptors, mGluR3 and mGluR4. *J. Neurosci.* **13**: 1372–1378.

Tang Y, Schlumpberger T, Kim T, Lueker M, Zucker RS (2000) Effects of mobile buffers on facilitation: experimental and computational studies. *Biophys. J.* **78**: 2735–2751.

Terrian DM, Green CL, Dorman RV, Wu PH (1987) Uptake, exchange, and

release of GABA by cerebellar glomeruli. *Neurochem. Res.* **12**:399–408.

Tessier-Lavigne M, Attwell D, Mobbs P, Wilson M (1988) Membrane currents in

retinal bipolar cells of the axolotl. *J. Gen. Physiol.* **91**: 49–72.

Tia S, Wang JF, Kotchabhakdi N, Vicini S (1996) Developmental changes of

inhibitory synaptic currents in cerebellar granule neurons: role of

GABA(A) receptor alpha 6 subunit. *J. Neurosci.* **16**: 3630–3640.

Tong G, Jahr CE (1994) Block of glutamate transporters potentiates postsynaptic

excitation. *Neuron* **13**: 1195–1203.

Trussell LO, Zhang S, Raman IM (1993). Desensitization of AMPA receptors

upon multiquantal neurotransmitter release. *Neuron* **10**: 1185–1196.

Tsien RY (1988) Fluorescence measurement and photochemical manipulation of

cytosolic free calcium. *Trends Neurosci.* **11**: 419-424.

Tsodyks MV, Markram H (1997) The neural code between neocortical pyramidal

neurons depends on neurotransmitter release probability. *Proc. Natl. Acad.

Sci. USA* **94**: 719-723

Tyrrell T, Willshaw D (1992) Cerebellar cortex: its stimulation and the relevance

of Marr's theory. *Phil. Trans. R. Soc. Lond. B* **336**: 239–257.

van den Pol AN, Gao XB, Patrylo PR, Ghosh PK, Obrietan K (1998) Glutamate

inhibits GABA excitatory activity in developing neurons. *J. Neurosci.* **18**:

10749–10761.

van Kan PL, Gibson AR, Houk JC (1993) Movement-related inputs to intermediate cerebellum of monkeys. *J. Neurophysiol.* **69**: 74–94.

Vetter P, Garthwaite J, Batchelor AM (1999) Regulation of synaptic transmission in the mossy fibre-granule cell pathway of rat cerebellum by metabotropic glutamate receptors. *Neuropharmacology* **38**: 805–815.

Vignes M, Collingridge GL (1997) The synaptic activation of kainate receptors. *Nature* **388**: 179–182.

Vogt KE, Nicoll RA (1999) Glutamate and gamma-aminobutyric acid mediate a heterosynaptic depression at mossy fibre synapses in the hippocampus. *Proc. Natl Acad. Sci. USA* **96**: 1118–1122.

Volterra A, Bezzi P, Rizzini BL, Trotti D, Ullensvang K, Danbolt NC, Racagni G (1996) The competitive transport inhibitor L-trans-pyrrolidine-2, 4-dicarboxylate triggers excitotoxicity in rat cortical neuron-astrocyte co-cultures via glutamate release rather than uptake inhibition. *Eur. J. Neurosci.* **8**: 2019–2028.

von Gersdorff H, Scheggenburger R, Weis S, Neher E (1997). Presynaptic depression at a calyx synapse: the small contribution of metabotropic glutamate receptors. *J. Neurosci.* **17**: 8137–8146.

Vos BP, Vofny-Luraghi A, De Schutter E (1999a) Cerebellar Golgi cells in the rat: receptive fields and timing of responses to facial stimulation. *Eur. J. Neurosci.* **11**: 2621–2634.

Vos BP, Maex R, Volny-Luraghi A, De Schutter E (1999b) Parallel fibers

synchronize spontaneous activity in cerebellar Golgi cells. *J. Neurosci.* **19**:

RC6.

Wadiche JI, Kavanaugh MP (1998) Macroscopic and microscopic properties of a

cloned glutamate transporter/chloride channel. *J. Neurosci.* **18**: 7650–

7661.

Wall MJ, Usowicz MM (1997) Development of action potential-dependent and

independent spontaneous GABAA receptor-mediated currents in granule

cells of postnatal rat cerebellum. *Eur. J. Neurosci.* **9**: 533–548.

Wang L-Y, Dudek EM, Browning MD, MacDonald JF (1994) Modulation of

AMPA/Kainate receptors in cultured murine hippocampal neurones by

protein kinase C. *J. Physiol.* (*Lond.*) **475**: 431–437.

Wang, X-J (1998) Calcium coding and adaptive temporal computation in cortical

pyramidal neurons. *J. Neurophysiol.* **79**: 1549–1566.

Warashina A (2001) Mechanism by which wortmannin and LY294002 inhibit

catecholamine secretion in the rat adrenal medullary cells. *Cell Calcium*

29: 239-247.

Watkins JC (2000) L-glutamate as a central neurotransmitter: looking back.

Biochem. Soc. Trans. **28**: 297-309.

Wehmeier U, Dong D, Koch C, Van Essen D (1989) Modeling the mammalian

visual system In : *Methods in neuronal modeling*, Koch C, Segev I eds pp

335–360. MIT Press, Cambridge, Massachusetts.

Wilkin GP, Hudson AL, Hill DR, Bowery NG (1981) Autoradiographic localization of GABAB receptors in rat cerebellum. *Nature* **294**: 584–587.

Wu LG, Saggau P (1994) Adenosine inhibits evoked synaptic transmission primarily by reducing presynaptic calcium influx in area CA1 of hippocampus. *Neuron* **12**: 1139–1148.

Wu LG, Saggau P (1995) GABAB receptor-mediated presynaptic inhibition in guinea-pig hippocampus is caused by reduction of presynaptic Ca2+ influx. *J. Physiol. (Lond.)* **485**: 649–657.

Wu SY, Dun NJ (1992) Presynaptic GABA$_B$ receptor activation attenuates synaptic transmission to rat sympathetic preganglionic neurons *in vitro*. *Brain Res.* **572**: 94–102.

Wurdig S, Kugler P (1991) Histochemistry of glutamate metabolizing enzymes in the rat cerebellar cortex. *Neurosci. Lett.* **130**: 165-168.

Yamada J, Saitow F, Satake S, Kiyohara T, Konishi S (1999) GABA(B) receptor-mediated presynaptic inhibition of glutamatergic and GABAergic transmission in the basolateral amygdala. *Neuropharmacology* **38**: 1743–1753.

Zeevalk GD, Nicklas WJ (1997) Activity at the GABA transporter contributes to acute cellular swelling produced by metabolic impairment in retina. *Vision Res.* **37**: 3463–3470.

Zucker RS (1989) Short-term synaptic plasticity. *Annu. Rev. Neurosci.* **12**: 13–31.